

Techno-Economic Analysis of the Arlington Microgrid

A Report prepared by the University of Washington
for Snohomish Public Utility District

February 28, 2022



This report was prepared for Snohomish Public Utility District by Daniel Kirschen and Chanaka Keerthisinghe of the Department of Electrical and Computer Engineering at the University of Washington. The project manager for Snohomish Public Utility District was Scott Gibson.

Appendices B and C were produced by Pacific Northwest National Laboratory.

Appendix D was written by John Glassmire of Hitachi.

This project was carried out under Washington State Grid Modernization CEF2 Contract Number 17-92110-001.

Executive Summary

This report describes the modeling, testing and data analytics work done by the University of Washington as part of Snohomish County Public Utility District’s Arlington Microgrid project. This project was funded by the Washington State Department of Commerce under the Clean Energy Fund 2.

The microgrid consists of a 1MW/1.4MWh Lithium-ion battery energy storage system, a 500 kW AC photovoltaic (PV) generation system, two vehicle-to-grid (V2G) systems, a 350-kW emergency backup generator, a microgrid controller and the Clean Energy Center load. The microgrid can also serve as an emergency backup power supply for the local data center. It will feed the Snohomish PUD’s Arlington office once it is built.

The microgrid controller has been designed to seize the full potential of the microgrid’s distributed energy resources while making sure that it is able to meet the critical loads during an emergency. To demonstrate the benefits of the Arlington Microgrid, this report discusses the analysis and tests carried out for four use-cases:

- Disaster recovery and grid resilience
- Renewable energy integration
- Grid support and ancillary services
- Vehicle-to-grid integration.

Pacific Northwest National Laboratory produced two complementary reports on the vehicle-to-grid (V2G) aspect of the microgrid. The first of these reports (Appendix B) is entitled “Economic Assessment of Vehicle-to-Grid (V2G) Tech for Fleets” and focuses on the life-time cost-benefit assessment of the use of electrified transportation fleets for V2G applications. In particular, this report discusses the value of V2G grid services provided by electric fleets of three types: i) Delivery vans, ii) School buses, and iii) Maintenance trucks. Four types of grid services were considered: i) Energy arbitrage, ii) Demand charge reduction, iii) Frequency regulation, and iv) Spinning reserve. The assessment included many factors that impact the economics of V2G, including, among others, battery degradation, replacement, roundtrip efficiencies, wholesale and retail energy prices to determine the long-term viability of V2G for both the utility and fleet

operators. The results indicate a strong correlation between the number of battery charge/discharge cycles and the cost of V2G.

The second PNNL report (Appendix C) discusses how standards development organizations from both the automotive and energy sectors need to coordinate the development of V2G standards. This coordination is currently happening, particularly between the SAE (Society of Automotive Engineers) and the IEEE (Institute of Electrical and Electronics Engineers). Members of these organization are working with Underwriters Laboratories (UL) to develop requirements for electric vehicles (EVs) and electric vehicle supply equipment (EVSE) to function as distributed energy resources for the grid e.g., UL1741 SC.

A CIGRE paper written by Hitachi Energy describing the lessons learned from the V2G integration at the Arlington microgrid is included as Appendix D.

Table of Contents

1.	Introduction	1
2.	Overview of the Arlington Microgrid	4
2.1	Design of the Arlington Microgrid.....	4
2.1.1	PV System	5
2.1.2	Battery Energy Storage System	7
2.1.3	Emergency Generator	9
2.1.4	Vehicle-to-Grid Systems	9
2.1.5	Electrical Load.....	10
2.1.5	Microgrid Controller.....	11
2.2	Operating Modes	12
2.2.1	Grid-Connected Operation	12
2.2.2	Islanded Operation	12
2.2.3	Transition from Grid-Connected to Islanded Mode.....	13
2.2.4	Transition from Islanded to Grid-Connected Mode.....	14
3.	Baseline Performance of the BESS	15
3.1	Summary of the Test Results	15
3.3	Detail of the Test Results	18
3.4	Conclusions	30
4.	Use-Cases of the Arlington Microgrid	31
4.1	UC1: Disaster Recovery and Grid Resilience	31
4.1.1	Background	31
4.1.2	Analysis.....	32
4.1.3	Value of Resilience	39

4.1.4	Summary	40
4.2	UC2: Renewable Energy Integration	41
4.2.1	Solar Smoothing.....	41
4.2.2	Capacity Firming	45
4.3	UC3: Grid Support and Ancillary Services	49
4.4	UC4: Vehicle-Grid Integration.....	50
4.4.1	Background	50
4.4.2	Analytics	51
5.	Microgrid Testing.....	53
5.1	UC1: Disaster Recovery and Grid Resilience	53
5.1.1	First Test.....	53
5.1.2	Second Test.....	56
5.1.3	Third Test	59
5.2	UC2: Renewable Energy Integration	62
5.2.1	First Day of Testing Solar Smoothing: Thursday September 2, 2021	62
5.2.2	Second Day of Testing Solar Smoothing: Tuesday September 7, 2021	65
5.2.3	Third Day of Testing Solar Smoothing: Wednesday September 8, 2021	68
5.2.4	Fourth Day of Testing Solar Smoothing: Monday October 18, 2021	71
5.2.5	Conclusion on Solar Smoothing Testing	72
5.3	UC3: Grid Support and Ancillary Services	73
5.4	UC4: Vehicle-Grid Integration.....	75
6.	Cost Breakdown of the Arlington Microgrid	79
7.	References	80
Appendix A: Site Acceptance Test Report on Integration of the Arlington Microgrid with the DERO Computer System.....		A

Appendix B: PNNL Report on Economics of Vehicle-to-Grid Integration	B
Appendix C: PNNL Report on Standards for Vehicle-to-Grid Integration	C
Appendix D: CIGRE Paper on V2G.....	D
Appendix E: Real-Time Digital Simulation of Microgrid Control Strategies	E
Appendix F: Capacity Firming Using Deep Learning	F

Table of Figures

Figure 1: Schematic representation of the components of the Arlington Microgrid and location of the various metering devices.	5
Figure 2: Median PV output profiles over the four seasons. The bars show the range between the 90th and 10th percentiles.	6
Figure 3: Energy flows and metering of the BESS.	7
Figure 4: Expected battery degradation over ten years assuming one energy throughput cycle per day.	9
Figure 5: Mean electrical load profiles of the Lynwood Office during the four seasons along with bars showing the 95th and 5th percentiles, as well as maximum and minimum values.	10
Figure 6: Round-trip-efficiency as a function of the discharge power.	16
Figure 7: Battery DC voltage as a function of the SoC for discharging at 1000, 500, and 250 kW.	17
Figure 8: Battery DC voltage as a function of the SoC for charging at 1000, 500, and 250 kW.	17
Figure 9: 1000 kW capacity test results: (a) battery SoC, (b) battery DC power, (c) battery DC voltage and (d) battery DC current.	20
Figure 10: 1000 kW capacity test results: (a) active power, (b) reactive power, (c) AC voltage, (d) AC current, (e) total energy in and (f) total energy out.	21
Figure 11: 500kW capacity test results: (a) battery SoC, (b) battery DC power, (c) battery DC voltage, (d) battery DC current, (e) battery enclosure temperatures and (f) auxiliary power.	24
Figure 12: 500 kW capacity test results: (a) active power, (b) reactive power, (c) AC voltage, (d) AC current, (e) total energy in and (f) total energy out.	25
Figure 13: 250kW capacity test results: (a) Battery SoC, (b) Battery DC power, (c) Battery DC voltage, (d) Battery DC current, (e) Battery enclosure temperatures and (f) Auxiliary power.	28

Figure 14: 250 kW capacity test results: (a) Active power, (b) reactive power, (c) AC voltage, (d) AC current, (e) total energy in and (f) total energy out.....	29
Figure 15: Continuous operating time (COT) simulation results considering both CEC and Arlington Office loads. (a) COT assuming the BESS is fully charged (b) PV generation and (c) electrical load of the microgrid at each hour (y-axis) over a year (x-axis). (d) COT assuming the initial BESS SoC at the moment of islanding at 12 pm is 100% and 50% vs. the day of the year.	34
Figure 16: Monthly maximum, mean and minimum COT assuming the BESS is fully charged at the moment of islanding for both CEC and Arlington Office loads.	35
Figure 17: Monthly maximum, mean and minimum COT assuming the BESS is half charged at the moment of islanding for both CEC and Arlington Office loads.	35
Figure 18: Continuous operating time simulation results considering Arlington Office load. (a) COT assuming the BESS is fully charged (b) PV generation and (c) electrical load of the microgrid at each hour (y-axis) over a year (x-axis). (d) COT assuming the initial BESS SoC at the moment of islanding at 12 pm is 100% and 50% vs. the day of the year.	36
Figure 19: Monthly maximum, mean and minimum COT assuming the BESS is fully charged at the moment of islanding for Arlington Office load.....	37
Figure 20: Monthly maximum, mean and minimum COT assuming the BESS is half charged at the moment of islanding for Arlington Office load.....	37
Figure 21: Effect of load curtailment on the COT when the BESS is half charged at the moment of islanding.	38
Figure 22: Interruption Cost Estimator Calculator results for a SAIFI of 2 and CAIDI of 315 in Washington State. Note that the total yearly load of a medium-large building is set to 392,720 kWh.	40
Figure 23: Raw and smoothed PV generation profile on June 23, 2020. The ramp rate limit of the smoothed profile is 3 kW/minute.	42

Figure 24: Number of battery energy throughput cycles as a function of the solar smoothing ramp rate	43
Figure 25: Net present value of solar smoothing as a function of the ramp rate limits in kW/minute, assuming replacement of the battery in ten years.....	44
Figure 26: PV generation and battery SoC on a cloudy day using encoder-decoder LSTM-RNN and persistence method.	47
Figure 27: PV generation and battery SoC on a less sunny day using encoder-decoder LSTM-RNN and persistence method.	47
Figure 28: PV generation and battery SoC on a sunny day using encoder-decoder LSTM-RNN and persistence method.	48
Figure 29: Net present value of capacity firming using encoder-decoder LSTM-RNN and 30/30 persistence after 10 years as a function of the battery replacement cost in 10 years. The revenue is fixed at \$5400 per year, the discount rate is assumed to be 5% and the battery degradation per cycle is based on Figure 4.	49
Figure 30: First islanding test on July 14, 2021. Islanding occurs at 13:45:04.	54
Figure 31: Microgrid operation during the islanded period (from 2704 second to 6087 second) of the first islanding test on July 14, 2021	55
Figure 32: Second islanding test on July 26, 2021. Islanding occurs at 14:41:44.....	57
Figure 33: Microgrid operation during the islanded period of the second islanding test on July 26, 2021. Islanding was triggered at 14:41:44 and lasted 34 minutes and 7 seconds.	58
Figure 34: Third islanding test on September 3, 2021. Islanding was triggered at 14:00:15	60
Figure 35: Microgrid operation during the islanded period of the third islanding test on September 3, 2021. Microgrid lasted from second 3615 to second 3932.	61
Figure 36: Solar smoothing on Thursday September 2, 2021, from 7am till 8pm. Note that the solar smoothing function was turned off at 5pm because the PUD crew was turning the battery off before they leave work. This was the case until all testing, training and fire safety systems were complete.	63

Figure 37: Solar smoothing on Thursday September 2, 2021, over the 20-minute period starting at 3.13pm when the PV generation was turned off and on using solar inverters.	64
Figure 38: Solar smoothing on September 7, 2021 (Tuesday) from 7am till 8pm. Note that the solar smoothing function was turned off at 5pm for safety reasons.....	66
Figure 39: Solar smoothing over a 20-minute period starting at 3.13pm on September 7, 2021.	67
Figure 40: Solar smoothing on Wednesday September 8, 2021, from 7am till 8pm. Note that the solar smoothing function was turned off at 5pm for safety reasons.....	69
Figure 41: Solar smoothing over a 30-minute period starting at 9.15am on Wednesday September 8, 2021.....	70
Figure 42: Solar smoothing over a 1-hour period starting at 2 pm on October 18, 2021.....	71
Figure 43: BESS charging and discharging at 250 kW over a day. (a) BESS AC power and (b) BESS DC power.....	73
Figure 44: BESS charging and discharging at 500 kW over a day. (a) BESS AC power and (b) BESS DC power.....	73
Figure 45: BESS charging and discharging at 1000 kW over a day. (a) BESS AC power and (b) BESS DC power.....	74
Figure 46: V2G test on January 19, 2022. The SoC and power input/output of the two electric vehicles. Note that the anomalies from measurement error are removed in this figure.	75
Figure 47: V2G test on January 19, 2022. Active power and reactive power at the outer microgrid (a and b) and inner microgrid (c and d). The outer microgrid includes the data center load.	76
Figure 48: V2G test on January 19, 2022. (a) BESS SoC; (b) BESS power; (c) PV generation; and (d) generator output.	76
Figure 49: V2G test on January 19, 2022. SoC and power of the two electric vehicles.	77
Figure 50: V2G test on January 19, 2022. (a) BESS SoC; (b) BESS power; (c) PV generation; and (d) generator output.	78

Figure 51: V2G test on January 19, 2022. Active power and reactive power at the outer microgrid (a and b) and inner microgrid (c and d)..... 78

Acronyms and Abbreviations

A	Ampere
AC	Alternating current
BESS	Battery energy storage system
BMS	Battery management system
BPA	Bonneville Power Administration
CEC	Clean Energy Center
CEF	Clean Energy Fund
COT	Continuous operating time
CSZ	Cascadia subduction zone
DC	Direct current
DER	Distributed energy resources
DG	Distributed generation
DoD	Depth-of-discharge
EV	Electric vehicle
HMI	Human machine interface
HVAC	Heating, ventilation, air conditioning
IED	Intelligent electronic device
kA	Kiloampere
kV	Kilovolt
kW	Kilowatt
kWh	Kilowatt hour
MW	Megawatt
MWh	Megawatt hour
PCC	Point of common coupling

POI	Point of interconnection
PV	Photovoltaic
PUD	Public Utility District
RTE	Roundtrip efficiency
SEI	Solid electrolyte interface
SoC	State of charge
UC	Use case
UL	Underwriters Laboratories
UPS	Uninterruptible power supply
V	Volt
V2G	Vehicle-to-grid
V2H	Vehicle-to-home
VAR	Volt Ampere reactive
VGI	Vehicle-grid integration
W	Watt
Wh	Watt hour

1. Introduction

The traditional interconnected electrical power system of the United States (US) is fragile and vulnerable to natural disasters and other power outages. The U.S. Department of Energy (DOE) stated that due to severe weather roughly 679 power outages affecting at least 50,000 customers occurred in the USA between 2003 to 2012 [1]. Some of the natural disasters that resulted in a large outage included hurricanes Katrina (2005), Sandy (2012), and Irma (2017) and the Pacific Northwest windstorm of 2006. The frequency and intensity of hurricanes, windstorms, blizzards, and floods is expected to increase because of climate change.

The Pacific Northwest is in the Cascadia Subduction Zone (CSZ). The last major CSZ earthquake and tsunami occurred in 1700 and science points to an 8-9 magnitude earthquake ripping across the 800-mile CSZ fault line on average once every 200 to 500 years. We can expect a large scale and long-term blackout from such a disaster [2].

Given the above reasons, improving the resilience of the electrical power grid has become an imperative topic. The U.S. DOE received \$4.5 billion through the American Recovery and Reinvestment Act of 2009 (“Recovery Act”) for investments in modern grid technology, which includes improving the resilience and reliability of the grid in the face of severe weather events. As stated by the DOE, a more resilient grid is one that is better able to sustain and recover from adverse events like severe weather while a more reliable grid is one with fewer and shorter power interruptions [1].

One way to improve grid resilience is to improve system flexibility and robustness by deploying microgrids. A microgrid is a group of interconnected loads and distributed energy resources (DER) within clearly defined electricity boundaries that acts as a single controllable entity with respect to the grid. A microgrid can connect and disconnect from the grid to enable it to operate in both grid-connected and islanded mode. During an emergency, the microgrid can supply electricity to critical end-user loads with little or no disruption by seamlessly isolating itself from the grid. Then, when the grid returns to the normal operation, the microgrid automatically resynchronizes and reconnects itself to the grid in an equally seamless fashion. A range of other methods used to improve grid resilience can be found in [1].

As a part of the Energy Freedom Program, the Washington State Department of Commerce has allocated \$36 million in 2013 as Clean Energy Fund 1 and \$40 million in 2015 as Clean Energy

Fund 2 (CEF-2) to expand clean energy projects and technologies throughout the state [3]. The Snohomish County Public Utility District (PUD) received \$3.5 million from the WA Department of Commerce to implement a microgrid in Arlington, Washington.

A large number of microgrids have been deployed in the past years and a detailed list can be found in DOE webpage [4]. Examples include the following:

- The Technology Applications Center (TAC) microgrid in Illinois was constructed by S&C Electric Co. of Chicago. This microgrid can supply up to 1415 kW using a wind turbine, photovoltaic (PV) array, natural gas generator and battery energy storage system. The novelty of their design is the capability to seamlessly transition the power source for an entire distribution circuit from exclusively distributed generation sources to the grid [5].
- Tesla Energy has successfully implemented microgrids in Kauai, Hawaii and Tau Island, American Samoa. The Kauai microgrid consists of a 13 MW PV array (54978 panels) and 52 MWh of battery storage (272 Tesla Powerpacks) and saves 1.6 million gallons of fossil fuel per year. Similarly, the Tau Island microgrid consists of a 1.4 MW PV array (5328 panels) and a 6 MWh of battery storage (60 Tesla Powerpacks) and saves 300 gallons of fossil fuel per day. According to Tesla, the island can remain fully supplied with electricity for three full days without sun [6].
- The Fort Carson microgrid in Colorado Springs is one of several microgrid projects under the SPIDERS (Smart Power Infrastructure Demonstration for Energy Reliability and Security) program. This military base has an ambitious plan to become a net zero facility using huge PV resources, potentially over 100 MW, as well as wind, ground-source heat pumps, biomass, and solar water heating [4].
- ABB developed a 1MWh/1MW lithium battery and diesel generator microgrid in Melbourne, Victoria, Australia for the AusNet's distribution electricity network in 2015 [7].

Snohomish PUD's Arlington Microgrid consists of a 500 kW PV system, a 1MW/1.4 MWh battery energy storage system (BESS), two vehicle-to-grid systems, and a 350-kW emergency generator. It can provide power to the Clean Energy Center (CEC) and the future Arlington Office of

Snohomish PUD during an emergency and provide other grid services during normal operation. It is designed to support four use-cases:

- UC1: Disaster recovery and grid resilience
- UC2: Renewable energy integration
- UC3: Grid support and ancillary services
- UC4: Vehicle-to-grid integration.

The rest of this report is structured as follows. Section 2 describes the design of the Arlington Microgrid and its operating modes. The results of the BESS baseline tests are presented in Section 3. Section 4 discusses the benefits of the four use-cases. Test results are presented and analyzed in Section 5. Section 6 summarizes the costs of the various components of the microgrid. Supplemental information is included in the appendices.

2. Overview of the Arlington Microgrid

The first part of this section describes the configuration and the design of the Arlington Microgrid, while the second and third explain the operating modes and the transition between these modes.

2.1 Design of the Arlington Microgrid

As depicted in Figure 1, the Arlington Microgrid consists of the following:

- A 1MW/1.4 MWh Lithium-Ion battery energy storage system (BESS), which adheres to the MESA standard
- A 500 kW AC PV system
- Two vehicle-to-grid (V2G) systems
- A 350-kW emergency backup diesel generator
- The loads provided by the completed Clean Energy Center (CEC) and data center, and the future Snohomish PUD's Arlington Office
- The microgrid controller.

The microgrid is located at latitude 48.17 and longitude -122.14, which is near the Arlington airport.

The main use-case of the Arlington Microgrid is to supply power reliably to critical end-user loads, such as the CEC, the data center, and Snohomish PUD's Arlington Office during an emergency. Following a natural disaster, the CEC could be used as a community shelter and the Arlington Office could be used as a location to dispatch repair crew to restore the rest of the power system. However, since such disasters are hopefully not common, the microgrid should provide other benefits. These benefits include facilitating the integration of renewable energy sources as well as providing grid support and ancillary services. These benefits are discussed in more details in Section 3.

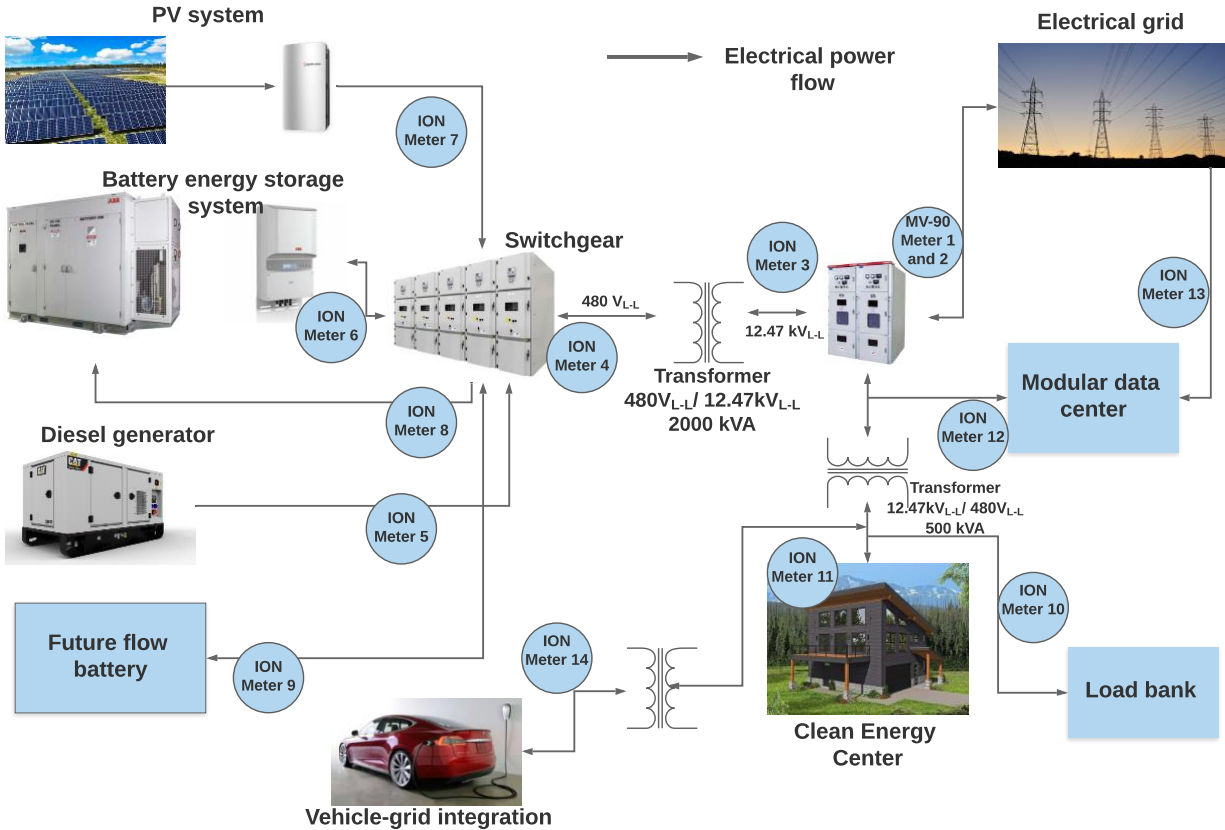


Figure 1: Schematic representation of the components of the Arlington Microgrid and location of the various metering devices.

2.1.1 PV System

The PV system consists of a PV array and 10 inverters with maximum power point tracking. Table 1 gives the parameters of this system. Figure 2 shows the median PV output over a day in each of the four seasons. As the 90th percentile bar indicates, the maximum PV generation of 500kW is achieved in during the summer, fall and spring. Over its first year of operation (2019/2020), this PV system generated 667 MWh.

Table 1: Parameters of the PV system

DC rating	615 kW
Module	REC TWINPEAK 2S MONO 72 SERIES
Number of modules	1618
AC rating	500 kW
Inverter	Sunny Tripower Core1 50kW
Azimuth	180°
Tilt	30°
Racking	Ground
DC:AC ratio	1:1.23
Degradation	0.7% per year and 17.5% over 25 years

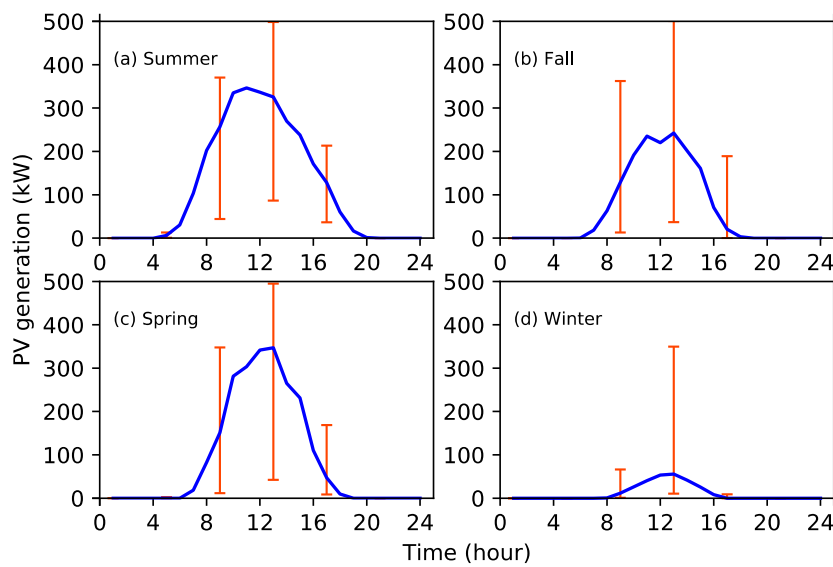


Figure 2: Median PV output profiles over the four seasons. The bars show the range between the 90th and 10th percentiles.

2.1.2 Battery Energy Storage System

The Hitachi-ABB PowerStore™ BESS is rated at 1 MW/1.4 MWh. Figure 3 illustrates the energy flows and the metering in the BESS.

Table 2 and Table 3 summarize the manufacturer’s BESS specifications. Figure 4 shows the expected battery degradation over 10 years.

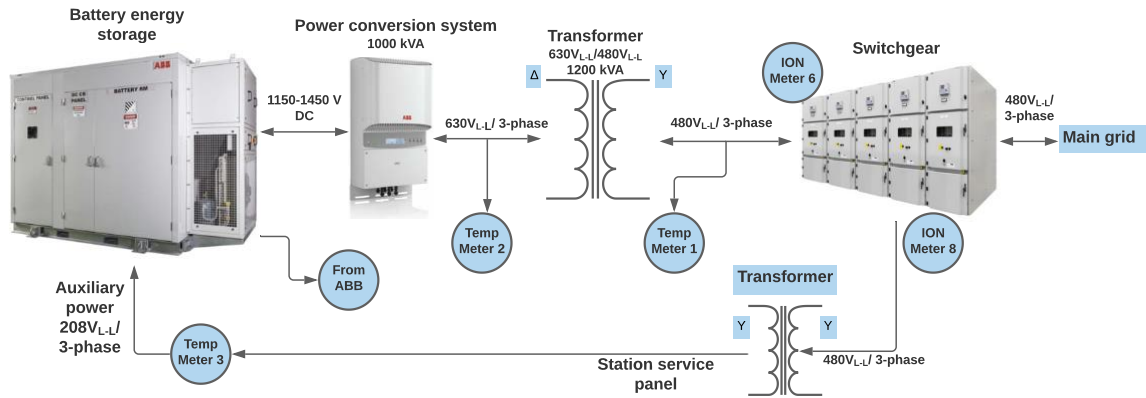


Figure 3: Energy flows and metering of the BESS.

Table 2: Specifications of the PowerStore™ PCS inverter

kVA rating	1,000kVA
AC Voltage Range	630 VRMS+10/-12%
Transformer	630Vac to 480Vac oil filled transformer
AC export capacity at 25C	1250kVA 1146A RMS
AC export capacity at 45C	1125 kVA 1031A RMS
AC import capacity at 25C	1004 kVA 920A RMS
AC Import Capacity at 25C	886 kVA 812A RMS
Inverter Type	3-Level VSC
Minimum Grid SCCR	2
Nominal frequency range	3-Level VSC
Harmonic distortion	UL1741/IEEE 1547

	<2%TDDi per IEEE 519
Power factor/ reactive power	0.0 leading 0.0 lagging (full 4-quadrant operation)
Max auxiliary power consumption	950W
Efficiency: max CEC Euro	98.6% (est.) >98% (est.) >98% (est.)
Ambient temperature (operation)	-20C to 60C
Protection degree	NEMA 3R/IP54
Relative humidity	5%-100% condensing
Max elevation	2,000m
Dimensions (estimate)	[108.6” x 39.4” x 47.2”]
Weight (estimate)	2,000lb
Cooling	Hybrid liquid/ air
Safety (pending)	UL1741 C22.2 No. 107.1-16
Utility Interconnect (pending)	16UL 1741:2010 R2.18 (SA) IEEE 1547.1-2005 CA Rule 21 No. 16-06- 052 Hawaii Rule 14 No. 2014-0192
AC protection	Motor operated fuses
DC protection	Motor operated fuses

Table 3: Manufacturer’s specifications of the battery module and battery container

Battery module	Samsung M2F 352S 121.8kkWh/rack 1,126.4-1,460.8Vdc
Nameplate energy rating	1,340kWh
Container type	Concrete
HVAC	Wall mount units
Fire suppression	NOVEC1230 (150ft2) and Siamese Connection and Sprinklers
Gas sensors louvers	Lithium Ion Tamer
Louvers	180CFM vent system with motor louvers
Deflagration panel	Included

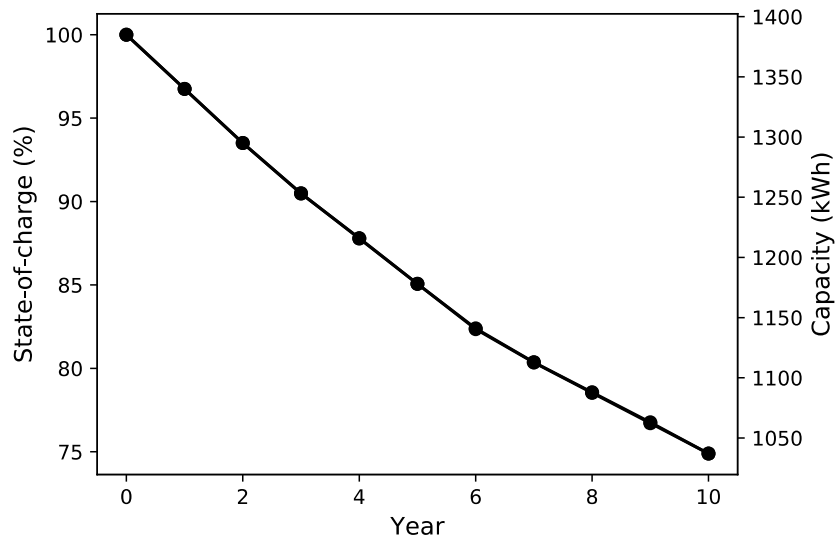


Figure 4: Expected battery degradation over ten years assuming one energy throughput cycle per day.

2.1.3 Emergency Generator

The diesel generator is rated at 350 kW and is expected to have enough fuel to run for 24 hours during an emergency. Its operation is discussed as part of UC2 “Disaster recovery and resilience”.

2.1.4 Vehicle-to-Grid Systems

Two electric vehicle (EV) charging stations with vehicle-to-grid capability have been incorporated in the microgrid. They are manufactured by Mitsubishi Electric (Japan) and are of the type Power Conditioner Smart V2H (vehicle-to-home), model EVP-SS60B3-M7-R. Each of them is rated at 6 kW during grid-connected mode. During islanded operation each of them is rated at 6 kVA because they must be able to supply reactive power to maintain the voltage closer to nominal.

Snohomish PUD purchased two Nissan Leaf electric vehicles for this project. The 2020 model has a 60-kWh battery while the 2019 model has only a 40-kWh battery. The 2020 Nissan Leaf can be

fully charged within 12 hours while a full charge of the 2019 Nissan Leaf takes less than 8 hours. The maximum power conversion efficiency according to the manufacturer is 90%.

2.1.5 Electrical Load

Actual data about the profiles of the loads that will be connected directly to the Arlington microgrid is unfortunately not available because the construction of the Arlington Office has not yet started, and the CEC was under construction during the planning phase of the microgrid. We expect the load of the new Arlington office to be similar to the load of the Lynnwood office building and the load of the CEC to be similar to the load of the Line Training Building. According to Snohomish PUD engineers, the peak office load is expected to be approximately 150 kW and the peak load of the CEC to be 50 kW. Their estimated average loads are 135 kW for the office load and 35 kW for the CEC. It was therefore decided to use the electrical load profile of the Lynnwood Office for modeling purposes. As shown in Figure 5, due to the high space heating requirements and low cooling requirements, this load is highest on winter days and lowest on summer days.

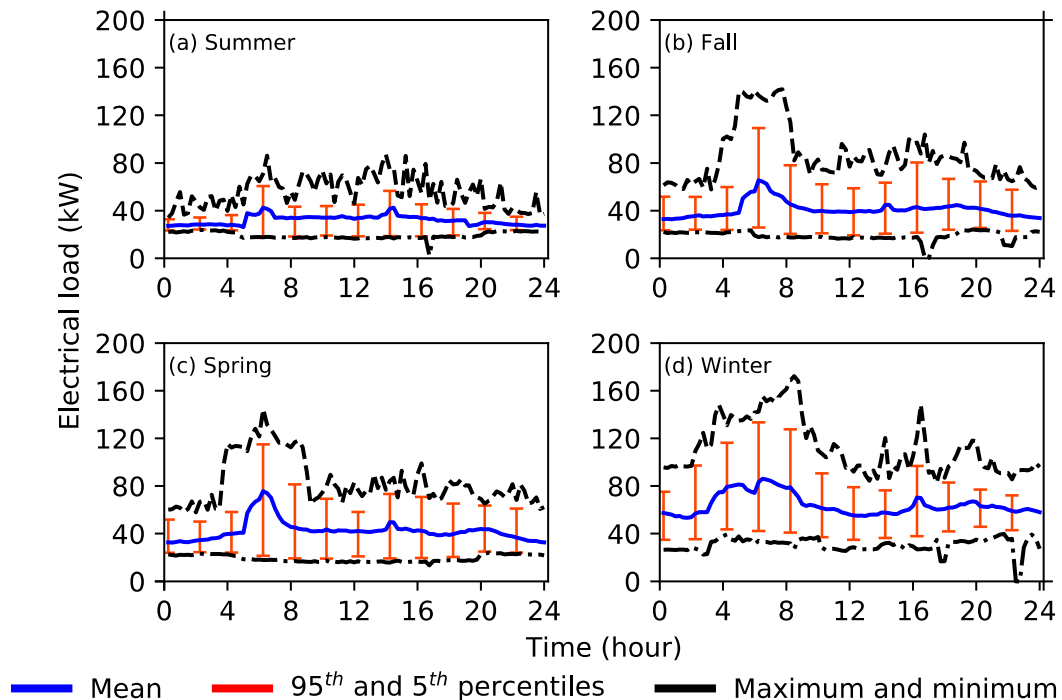


Figure 5: Mean electrical load profiles of the Lynnwood Office during the four seasons along with bars showing the 95th and 5th percentiles, as well as maximum and minimum values.

Note that the electrical load during an emergency is difficult to predict as it depends on the number of employees and their behavioral pattern. The building energy management system will have different load shedding options so power can be saved for critical uses during an emergency.

The electricity cost of the Lynwood Office consists of the demand and energy charges. The demand charge is based on the maximum electricity consumption rate during each month, measured in kW. The energy charge is based on the total amount of electrical energy consumed during the month, measured in kWh. Table 4 gives the energy and demand charges for the Lynwood Office in 2017. The demand charge is only applicable if the peak load is above 100 kW. The peak load is measured at 15-minute intervals.

Table 4: Electricity costs of the Lynwood Office in 2017

Month	Posting Period	kWh	Billed KW	Energy Charges	Billed KW Charges	Total Charges
1	Jan-17	55,360	148.2	\$4,373	\$217	\$4,590
2	Feb-17	41,520	148.0	\$3,421	\$216	\$3,637
3	Mar-17	40,000	172.2	\$3,316	\$325	\$3,641
4	Apr-17	34,800	144.5	\$2,980	\$211	\$3,192
5	May-17	26,320	129.1	\$2,345	\$144	\$2,489
6	Jun-17	21,680	90.4	\$1,932	\$0	\$1,932
7	Jul-17	24,160	87.0	\$2,153	\$0	\$2,153
8	Aug-17	21,840	86.1	\$1,946	\$0	\$1,946
9	Sep-17	24,400	75.3	\$2,174	\$0	\$2,174
10	Oct-17	23,600	104.4	\$2,117	\$22	\$2,139
11	Nov-17	35,360	141.9	\$3,086	\$215	\$3,301
12	Dec-17	43,680	148.5	\$3,667	\$248	\$3,915
Total		392,720		\$33,509	\$1,599	\$35,107

2.1.5 Microgrid Controller

The operation of the microgrid controller provided by Hitachi-ABB is discussed in the section on microgrid operating modes.

2.2 Operating Modes

This section describes the two operating modes of the microgrid: grid-connected and islanded.

2.2.1 Grid-Connected Operation

This is the most common mode of operation where the microgrid is connected to the electrical grid i.e., the POI circuit breaker is closed. While in this mode, the BESS will be used for energy arbitrage (UC3) and solar smoothing (UC2).

When grid-connected, the inverters of both the PV and the BESS inverters typically operate in grid-following mode. However, Hitachi-ABB decided to keep the BESS inverter in grid-forming mode to achieve seamless islanding

2.2.2 Islanded Operation

The microgrid is islanded when the breaker at the PCC/ POI is open and the connection with the utility power system is lost. The BESS maintains the microgrid voltage and frequency at the desired levels by operating the BESS inverter in grid-forming mode. The PV inverter operates in grid-following mode based on the dispatch setpoint from the microgrid controller.

When the PV generation is greater than the total load, the excess power is used to charge the battery. If the battery SoC reaches the maximum SoC limit of the battery, the microgrid controller automatically curtails the PV generation.

On the other hand, when the PV generation is less than the total load, the BESS is discharged to meet the load. The PV set point is maintained at the maximum power point.

During an extended power outage, once the SoC of the BESS drops below the operator configurable minimum SoC limit, the microgrid controller sends a command to start the emergency generator. The emergency generator then supplies the load and charge the BESS to the required level. The PV inverters operate at their maximum power point if there is enough energy capacity left in the BESS.

2.2.3 Transition from Grid-Connected to Islanded Mode

When in grid-connected mode i.e., the PCC breaker is closed, the PV inverters operate in grid-following mode according to dispatch setpoints from the microgrid controller while the BESS inverter operates in grid forming mode. Islanding of the microgrid can be unplanned or planned.

Unplanned Islanding

The microgrid control system constantly collects information from the relay at the PCC and initiates an islanding based on any of the following conditions:

- Flow of fault current from the microgrid to the main grid
- Voltage sag duration per IEEE 1547-2018
- Frequency excursion per IEEE 1547-2018

Once the relay at the PCC trips the breaker open, the BESS reacts to the transient event and maintains the system voltage and frequency within the islanded microgrid. During this event, the microgrid control system automatically transfers from grid-connected mode to islanded mode and sends proper protection group setting to the intelligent electronic devices (IEDs) and send set points to the PV system and the diesel generator.

Planned Islanding

When islanded operation is planned, the operator commands the system through the human machine interface (HMI) to enter islanded mode. Upon receiving this command, the microgrid controller brings appropriate generation and storage online if required to meet the demand and adjusts the output of these sources such that there is null power flow at the PCC. Once the null power flow is achieved, the system opens the breaker at the PCC and send proper protection group settings to the IEDs.

The transition of the BESS from grid-connected mode to islanded mode is expected to be seamless. If the microgrid requires black start for any reason, the microgrid control system first commands the emergency generator or BESS to start so that the main bus can be energized. The microgrid control system recalls the last demand prior to going dark and bring up enough generation and storage to comfortably handle the load.

2.2.4 Transition from Islanded to Grid-Connected Mode

The microgrid control system transitions from islanded mode to grid-connected mode in a seamless manner. During islanded mode operation, the microgrid control system detects the presence of voltage on the main grid through the relay at the PCC and alerts the operator. At this point, the operator can command the microgrid control system to initiate a resynchronization to the grid. The microgrid control system will slightly speed up or slow down the microgrid frequency to bring it into sync with the main grid. Once synchronized it will hold the two frequencies and alert the operator that the PCC breaker can be closed. Note that re-synchronization is disabled when the microgrid is manually islanded by the operator.

During an extended power outage, after the BESS has been on stand-by for a long period and the uninterruptible power supply (UPS) battery used for the controllers is completely drained, power to the microgrid controller and breaker will be lost. In such situations, Snohomish PUD crew will need to go to the site to close the PCC breaker.

3. Baseline Performance of the BESS

The BESS underwent baseline tests to determine the beginning-of-life reference performance. Repeating these baseline performance tests and comparing with these baselines will allow Snohomish PUD to determine BESS degradation. The test plans were developed by Hitachi-ABB and Burns & McDonnell and are provided in Appendix A.

The DOE-OE (Department of Energy - Office of Electricity) sponsored protocol development effort identified the following general performance metrics:

- Round-trip efficiency (RTE)
- Response time and ramp rate (this was an application-specific metric in the protocol but has been moved up to general metrics)
- Energy capacity stability (this can be performed at any time during BESS operation)
- Internal resistance during charge and discharge
- Stability of internal resistance over time

3.1 Summary of the Test Results

Snohomish PUD and Hitachi-ABB carried out three capacity tests at three discharge rates (1MW, 500kW and 250kW). Each capacity test consists of 2 or 3 cycles with a fixed 15-minutes rest time between charge and discharge and between cycles. The upper limit of the BESS SoC was set at 95% while the lower limit was set at 0%. The test results of the capacity tests enable us to calculate the RTE and capacity of the BESS. Note that response time and ramp rates and internal resistances are also obtained from these tests instead of repeating the same experiments again. Figure 6 illustrates the dependence of the RTE on the discharge rate. Figure 7 shows how the battery DC voltage varies with the SoC as the battery is discharged and Figure 8 as it is charged. The details of the tests can be found in Table 5, Table 6 and Table 7.

Important findings are as follows:

- The RTE of the BESS without auxiliary power is highest for lower C-rates. The RTE at 1C, 0.5C and 0.25C are 90.52%, 92.79% and 92.94%, respectively.

- The RTE of the BESS with auxiliary power is highest for 0.5C rate because the 0.25C rate test takes longer, which results in a much higher HVAC load (heating, ventilation, and air conditioning). The RTE at 1C, 0.5C and 0.25C are 88.53%, 90.4% and 88.84%, respectively.
- The RTE including the rest period between the charge discharge is slightly lower. The RTE at 1C, 0.5C and 0.25C are 88.762%, 90.31% and 88.38%, respectively.
- The charge internal resistance of the BESS is higher than the discharge internal resistance for all the tests. This is because the solid electrolyte interface (SEI) layer is mainly formed at the anode. The average internal resistance ranges between 20 and 50 mΩ.

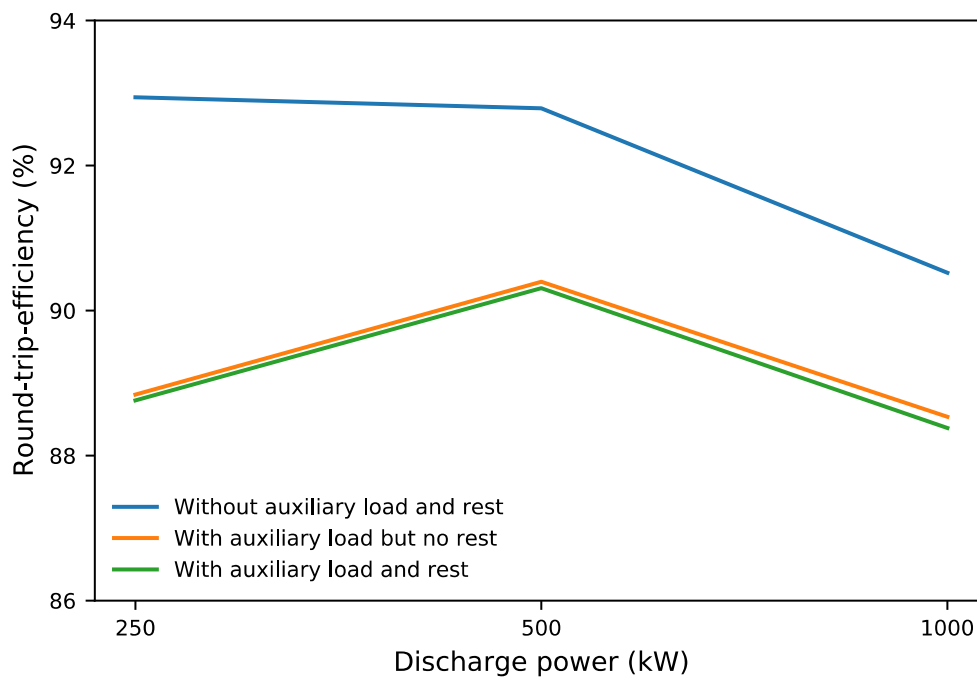


Figure 6: Round-trip-efficiency as a function of the discharge power.

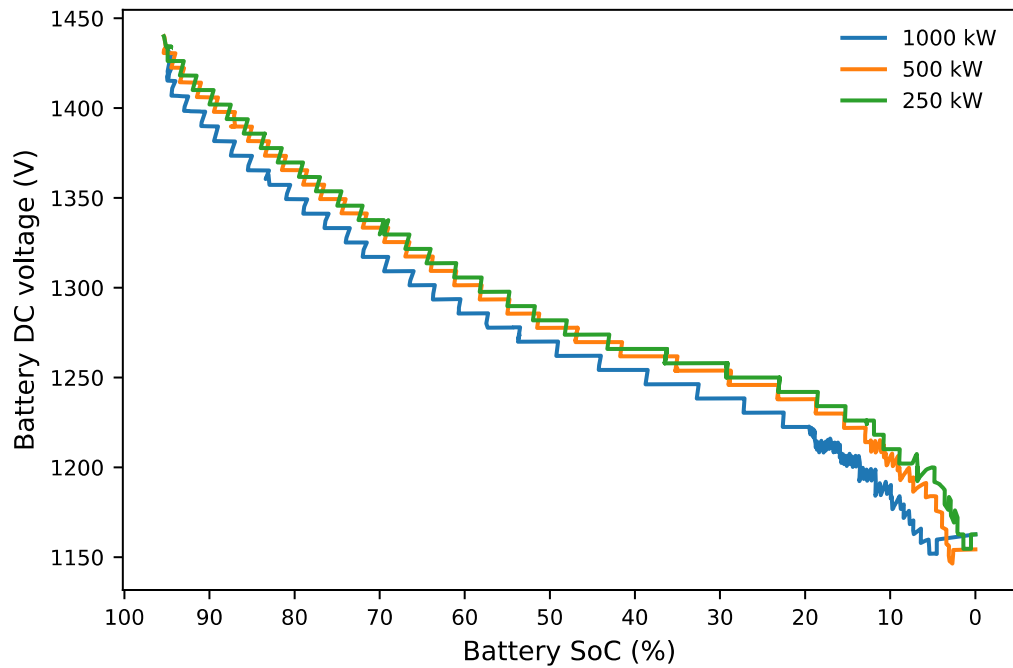


Figure 7: Battery DC voltage as a function of the SoC for discharging at 1000, 500, and 250 kW

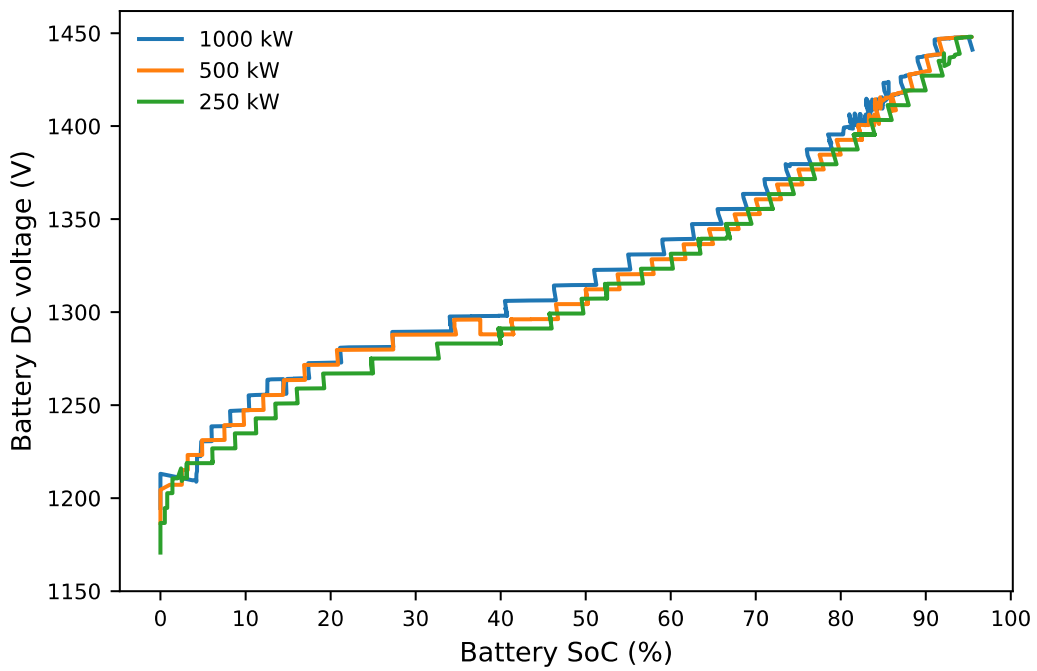


Figure 8: Battery DC voltage as a function of the SoC for charging at 1000, 500, and 250 kW.

3.3 Detail of the Test Results

The following tables and figures provide the detail of the tests that were carried out to obtain a baseline of the performance of the BESS.

Table 5: Summary of the 1000 kW capacity test results

	Cycle 1	Cycle 2	Average	
SoC range	0% - 95%			
Total input energy (charge)	1440 kWh	1389 kWh	1414.5 kWh	
Total output energy (discharge)	1280 kWh	1280 kWh	1280 kWh	
Charging				
Average charge power	988.723 kW	988.558 kW	988.641 kW	
Charge time at full power	86 minutes and 40 seconds	83 minutes and 41 seconds		
Initial ramp up time (charging)	12 seconds	12 seconds		
Final ramp down time (charging)	287 seconds	243 seconds		
Total charge time	91 minutes and 39 seconds	87 minutes and 56 seconds		
Initial ramp up rate (charging)	81.056 kW/ second	81.448 kW/ second		
Final ramp down rate (charging)	3.427 kW/ second	4.051 kW/ second		
Discharging				
Average discharge power	967.125 kW	967.458 kW	967.292 kW	
Discharge time at full power	77 minutes and 25 seconds	78 minutes and 18 minutes		
Initial ramp up time (discharging)	13 seconds	13 seconds		
Final ramp down time (discharging)	69 seconds	83 seconds		
Total discharge time	78 minutes and 47 seconds	79 minutes and 54 seconds		
Initial ramp up rate (discharging)	74.834 kW/ second	74.797 kW/ second		
Final ramp down rate (discharging)	14.109 kW/ second	11.730 kW/ second		

RTE (without auxiliary power)	88.89%	92.15%	90.52%	
Auxiliary power charging	10.46 kW	10.96 kW		
Auxiliary energy charging	15.98 kWh	16.063 kWh		
Auxiliary power discharging	10.88 kW	10.28 kW		
Auxiliary energy discharging	14.286 kWh	13.69 kWh		
RTE (with auxiliary power)	86.93%	90.13%	88.53%	
Rest time between charge/ discharge	14 minutes and 53 seconds	14 minutes and 52 seconds		
Auxiliary power during rest	9.405 kW	9.727 kW		
RTE (with auxiliary power and rest)	86.793%	89.97%	88.38%	
Charge internal resistance at 0% SoC	0.032 ohms	0.0253 ohms	0.0287 ohms	
Discharge internal resistance at 95% SoC	0.01414 ohms	0.024 ohms	0.01907 ohms	

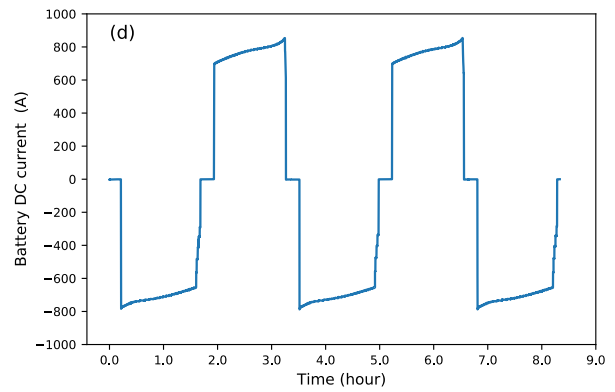
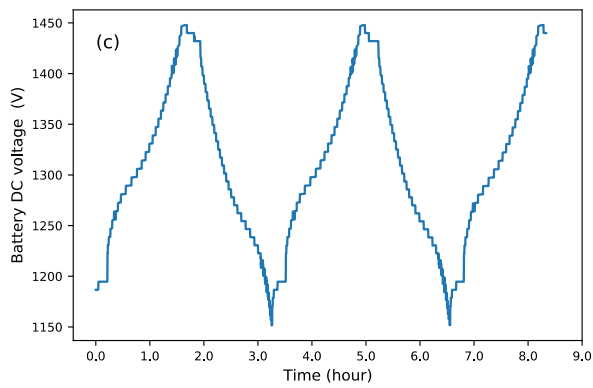
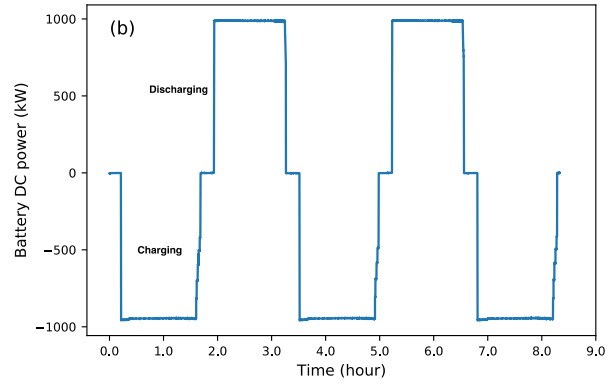
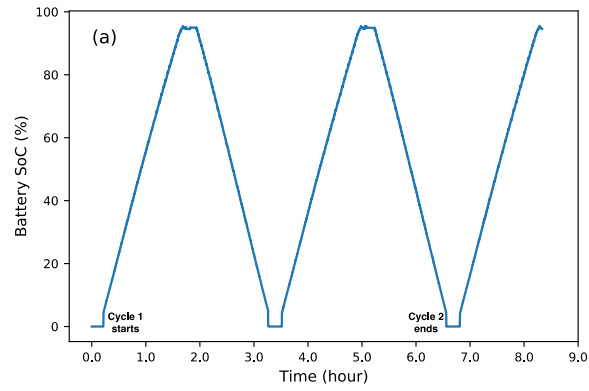


Figure 9: 1000 kW capacity test results: (a) battery SoC, (b) battery DC power, (c) battery DC voltage and (d) battery DC current.

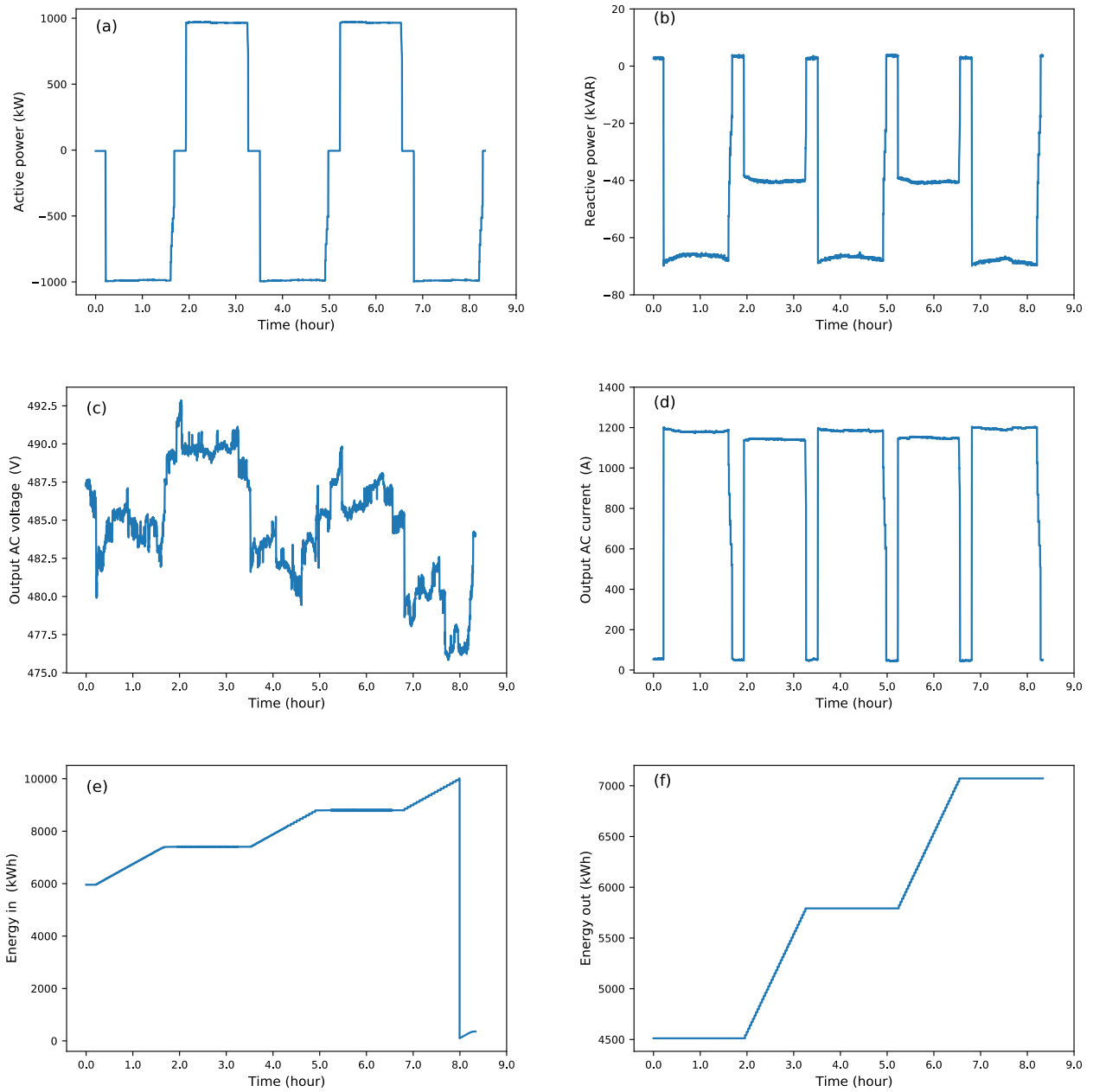


Figure 10: 1000 kW capacity test results: (a) active power, (b) reactive power, (c) AC voltage, (d) AC current, (e) total energy in and (f) total energy out.

Table 6: Summary of the 500 kW capacity test results

	Cycle 1	Cycle 2	Cycle 3	Average
SoC range	0% - 95%			
Total input energy (charge)	1428 kWh	1452 kWh	1440 kWh	1440 kWh
Total output energy (discharge)	1344 kWh	1320 kWh	1344 kWh	1336 kWh
Charging				
Average charge power	481.441 kW	481.959 kW	482.432 kW	481.944 kW
Charge time at full power	175 minutes and 4 seconds	175 minutes and 29 seconds	175 minutes and 8 seconds	175 minutes and 13.7 seconds
Initial ramp up time (charging)	6 seconds	7 seconds	7 seconds	6.7 seconds
Final ramp down time (charging)	305 seconds	337 seconds	327 seconds	323 seconds
Total charge time	180 minutes and 15 seconds	181 minutes and 13 seconds	180 minutes and 42 seconds	180 minutes and 43.3 seconds
Initial ramp up rate (charging)	80.190 kW/second	70.493 kW/second	68.719 kW/second	73.134 kW/second
Final ramp down rate (charging)	1.562 kW/second	1.418 kW/second	1.459 kW/second	1.48 kW/second
Discharging				
Average discharge power	491.264 kW	492.008 kW	492.401 kW	491.891 kW
Discharge time at full power	161 minutes and 29 seconds	161 minutes and 22 seconds	161 minutes and 6 seconds	161 minutes and 19 seconds
Initial ramp up time (discharging)	6 seconds	6 seconds	7 seconds	6.3 seconds
Final ramp down time (discharging)	70 seconds	68 seconds	109 seconds	82.33 seconds

Total discharge time	162 minutes and 45 seconds	162 minutes and 36 seconds	163 minutes and 2 seconds	162 minutes and 48 seconds
Initial ramp up rate (discharging)	82.624 kW/second	82.428 kW/second	70.508 kW/second	78.52 kW/second
Final ramp down rate (discharging)	7.095 kW/second	7.326 kW/second	4.567 kW/second	6.33 kW/second
RTE (without auxiliary power and rest)	94.12%	90.91%	93.33%	92.79%
Auxiliary power charging	7.83 kW	6.451 kW	5.287 kW	6.523 kW
Auxiliary energy charging	23.523 kWh	19.484 kWh	15.923 kWh	19.643 kWh
Auxiliary power discharging	7.452 kW	5.792 kW	5.138 kW	6.127 kW
Auxiliary energy discharging	20.214 kWh	15.696 kWh	13.961 kWh	16.624 kWh
RTE (with auxiliary power)	91.2%	88.639%	91.354%	90.398%
Rest time between charge/ discharge	14 minutes and 57 seconds	14 minutes and 57 seconds	14 minutes and 56 seconds	14 minutes and 56.67 seconds
Auxiliary power during rest	7.115 kW	5.454 kW	5.265 kW	5.945 kW
RTE (with auxiliary power and rest)	91.1%	88.557%	91.272%	90.31%
Charge internal resistance at 0% SoC	0.0527 ohms	0.0255 ohms	0.0729 ohms	0.05037 ohms
Discharge internal resistance at 95% SoC	0.03224 ohms	0.02682 ohms	0.03277 ohms	0.03061 ohms

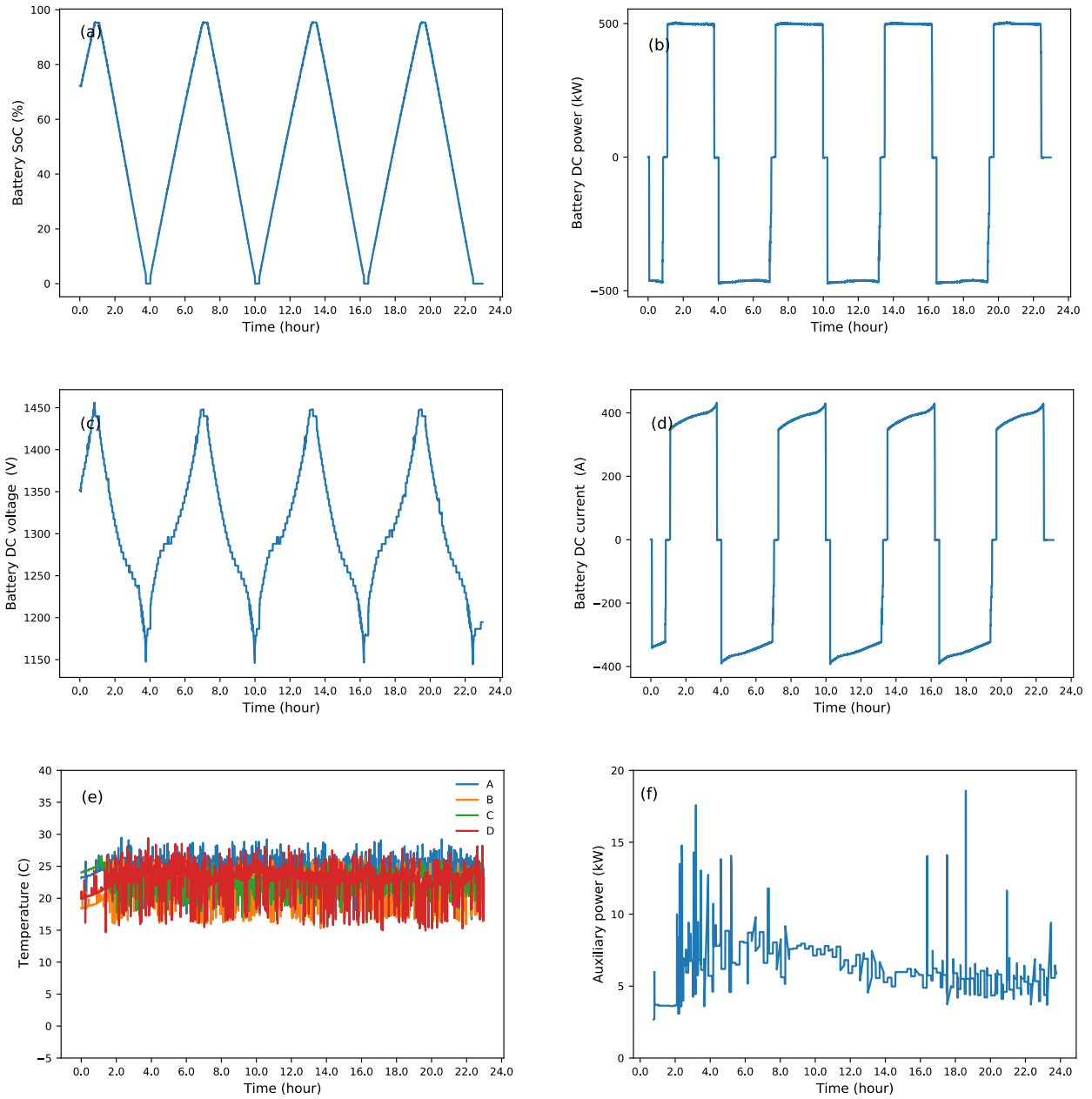


Figure 11: 500kW capacity test results: (a) battery SoC, (b) battery DC power, (c) battery DC voltage, (d) battery DC current, (e) battery enclosure temperatures and (f) auxiliary power.

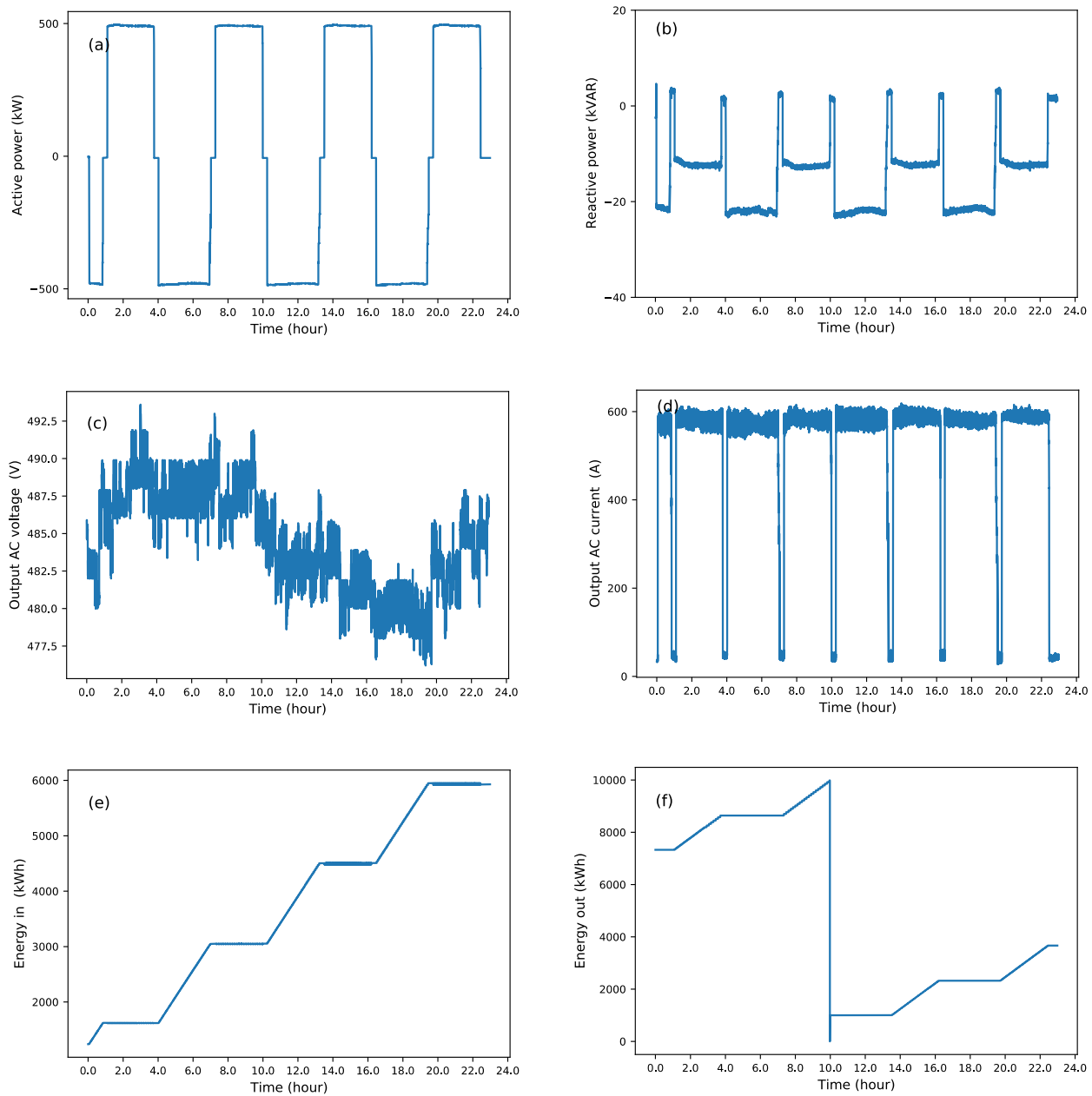


Figure 12: 500 kW capacity test results: (a) active power, (b) reactive power, (c) AC voltage, (d) AC current, (e) total energy in and (f) total energy out.

Table 7: Summary of the 250 kW capacity test results

	Cycle 1	Cycle 2	Cycle 3	Average
SoC range	0% - 95%			
Total input energy (charge)	1463 kWh	1456 kWh	1467 kWh	1462 kWh
Total output Energy (discharge)	1352 kWh	1344 kWh	1376 kWh	1357.33 kWh
Charging				
Average charge power	232.6725 kW	232.513 kW	232.842 kW	232.68 kW
Charge time at full power	375 minutes and 44 seconds	375 minutes and 51 seconds	375 minutes and 18 seconds	375 minutes and 37.67 seconds
Initial ramp up time (charging)	4 seconds	5 seconds	5 seconds	4.67 seconds
Final ramp down time (charging)	6 seconds	5 seconds	5 seconds	5.33 seconds
Total charge time	375 minutes and 54 seconds	376 minutes and 1 second	375 minutes and 28 seconds	375 minutes and 47.67 seconds
Initial ramp up rate (charging)	57.6746 kW/second	46.309 kW/second	46.199 kW/second	50.061 kW/second
Final ramp down rate (charging)	38.148 kW/second	45.639 kW/second	45.823 kW/second	42.203 kW/second
Discharging				
Average discharge power	243.692 kW	243.931 kW	243.883 kW	243.84 kW
Discharge time at full power	330 minutes and 40 seconds	330 minutes and 39 seconds	330 minutes and 9 seconds	330 minutes and 29.33 seconds
Initial ramp up time (discharging)	4 seconds	4 seconds	5 seconds	4.33 seconds
Final ramp down time (discharging)	9 minutes and 6 seconds	9 minutes and 7 seconds	8 minutes and 57 seconds	9 minutes and 3.33 seconds

Total discharge time	339 minutes and 50 seconds	339 minutes and 50 seconds	339 minutes and 11 seconds	339 minutes and 37 seconds
Initial ramp up rate (discharging)	61.725 kW/second	61.865 kW/second	49.382 kW/second	57.66 kW/second
Final ramp down rate (discharging)	453 W/second	451 W/second	460 W/second	455 kW/second
RTE (without auxiliary power and rest)	92.413%	92.31%	93.797%	92.94%
Auxiliary power charging	5.07 kW	5.662 kW	5.031 kW	5.254 kW
Auxiliary energy charging	31.764 kWh	35.4835 kWh	31.483 kWh	32.91 kWh
Auxiliary power discharging	4.642 kW	6.091 kW	4.751 kW	5.161 kW
Auxiliary energy discharging	26.292 kWh	34.499 kWh	26.858 kWh	29.22 kWh
RTE (with auxiliary power)	88.69%	87.799%	90.034%	88.841%
Rest time between charge/ discharge	14 minutes and 55 seconds			
Auxiliary power during rest	4.31 kW	6.5144 kW	5.312 kW	5.38 kW
RTE (with auxiliary power and rest)	88.63%	87.7%	89.955%	88.762%
Charge internal resistance at 0% SoC	0.0221 ohms	0.0414 ohms	0.04143 ohms	0.035 ohms
Discharge internal resistance at 95% SoC	0.0178 ohms	0.02864 ohms	0.0336 ohms	0.0267 ohms

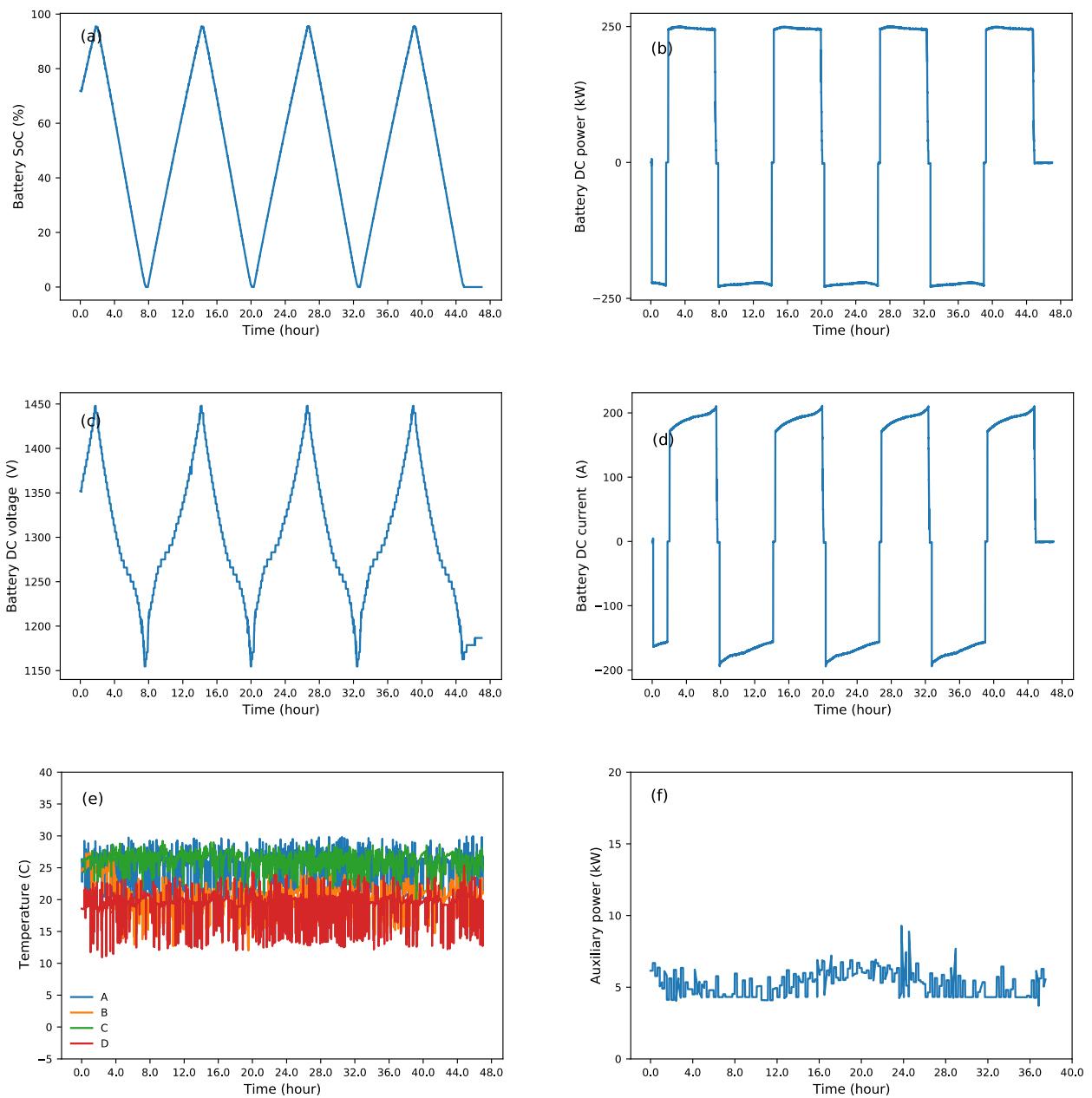


Figure 13: 250kW capacity test results: (a) Battery SoC, (b) Battery DC power, (c) Battery DC voltage, (d) Battery DC current, (e) Battery enclosure temperatures and (f) Auxiliary power.

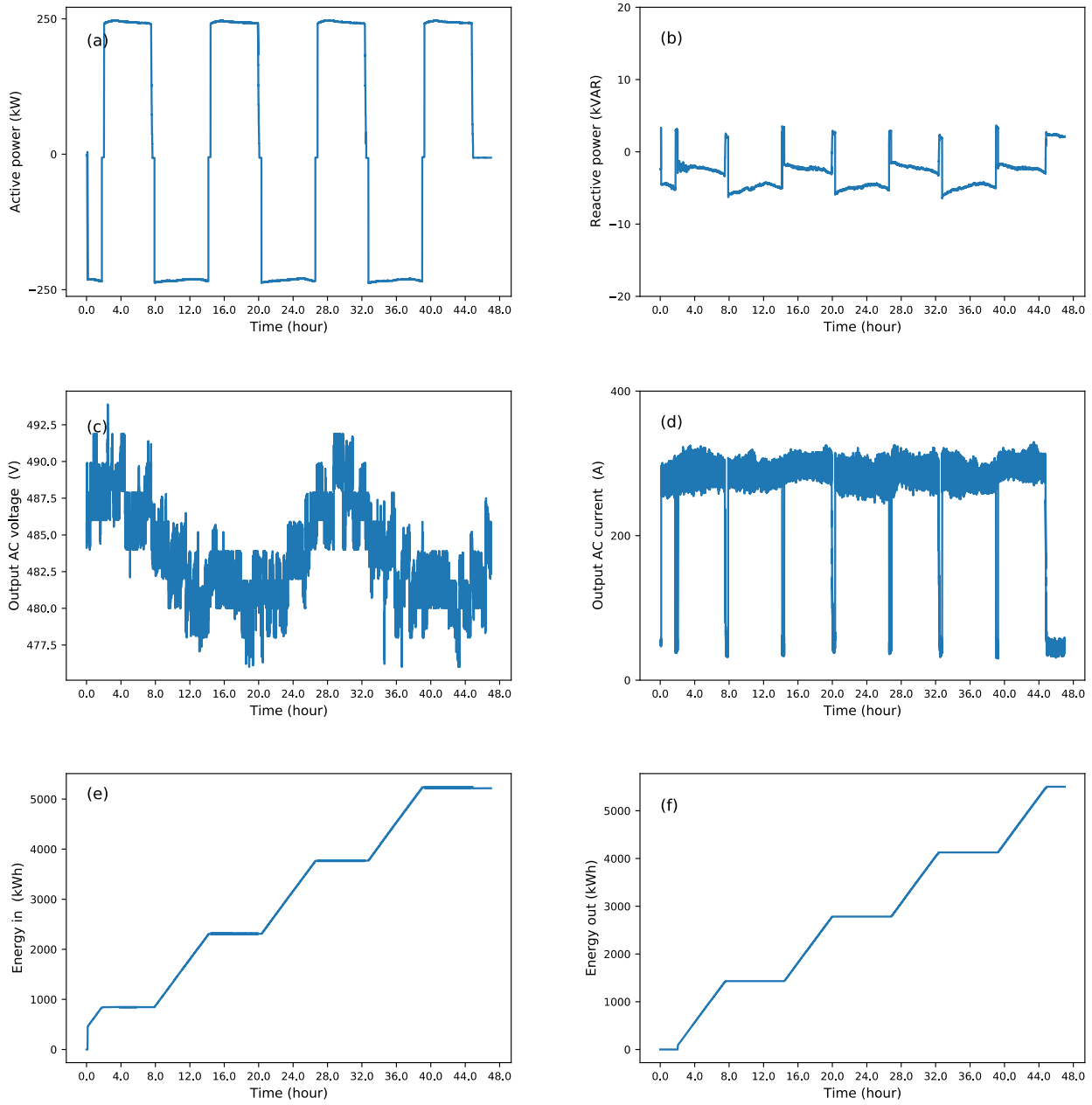


Figure 14: 250 kW capacity test results: (a) Active power, (b) reactive power, (c) AC voltage, (d) AC current, (e) total energy in and (f) total energy out.

3.4 Conclusions

The purpose of these baseline tests is to calculate BESS characteristics such as battery capacity, round-trip-efficiency (RTE), internal resistance, rated power, ramp rates and response times. These baseline parameters can be used to compare the BESS performance throughout the lifetime of the project. As advised by Washington State Department of Commerce, these baseline tests were informed by the procedure that PNNL used to analyze their CEF-1 projects.

The following quantities were measured and calculated based on the test results:

- AC-AC RTE vs. C-rate (with and without auxiliary power)
- DC BESS voltage vs. the SoC for all C-rates. It is important to note that the DC BESS voltage would depend on the charge/discharge rate because of the internal resistance of the BESS.
- Auxiliary power (for HVAC and fire safety) vs. the SoC at different C-rates.
- Ramp up/down rates and response times of the BESS at different C-rates.
- Internal resistances of the BESS.
- Energy capacity of the BESS. This will help Snohomish PUD analyze battery degradation as a function of the number of charge/discharge cycles used during lifetime of the microgrid.

4. Use-Cases of the Arlington Microgrid

The four use-cases that are considered for the Arlington Microgrid are:

UC1: Disaster recovery and grid resilience

UC2: Renewable energy integration

UC3: Grid support and ancillary services

UC4: Vehicle-to-grid integration

4.1 UC1: Disaster Recovery and Grid Resilience

4.1.1 Background

The only use-case in islanded operation is to provide power to the loads during a power outage. The authors of [8] propose a resilience-oriented service restoration method using microgrids to restore critical loads after a natural disaster and a resilience index to assess a microgrid's ability to feed critical loads during sudden power disruptions. This resilience index is defined using the following terms:

- *Feasible Islanding* is the ability of the microgrid to switch from grid-connected mode to islanded mode without curtailing its most critical loads.
- *Survivability* is defined as the ability of the microgrid to feed the maximum load of the microgrid without compromising its most critical loads during the emergency period.

Considering the scarcity of power generation resources, the concept of *continuous operating time* (COT) is introduced to determine the availability of the microgrid for critical load restoration and to assess the service time. At the time of this report, a load profile was not available for the planned Arlington Office to be located near the microgrid. Therefore, the analysis is carried out using the estimated load profile mentioned in Section 2.1, which has not been divided into critical and non-critical loads.

Since the occurrence of hurricanes, windstorms, blizzards, and floods can be predicted, the BESS could be charged to its maximum SoC so it can provide the longest possible COT for the microgrid after grid power is lost. On the other hand, since earthquakes and blackouts induced by a grid

failure cannot be predicted, a minimum level of BESS SoC should be maintained at all times to support continuous operation for some time. How to balance maintaining this minimum SoC with the desire to use the battery for other use cases is a challenging question because it involves weighing well-defined minor benefits against a major benefit that may or may not occur. Note that the emergency generator has been omitted from the analysis because we are interested in studying the resilience benefits from a PV and BESS microgrid.

4.1.2 Analysis

Prior to testing this use-case, we investigated the COT of the Arlington Microgrid at each hour over a year under the variable PV and load shown in Figure 15 (both CEC and Arlington Office loads) and Figure 18 (Arlington Office load). We assume that the BESS is either fully or half charged at the moment of islanding and that both the BESS and PV system supply power to the specified load. The total load is modeled on Snohomish PUD's Lynwood office load in 2017 and the estimated average CEC load of 35 kW. The PV generation data was measured during 2019/2020.

Our analysis shows that the COT of the combined Arlington Office and CEC load varies between 6 to 552 hours if the BESS is fully charged at the moment of islanding. This decreases to between 2 to 532 hours if the SoC of the BESS is 50% at the moment of islanding. As shown in Figure 15, Figure 16 and Figure 17, the highest COT would be achieved between June and July because the PV generation is then significantly higher than during the winter months and the load is minimum. Since the maximum discharge rate of the BESS is higher than the maximum load of the Arlington Microgrid, we can safely assume that no load would need to be curtailed in order to island the microgrid as long as there is enough energy in the BESS.

According to Snohomish PUD, CEC load could be reduced to zero during an emergency to make sure enough energy is available to supply the Arlington Office. Given this, we investigate the COT assuming only the Arlington Office load in Figure 18, Figure 19 and Figure 20. The COT varies between 8 hours to 199 days if the BESS is fully charged at the moment of islanding while it decreases to 3 hours to 198 days if the SoC of the BESS is 50% at the moment of islanding. These results are summarized in Table 8.

Table 8: Summary of COT analysis of the Arlington Microgrid under different load conditions

COT (fully charged battery)	Arlington Office + CEC	Arlington Office
Minimum	6 hours	8 hours
Maximum	552 hours	199 days
Median	23 hours	55.32 days
Mean	69.75 hours	16.6 days
COT (half charged battery)		
Minimum	2 hours	3 hours
Maximum	532 hours	198 days
Median	9 hours	10 days
Mean	44.22 hours	51 days

The Arlington Microgrid can provide power to the entire load during an emergency as long as we maintain the minimum required BESS SoC. Table 9 summarizes the historical power outages of the two feeders that feeds the Arlington Microgrid. One important finding is that the power outages of the two feeders did not occur at the same time so at least one feeder would have supplied power to the Arlington Microgrid. Unfortunately, this would not be the case during a major emergency, so we have to maintain the minimum required battery SoC to achieve the required COT.

A total of 50 power outages affected East Arlington Substation’s Feeder 12-2619 while only 8 outages affected the Portage Substation’s Feeder 12-3502. However, the longest power outage of the Portage Feeder lasted 26 hours while the longest of the East Arlington Feeder was less than 13 hours. On average East Arlington Feeder experienced 31 hours of outages in a year while the Portage Feeder experienced only 8 hours and 23 minutes of outages. If only one of the feeders was connected to the Arlington Microgrid, then the damage caused by these power outages could have been avoided using this microgrid and maintaining the BESS SoC at a suitable level.

It is important to note that the minimum BESS SoC required can be less if sunny, low demand days are anticipated. However, to calculate this we would need to forecast the PV generation and the Arlington Office load. Since the cost of implementing this feature would be much higher than

the minor financial benefits of having to maintain a lower BESS SoC, we will not consider this option further in this report.

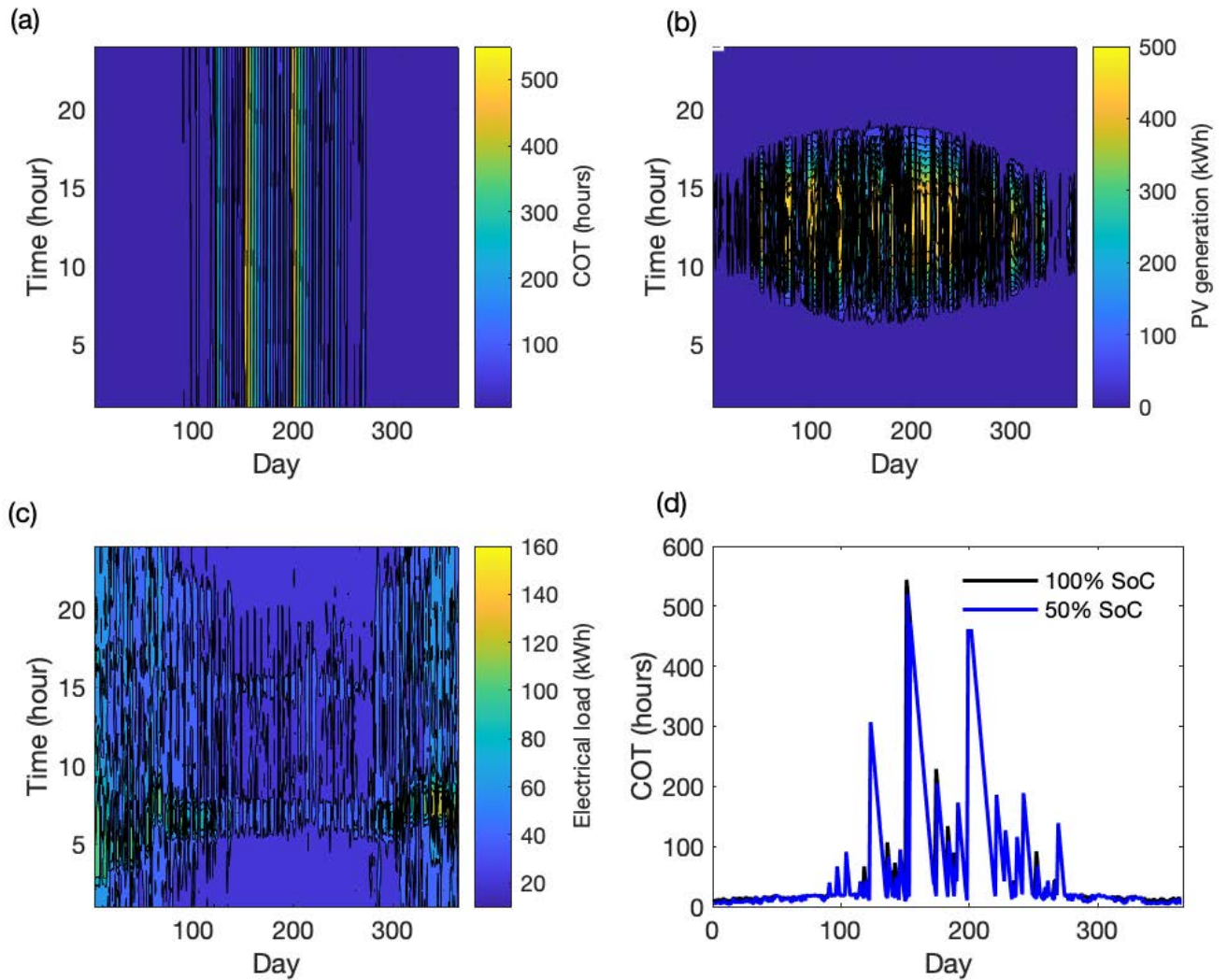


Figure 15: Continuous operating time (COT) simulation results considering both CEC and Arlington Office loads. (a) COT assuming the BESS is fully charged (b) PV generation and (c) electrical load of the microgrid at each hour (y-axis) over a year (x-axis). (d) COT assuming the initial BESS SoC at the moment of islanding at 12 pm is 100% and 50% vs. the day of the year.

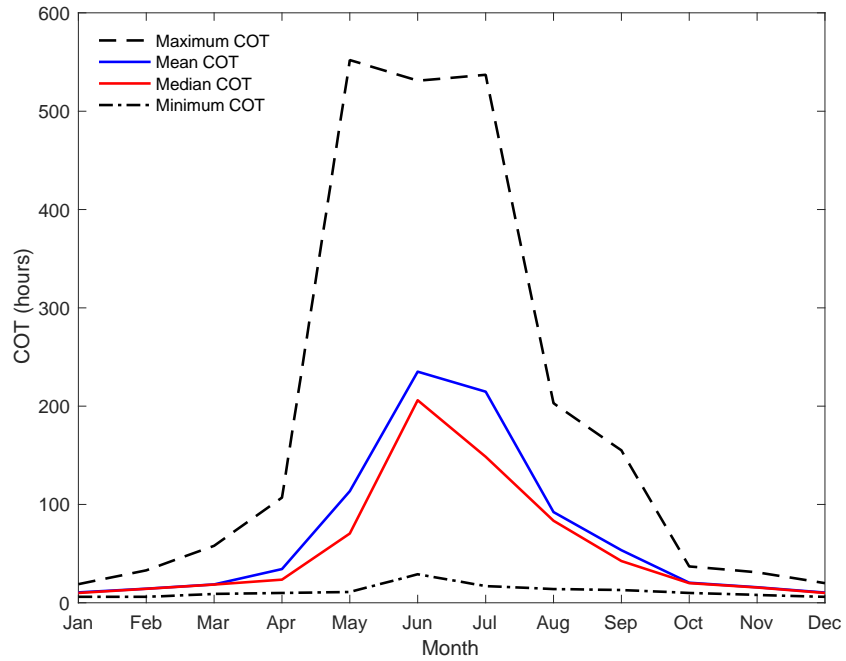


Figure 16: Monthly maximum, mean and minimum COT assuming the BESS is fully charged at the moment of islanding for both CEC and Arlington Office loads.

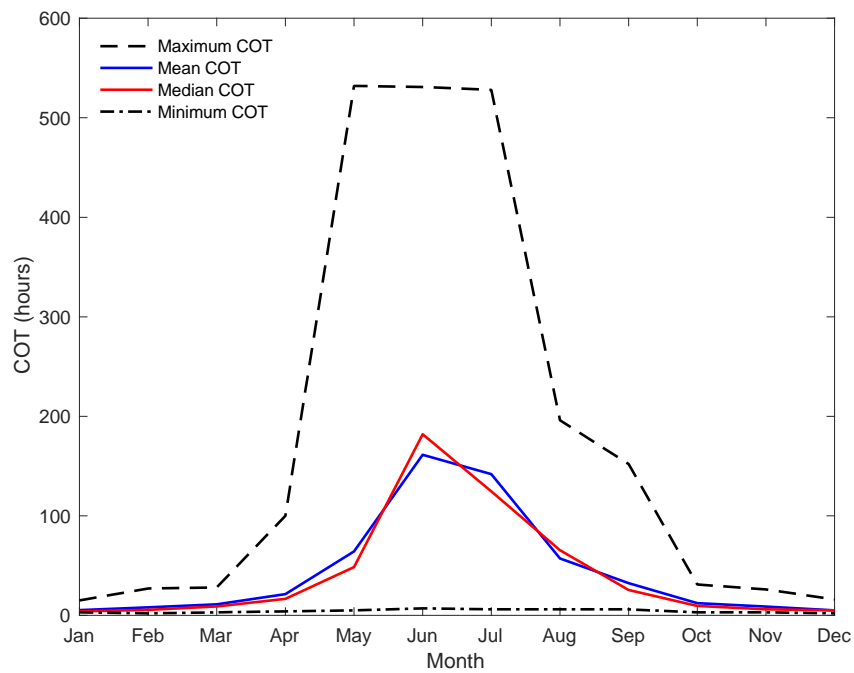


Figure 17: Monthly maximum, mean and minimum COT assuming the BESS is half charged at the moment of islanding for both CEC and Arlington Office loads.

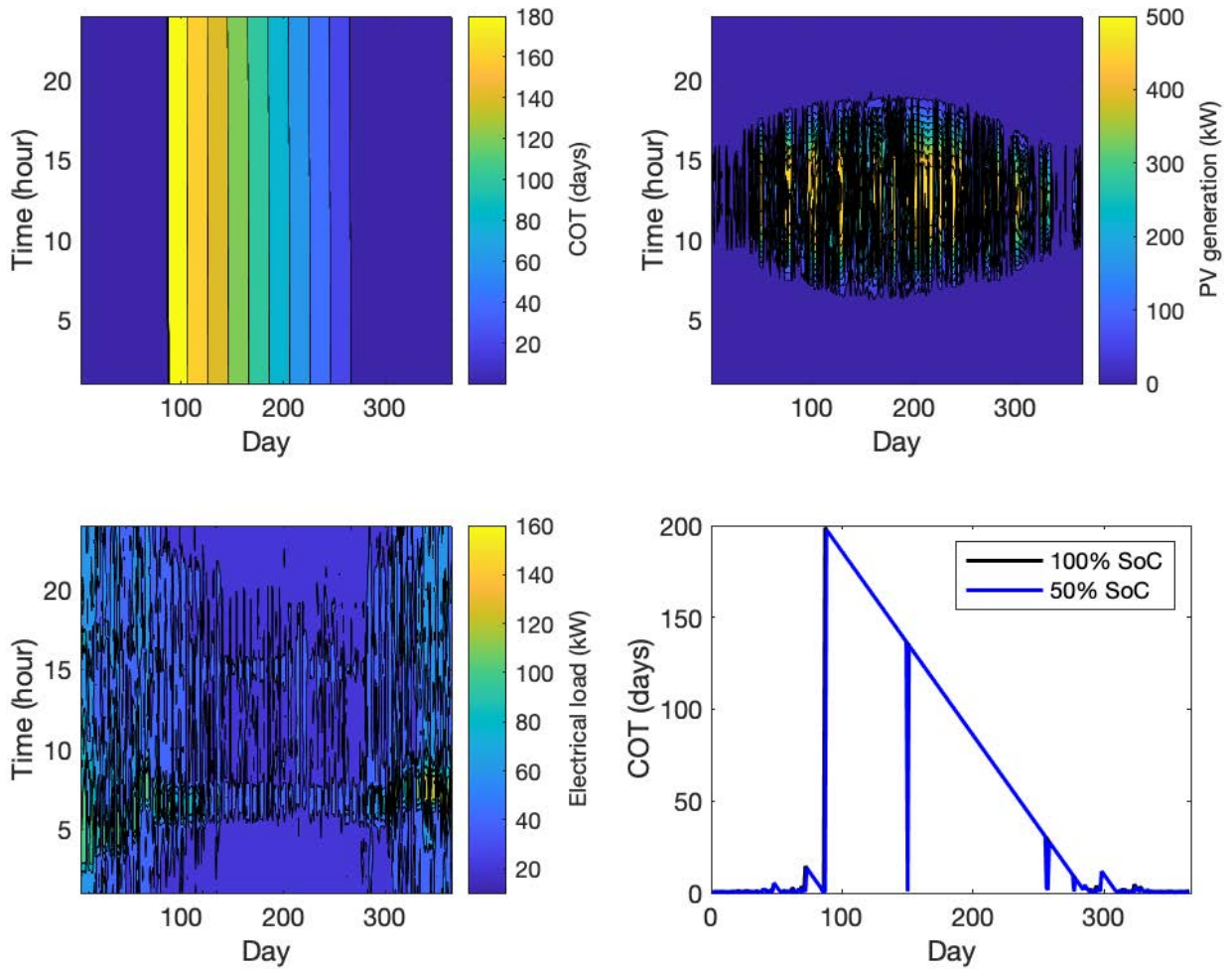


Figure 18: Continuous operating time simulation results considering Arlington Office load. (a) COT assuming the BESS is fully charged (b) PV generation and (c) electrical load of the microgrid at each hour (y-axis) over a year (x-axis). (d) COT assuming the initial BESS SoC at the moment of islanding at 12 pm is 100% and 50% vs. the day of the year.

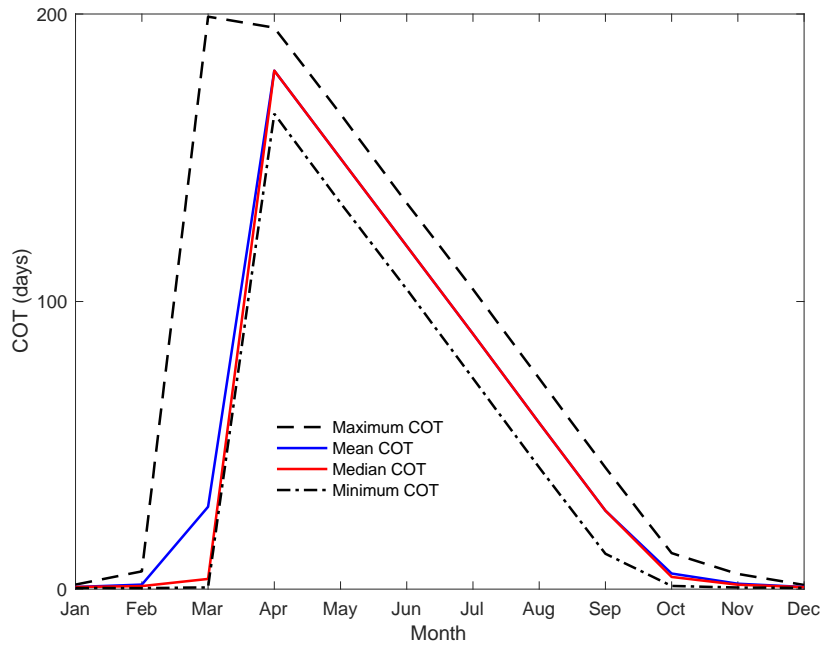


Figure 19: Monthly maximum, mean and minimum COT assuming the BESS is fully charged at the moment of islanding for Arlington Office load.

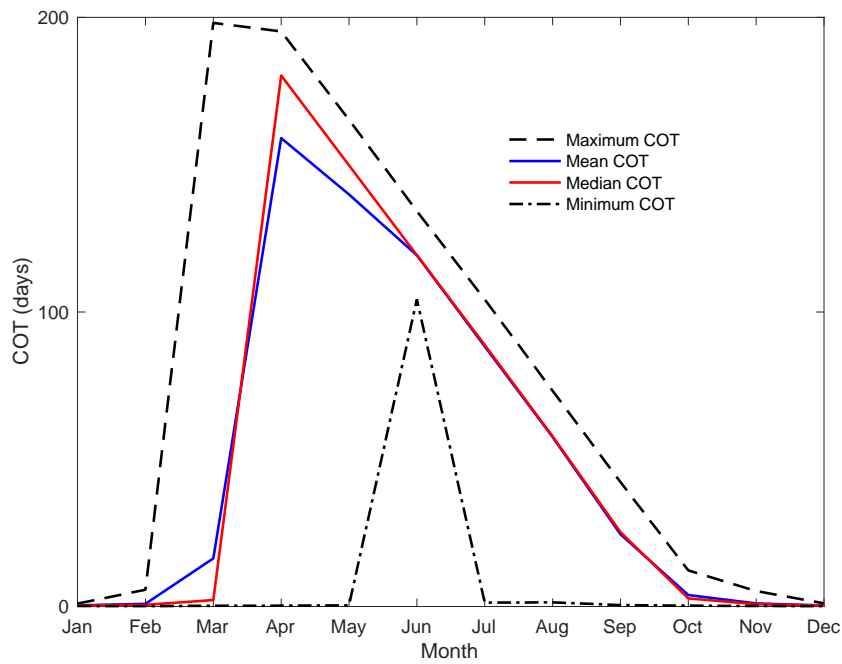


Figure 20: Monthly maximum, mean and minimum COT assuming the BESS is half charged at the moment of islanding for Arlington Office load.

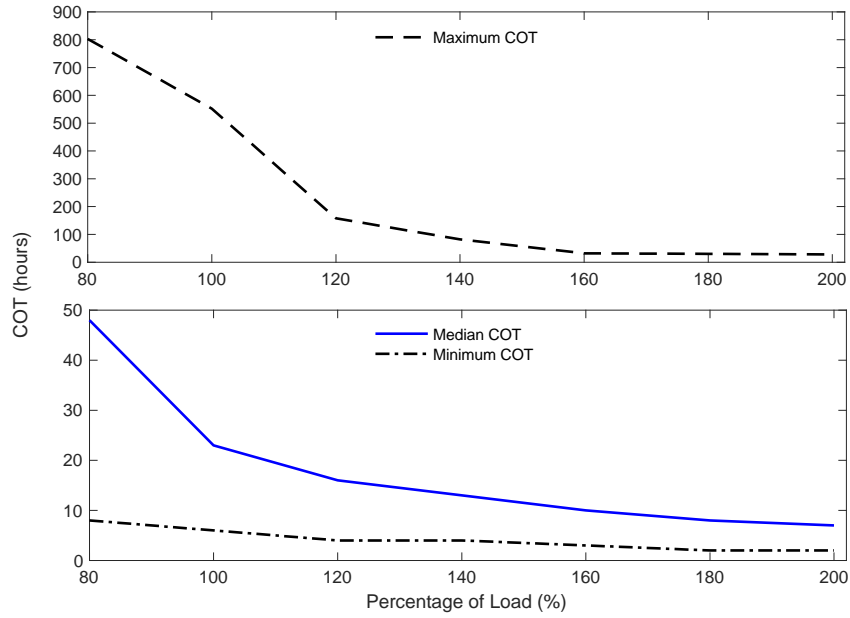


Figure 21: Effect of load curtailment on the COT when the BESS is half charged at the moment of islanding.

Figure 21 shows how the COT varies if the load is adjusted between 80% to 200% of the assumed base value. As expected, the COT increases if the load is curtailed and decreases if the load is increased. The maximum COT over a year increases at a significant rate when the load is curtailed, however, the increase in median COT is less significant.

Table 9: Historical power outages at the Arlington Microgrid site over 5 years

Years: 2012 - 2017	Portage Substation (Feeder: 12-3502)	Eagle Arlington Substation (Feeder: 12-2619)
Total outages	8	50
Total outage duration	2515.0	9308.0
Mean outage duration	314.375	186.16
Median outage duration	144.0	157.5
Maximum outage duration	1585.0	763
Minimum outage duration	43.0	2

4.1.3 Value of Resilience

A value of resilience specific to the Arlington Microgrid is difficult to obtain because we are unable to assign a cost for the lost load during an outage without carrying out a survey of the people who would benefit from the Arlington Microgrid. The currently used tools for valuing resilience are summarized in [9]. Given this, we suggest two approaches to assign an approximate value of resilience. First is the Interruption Cost Estimator calculator [10] developed by Lawrence Berkeley National Laboratory, which is built upon surveys carried out over a long period of time. The user needs to input the SAIDI, SAIFI and CAIDI values to calculate the total cost of power outages in the desired location as shown in Figure 22. If we assume that the SAIFI is 2 and SAIDI is 315 then the total yearly value of resilience according to this calculator is \$26,783.77.

The second approach is to consider that the value of the resilience provided by the microgrid is equal to the avoided cost of not having to install, maintain and fuel a conventional generator that would provide the same benefit. The Arlington Microgrid would need a 350-kW emergency generator to power the entire load during power outages that occur few times a year. However, generators can provide a higher COT, especially during the winter, if we have enough fuel reserve. Table 10 summarizes the emergency generator information.

Note that the emergency generator of the Arlington Microgrid is considered only as a backup if the PV and BESS are not able to provide continuous power to the loads. The purpose of our research is to fully study resilience benefits of PV and BESS microgrids so the future microgrids will only need a smaller emergency generator or not have one at all.

Another approach would be to use the Customer Damage Function Calculator developed by the National Renewable Energy Laboratory [9]. This approach would require details about the individual loads in the Arlington Office and CEC. Snohomish PUD could explore this approach in the future.

Table 10: Cost associated with a backup generator

Emergency generator rating	350 kW
Cost of the generator	\$150,000
Maintenance cost (labor and fuel cost for testing)	\$10,000/ year

Fuel cost (1000 gallons)	\$4/ gallon
--------------------------	-------------

This module provides estimates of cost per interruption event, per average kW, per unserved kWh and the total cost of sustained electric power interruptions.

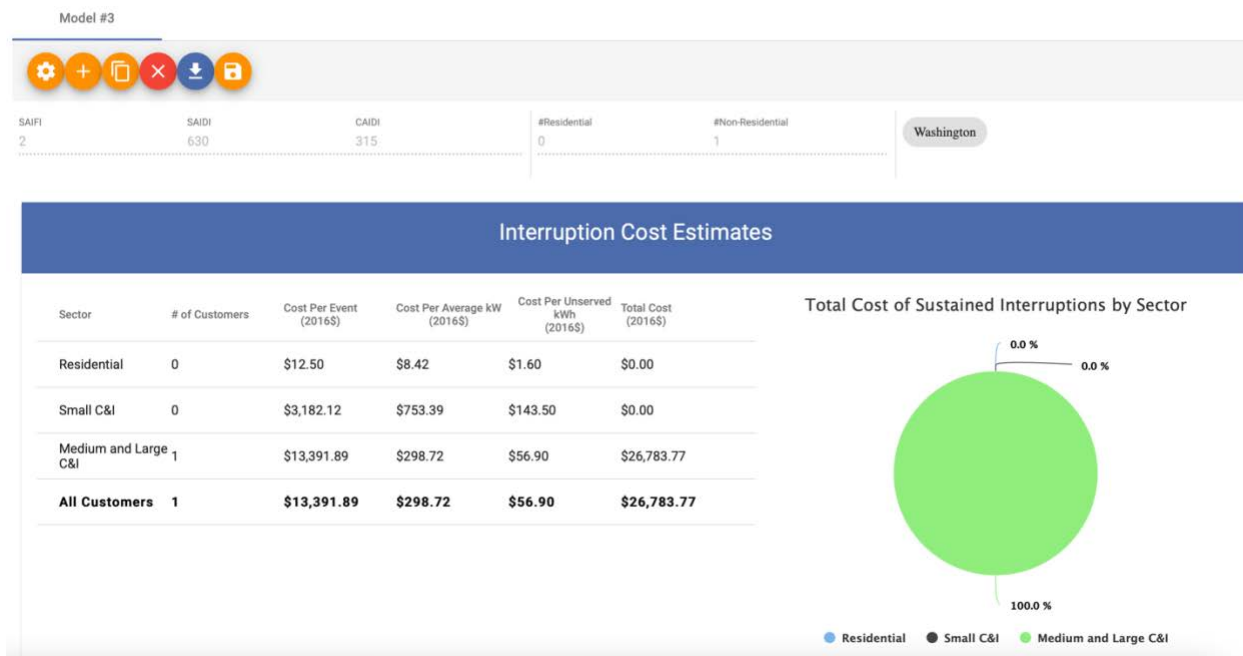


Figure 22: Interruption Cost Estimator Calculator results for a SAIFI of 2 and CAIDI of 315 in Washington State. Note that the total yearly load of a medium-large building is set to 392,720 kWh.

4.1.4 Summary

- Snohomish PUD said that they would most likely power up the Arlington Office during an emergency and shut off all other loads. The microgrid could then provide continuous power for close to 200 days during summer months if only the Arlington Office is used during an emergency.
- The continuous operating time of the microgrid is significantly higher during sunny low demand months.
- The yearly Arlington Office load represents only 59% of the total yearly PV generation.
- The continuous operating time can be significantly increased by curtailing the Arlington Office load.

- The Arlington Microgrid would have continued operating through any power outage that occurred in the past five years as long as sufficient energy had been maintained in the BESS prior to the outage.
- The emergency generator will improve the continuous operating time of the microgrid during cloudy weeks.

4.2 UC2: Renewable Energy Integration

Providing the resources needed to balance the increasing amount of naturally variable and uncertain generation from solar and wind can be very costly for the balancing authorities (BA) that are responsible for maintaining the balance between load and generation within their territory. The Bonneville Power Administration (BPA) is the balancing authority of the Snohomish PUD territory and has given Snohomish PUD a choice between paying a balancing fee and firming or smoothing up the output of its plants using its own resources.

The BESS of the Arlington Microgrid will be used to demonstrate the improved integration of a PV system with the Snohomish PUD's distribution system. This can be achieved using solar smoothing and capacity firming.

4.2.1 Solar Smoothing

Figure 23 (a) shows that the PV generation from the Arlington microgrid can be highly variable at a 1-minute time resolution. These variations can be smoothed using the BESS. In addition to the original PV generation profile for June 23, 2020, Figure 23 (b) shows what this profile would look like if it were smoothed with a ramp rate limit of 3 kW/ minute. The standard ABB E-Mesh Solar Smoothing algorithm controls the BESS to counteract fluctuations in the PV output so that the combined PV and BESS output only changes at a linear ramp-up or ramp-down rate. This open-

loop control algorithm uses a real-time calculation and does not incorporate a PV forecast. Note that the load can also be included in the calculations so the smoothing works on both PV generation and the load.

The analysis presented in this section using the 1-minute PV generation data of the Arlington Microgrid from March 27, 2020, to March 27, 2021, should only be considered as a reference because the exact operation of the solar smoothing algorithm embedded in the ABB microgrid controller is unknown to us. Table 11 summarizes the ramp rates observed in the PV generation data of the Arlington microgrid during the period from March 27, 2020, to March 27, 2021. The maximum ramp rate was 372 kW/minute while the median was 1.2 kW/minute.

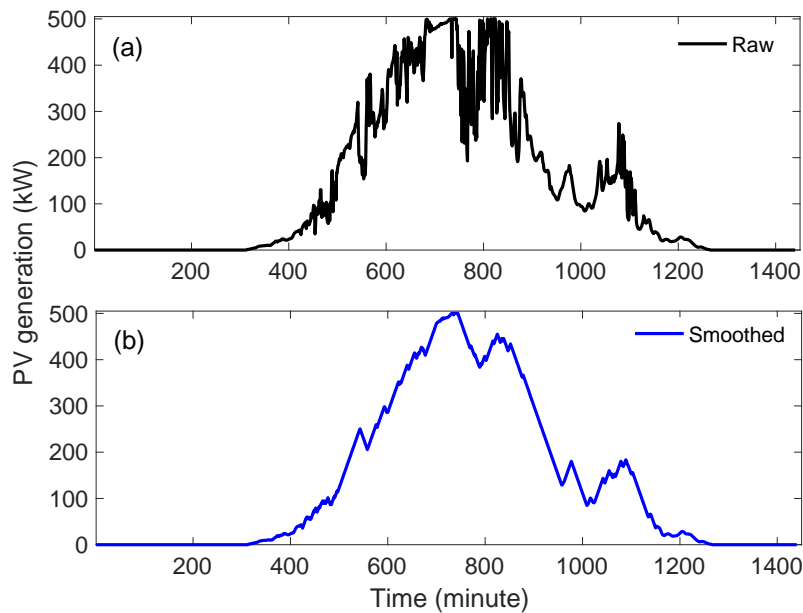


Figure 23: Raw and smoothed PV generation profile on June 23, 2020. The ramp rate limit of the smoothed profile is 3 kW/minute.

Table 11: Ramp rates of the raw PV generation data from March 27, 2020 to March 27, 2021 in kW/minute.

Percentile	Ramp rate (kW/minute)
10%	0.11
25%	0.37
50% (median)	1.24

75%	3.5
90%	13.03
100% (maximum)	372.3

Some PV inverters are also able to control the upward ramp rate to maintain a smoother PV profile. If the solar irradiance significantly increases these PV inverters operate at a lower power point i.e., not at the maximum power point, to maintain the upward ramp rate at the desired limit. The drawback of not using the BESS to control the upward ramp rate is that the amount of PV energy produced is reduced. The exact operation of the solar smoothing algorithm will be studied in Section 5. The aim of this section is to analyze the existing data and determine the optimal ramp rate limits.

Figure 24 shows the battery energy throughput cycles needed to achieve a range of ramp rate limits. The most important finding is that a ramp rate limit above 2 kW/minute will require less than 40 battery cycles per year.

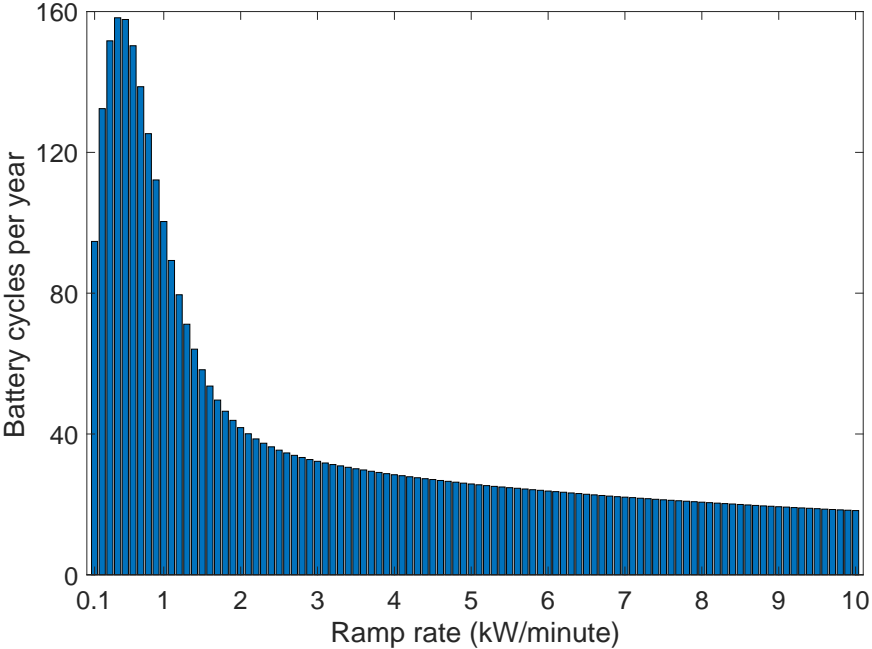


Figure 24: Number of battery energy throughput cycles as a function of the solar smoothing ramp rate

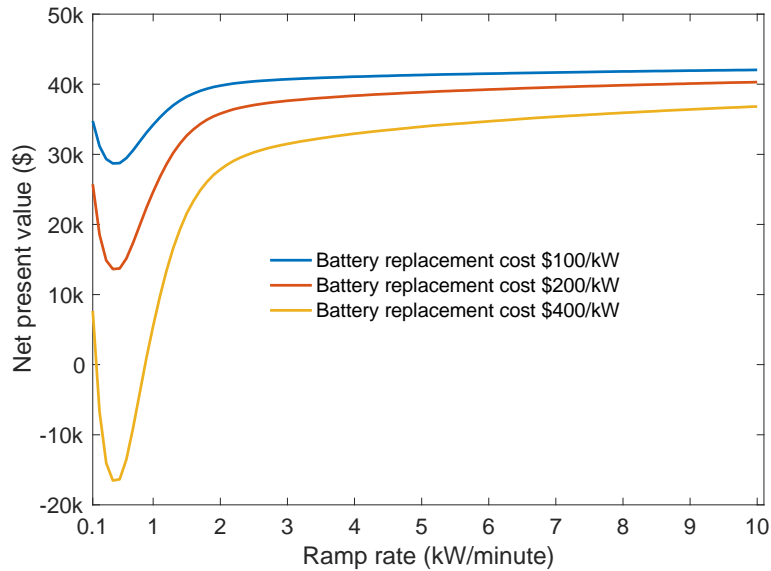


Figure 25: Net present value of solar smoothing as a function of the ramp rate limits in kW/minute, assuming replacement of the battery in ten years.

To calculate the value of solar smoothing, we need to consider both the value that it provides and its cost. The value of solar smoothing is assumed to be \$5400 per year, which is the amount that Snohomish PUD would not have to pay to BPA if it implemented solar smoothing. The cost of solar smoothing is the cost of the battery degradation caused by the additional charge/discharge cycles required. It is assumed to be 0.00687945% per cycle based on Figure 4.

Because the battery replacement cost is difficult to predict in 10 years, Figure 25 shows the NPV of solar smoothing for a range of battery replacement costs in ten years and the yearly battery energy throughput cycles from Figure 24. The interest rate is assumed to be 5%.

The NPV from solar smoothing is likely to be above \$40,000 if BPA and Snohomish PUD can negotiate a ramp rate above 2 kW/min and the battery replacement cost in ten years is below \$100/kW. If the battery replacement cost in ten years is \$200/ kW, then the ramp rate limit has to be above 4 kW/minute to achieve a similar NPV.

Conclusions and Recommendations

- The raw PV data analyzed in this section exhibits significant up and down ramp rates that could be reduced using solar smoothing.

- These ramp rates could be smoothed using the BESS. We calculated how much energy throughput and how many battery cycles would be required to implement this smoothing for a range of ramp rate limits.
- Snohomish PUD and BPA could use this report to negotiate suitable ramp rate limits for the Arlington Microgrid.
- A maximum ramp rate larger than 2 or 4 kW/minute is recommended because it would reduce the number of battery energy throughput cycles to less than 40 cycles per year.

4.2.2 Capacity Firming

Capacity firming keeps the PV generation at a one-hour-ahead target determined based on the PV forecast, the maximum allowed ramp rate of the PV profile and the BESS state-of-charge (SoC) that should be achieved at the next time-step. The BESS is charged when the PV generation is above the target value and discharged when the PV generation is below this value. In most cases the BESS has enough power and energy capacity to achieve this goal. However, the more inaccurate the forecast is, the more the battery has to compensate with deeper cycles. Since deeper cycles cause more battery degradation, it may be more economical in the long run to pay a fee for capacity firming to BPA rather than firming the capacity using the battery. Since more accurate forecasts extend the life of the battery, a careful analysis of the benefits of improved accuracy is required.

Our article attached in Appendix F compares state-of-the-art PV forecasting techniques, such as long short-term memory recurrent neural networks (LSTM-RNN), encoder-decoder LSTM-RNN, multi-layer perceptrons (MLP), and the persistence method suggested by BPA.

Because of its simplicity, BPA has suggested to Snohomish PUD to use the persistence forecasting technique for one-hour-ahead PV forecasting. For example, under 30/30 persistence forecasting, the net generation for the 2:00 PM to 2:30 PM interval is calculated by taking the average of the generation output from 1:00 PM to 1:30 PM. Similarly, the schedule for the 3:00 PM to 3:30 PM interval is calculated by taking the average of the generation output from 2:00 PM to 2:30 PM.

Figure 26 show the actual and forecast PV generation and the battery SoC for typical cloudy day, while Figure 27 and Figure 28 show the same for less sunny and sunny days, respectively. Table

12 compares the root-mean-square error (RMSE), mean-absolute error (MAE) and mean-bias error (MBE), and the resulting battery cycles of the LSTM-RNN, encoder-decoder LSTM-RNN, MLPs and the 30/30 persistence forecasting techniques. In all cases, machine learning forecasts are significantly better than the 30/30 persistence forecasts. The RMSE and MAE over a year from the encoder-decoder are respectively 35.7% and 42.6% better than the persistence method. The accuracy of the PV forecast varies with the type of day and machine learning technique (See the paper for details).

The number of yearly energy throughput cycles can be reduced by 29.1% (66 cycles per year) using the encoder- decoder LSTM-RNN forecasts. Battery cycles involving more than a 10% depth of discharge (DoD) can be reduced by 51%. Such deep cycles have a disproportionate effect on lithium-ion battery degradation. Unfortunately, due to the limited amount of data available about battery degradation, it has not been possible to quantify this effect more accurately. The benefit of using machine learning based forecasts is much higher during sunny days because incorrect forecasts result in higher battery energy throughput, as shown in Figure 28.

Figure 29 compares how using the best machine learning forecast and persistence forecast affects the NPV (net present value) of capacity firming. Since it is difficult to know what the battery replacement cost will be in ten years, these values have been calculated for a range of replacement costs. This figure shows that encoder-decoder LSTM-RNN based PV forecasting makes capacity firming more profitable than persistence forecasting. If the battery replacement cost is high, capacity firming is not profitable if persistence forecasting is used. In these NPV calculations, the revenue from capacity firming is assumed to be \$5400 per year (i.e., the amount that Snohomish PUD would not have to pay to BPA), the interest rate is assumed to be 5%, the battery degradation is assumed to be 0.00687945% per cycle based on Figure 4, and the yearly battery cycles are from Table 12.

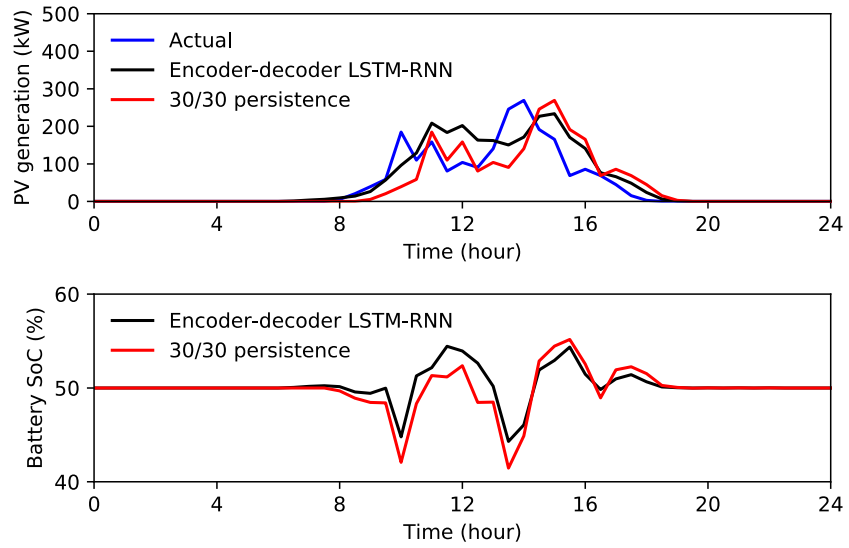


Figure 26: PV generation and battery SoC on a cloudy day using encoder-decoder LSTM-RNN and persistence method.

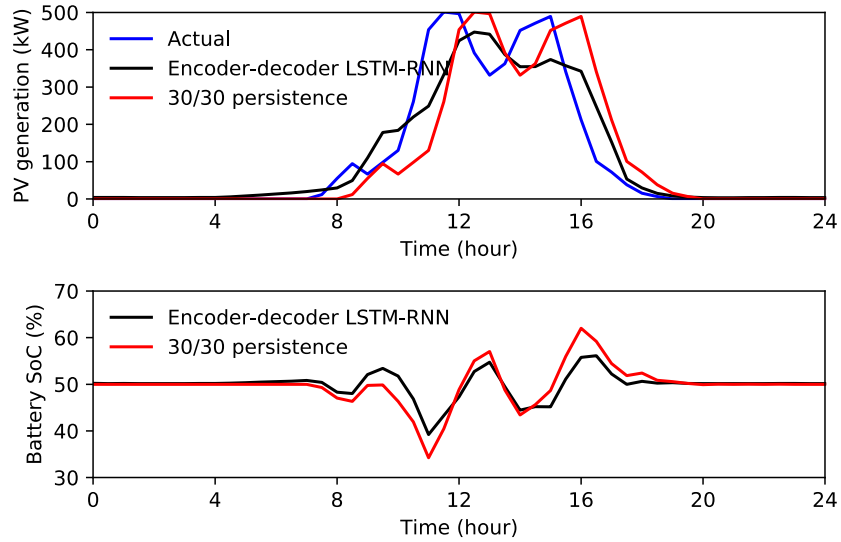


Figure 27: PV generation and battery SoC on a less sunny day using encoder-decoder LSTM-RNN and persistence method.

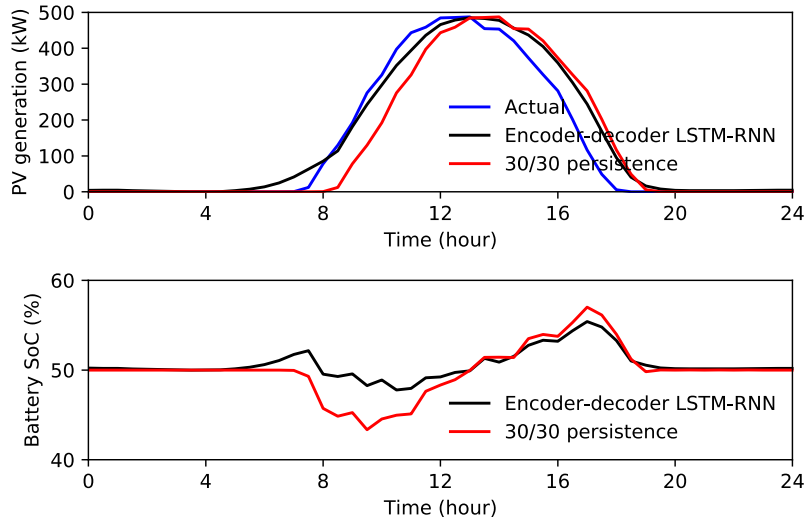


Figure 28: PV generation and battery SoC on a sunny day using encoder-decoder LSTM-RNN and persistence method.

Table 12: Simulation results based on NREL data over a year using five years training data. The improvements from the persistence method are given as percentages in parenthesis.

	RMSE (kW)	MAE (kW)	MBE (kW)	Battery cycles (energy throughput)	Battery cycles above 10% DoD	Training time (minutes)
30/30 Persistence	51.12	27.86	0	227	286	-
LSTM-RNN (no day-types)	35.88 (29.8%)	14.41 (48.3%)	0.55	180 (20.7%)	175 (38.8%)	14.7 e=20 b=32 h=100
LSTM-RNN (with day-types)	32.73 (36%)	13.64 (51.0%)	1.24	168 (26%)	153 (46.5%)	14.2 e=20 b=32 h=100
MLP (no day-types)	35.95 (29.7%)	18.18 (34.8%)	-2.1	177 (22%)	163 (43%)	1.3 e=20 b=16 h=200
MLP (with day-types)	34.53 (32.5%)	17.85 (35.9%)	1.9	163 (28.2%)	142 (50.4%)	1.4 e=20 b=16 h=200
Encoder-decoder LSTM-RNN (no day-types)	35.59 (30.4%)	15.79 (43.3%)	1.8	173 (23.8%)	157 (45.1%)	21.7 e=20 b=16 h=50, 25
Encoder-decoder LSTM-RNN (with day-types)	32.87 (35.7%)	15.98 (42.6%)	-1.85	161 (29.1%)	140 (51%)	21.4 e=20 b=16 h=50, 25

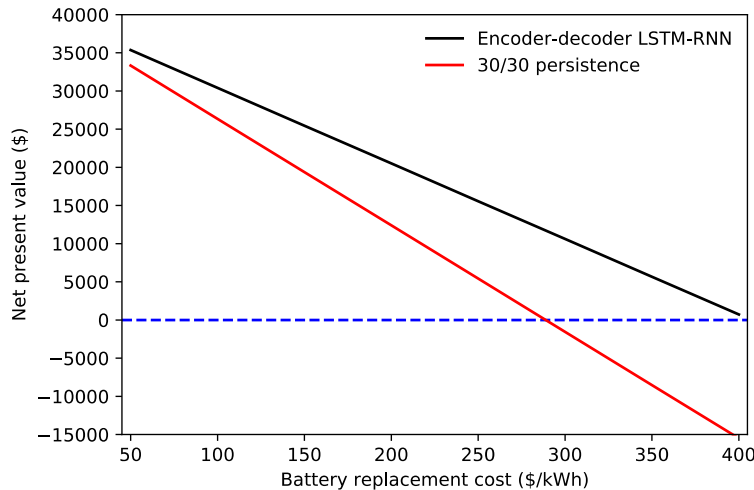


Figure 29: Net present value of capacity firming using encoder-decoder LSTM-RNN and 30/30 persistence after 10 years as a function of the battery replacement cost in 10 years. The revenue is fixed at \$5400 per year, the discount rate is assumed to be 5% and the battery degradation per cycle is based on Figure 4.

Conclusions and Recommendations

- Our analysis shows that it is beneficial to do capacity firming if the PV forecasts are based on a state-of-the-art machine learning technique and the capacity firming is already implemented in the BESS or the cost of implementing capacity firming in the BESS is low.
- The NPV for Snohomish PUD is higher for solar smoothing than for capacity firming. However, the benefits of capacity firming for BPA will significantly increase with the size of the PV system so it would be beneficial for BPA to study capacity firming with this 500 kWac PV system.

4.3 UC3: Grid Support and Ancillary Services

The Arlington Microgrid is integrated with Snohomish PUD’s other storage system, MESA 1, via the *distributed energy resource optimizer* (DERO) developed by Doosan GridTech. DERO enables the microgrid battery storage system to provide grid support while in grid-connected mode. The additional storage capacity of the BESS of the microgrid thus enhances the capacity of DERO to provide grid support and ancillary services. These services include peak shifting, energy arbitrage, energy imbalance mitigation.

Energy imbalance mitigation involves real-time automatic within-hour battery charge and discharge adjustments used to mitigate forecast errors in demand and generation. DERO looks ahead 5 - 120 minutes and calculates battery charge and discharge schedules every 5 - 10 minutes.

Energy arbitrage develops day-ahead schedules of the battery storage system based on load, price and weather forecasts over the next 1-7 days.

For a detailed analysis of the benefits that the microgrid can provide in terms of grid support and ancillary, please refer to the report produced by Pacific Northwest National Laboratory as part of the Washington State Clean Energy Fund I [10].

The ability of battery energy storage systems to provide services is limited in the Pacific Northwest due to the absence of an organized market for such services like those that exist in centralized electricity markets such as PJM (Pennsylvania, New Jersey, and Maryland), CAISO (California Independent System Operator), ISO-NE (ISO New England) and others. The Energy Imbalance Market (EIM) that links local utilities to the California market and other utilities is not yet setup to accommodate ancillary services.

4.4 UC4: Vehicle-Grid Integration

4.4.1 Background

The number of electric vehicles (EV) is growing rapidly in the USA and around the world due to growing concerns about climate change and decreasing battery technology costs. In 2019, over 2 million EVs were sold around the world and this number is expected to rise in the future. Another possible benefit of EVs is the ability to send power back to the electrical grid using a bi-directional inverter when the EV is parked. We refer to this as vehicle-grid integration (VGI) or vehicle-to-grid (V2G).

A V2G system enables the EV battery to be used as a conventional BESS. This means the EV battery power can be used to supply local loads as a distributed storage, to integrate intermittent renewable energy sources and to provide ancillary services to the distribution system. In return the owner of the EV should be compensated for the services provided. If putting power back into the grid is not possible or needed, the EV charge rate can also be throttled to provide demand response services. The global V2G market is expected to grow by approximately \$5.01 billion in the next

four years. Researchers at EPRI (Electric Power Research Institute) made the following forecast about California's V2G market:

- V2G technology can provide 2–3 times the value of managed charging.
- V2G technology can provide \$671 million in annual grid benefits, based on 3.3 million EVs in 2030 (medium EV forecast) with half of those EVs V2G-enabled.
- V2G technology can provide \$1 billion in annual grid benefits, given 5 million EVs in 2030 (aggressive EV forecast and a California goal) with half of those V2G-enabled.
- If half of California's 600,000 EVs today were V2G-enabled, they could provide \$39 million in annual net value from peak shaving and ramping support.

Unfortunately, similar research has not been carried out for Washington State but learning about V2G systems will be beneficial for Washington State utilities.

The V2G systems of the Arlington Microgrid can be used for renewable integration and ancillary services. However, they are not expected to be in use day-to-day because the degradation cost of the EV battery is unknown. Therefore, we mainly expect to use the EV battery systems to support the microgrid during islanded mode. Note that additional back-up battery systems add investment costs and a V2G system can provide the required services at a significantly lower cost.

The V2G system installed at the Arlington microgrid should be viewed as a limited proof of concept. The economics of expanding such systems need further analysis and the PNNL report on V2G economics included in appendix is a first step in that direction. As discussed in the second PNNL report, standardization of V2G systems should help bring their cost down and improve the economics. Other projects under consideration by the Washington State Clean Energy Fund and involving utilities and transit agencies should help clarify the benefits of this technology.

4.4.2 Analytics

The Arlington Microgrid will only host EVs owned by Snohomish PUD. The possibility of using privately owned EVs for the above services is still up to debate because of the battery degradation risks. In order to overcome the battery degradation problem and EV owners next trip preference, the EV battery should only be discharged up to a certain level. For example, some researchers decided to use 80% of the EV battery as the discharge limit in their scheduling problem. In some

situations, this limit could be lower assuming the EV battery can be charged back to the required level before the driver leaves for the next trip.

Another limiting factor is that the availability of power from the V2G system is intermittent because of the random plug-in patterns of the EV. The plug-in patterns of the Snohomish PUD fleet vehicles could be estimated in the future to design more efficient control algorithms.

The energy consumption of the EVs is also uncertain and is difficult to estimate. According to existing literature, an average driver drives 29 miles per day in the USA. However, we expect this value to be different for Snohomish PUD's vehicles.

The maximum V2G power is determined by the ratings of the power electronic converters used for charging and discharging the EV batteries. Since the rating of the power electronic converters is significantly lower than the EV battery rating, the EV battery ratings can be ignored. For example, Mitsubishi MiEV's battery is rated at 80 kW compared to its converter rating of 2.5 kW.

EV availability and its battery consumption is also difficult to estimate during normal operation and much harder during an emergency. However, in both modes of operations, we can safely assume that the EV battery is available between 6 pm and 7 am for charging and grid support. The mileage of the Snohomish PUD vehicles can be recorded. Given the mileage, we can estimate the EV battery SoC available by 6 pm.

5. Microgrid Testing

5.1 UC1: Disaster Recovery and Grid Resilience

Section 4.1 estimates the grid resilience benefits of the microgrid over the course of a year. This section presents test results showing that the microgrid can actually operate in islanded mode. Table 13 summarizes the three islanding tests that were performed. During the first test, the PV system was generating power and the BESS charged during the period of islanded operation. During the second test, the diesel generator was turned on after the microgrid was islanded. For the third test the PV inverters were turned off before the microgrid was islanded via the HMI, and the BESS was discharged to power the loads.

Table 13: Summary of the three islanded operation test

	PV system	BESS	Diesel generator
First test	On	Charged	Not used
Second test	On	Charged	Turned on after the microgrid is islanded
Third test	Off	Discharged	Not used

5.1.1 First Test

This first test was carried out on July 14, 2021. Islanding occurred at 13:45:04 and lasted 56 minutes and 23 seconds. Figure 30 illustrates the operation over the entire day, while Figure 31 focuses on the period of islanded operation. As these figures show, the microgrid islanding was seamless and the extra solar generation was fed into the BESS. The diesel generator was not used. The microgrid was then successfully resynchronized with the grid.

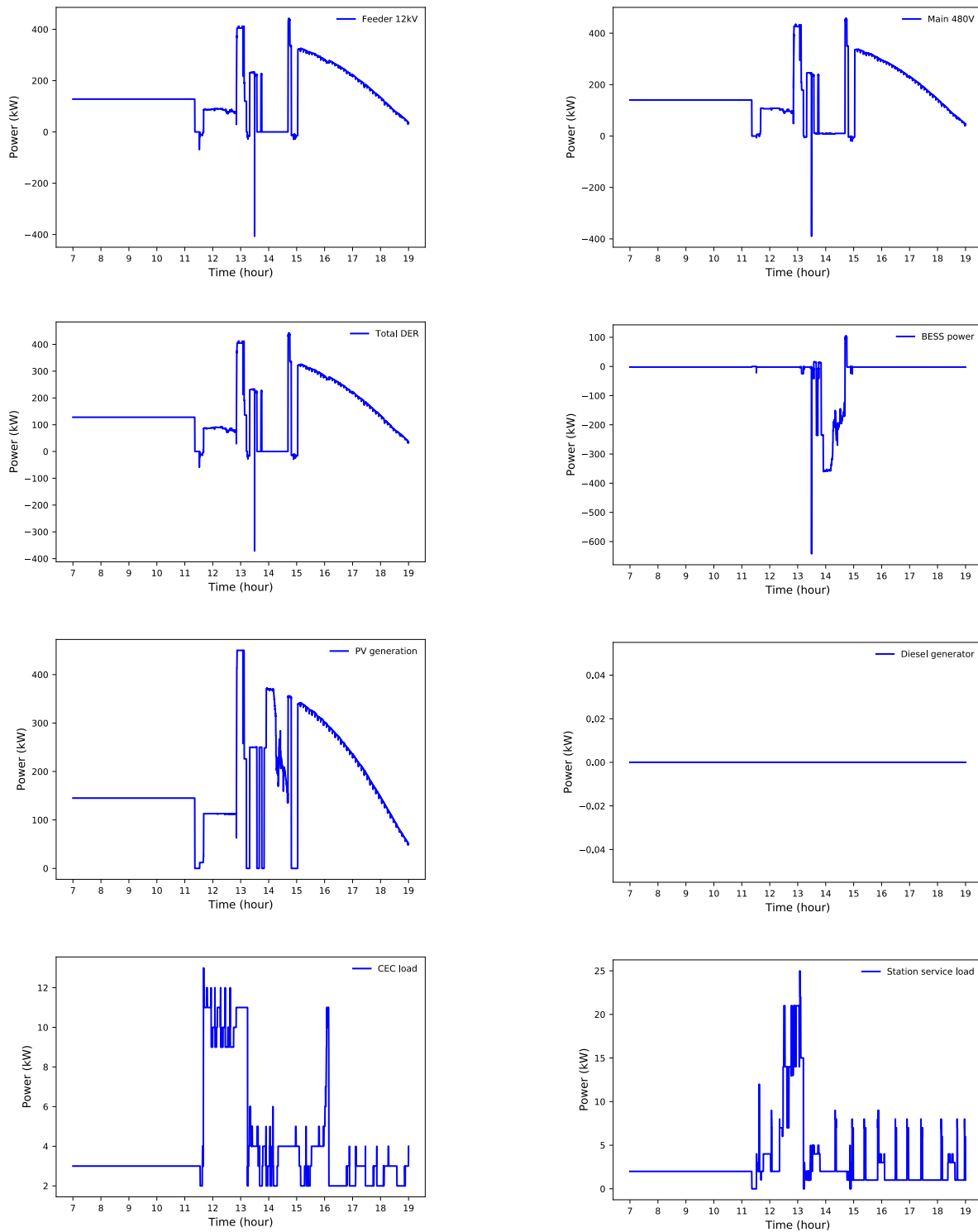


Figure 30: First islanding test on July 14, 2021. Islanding occurs at 13:45:04.

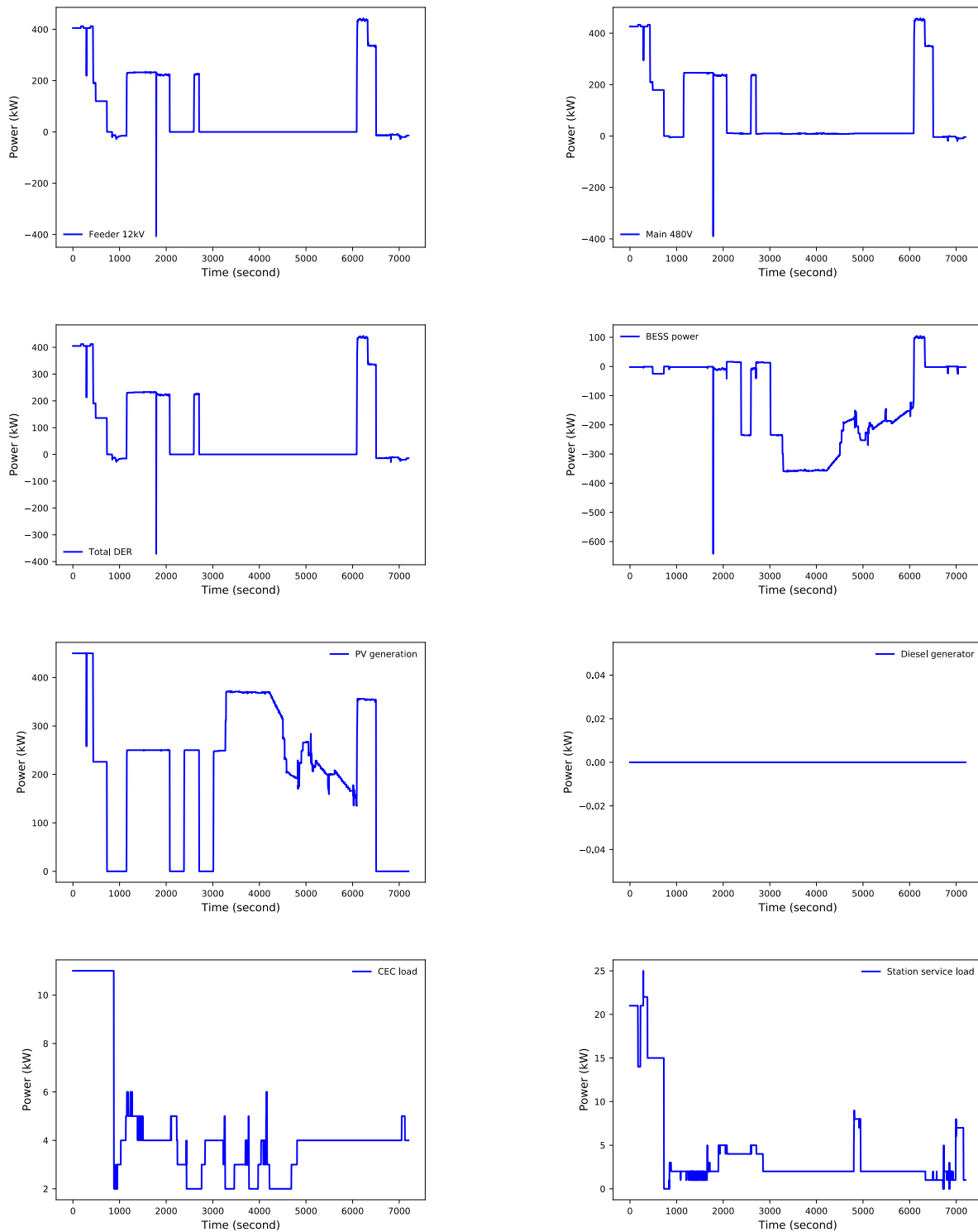


Figure 31: Microgrid operation during the islanded period (from 2704 second to 6087 second) of the first islanding test on July 14, 2021

5.1.2 Second Test

This second test was carried out on July 26, 2021. Islanding was triggered at 14:41:44 and lasted 34 minutes and 7 seconds. Figure 32 illustrates the operation over the entire day, while Figure 33 focuses on the period of islanded operation. As these figures show, the microgrid was islanded seamlessly and the extra solar generation was fed into the BESS. After a while the diesel generator was turned on to charge the battery and solar generation was temporarily curtailed. The microgrid was then successfully resynchronized with the grid.

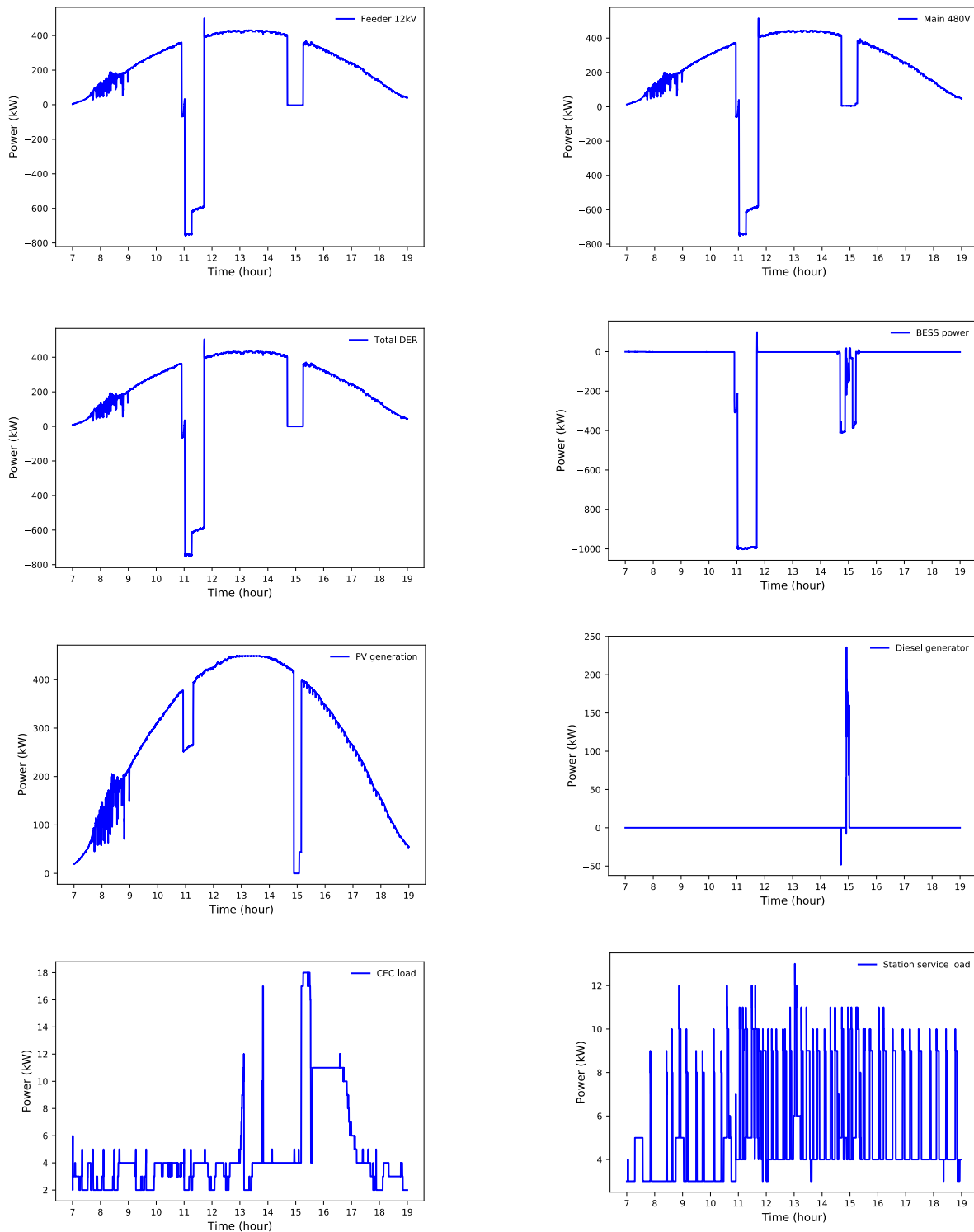


Figure 32: Second islanding test on July 26, 2021. Islanding occurs at 14:41:44.

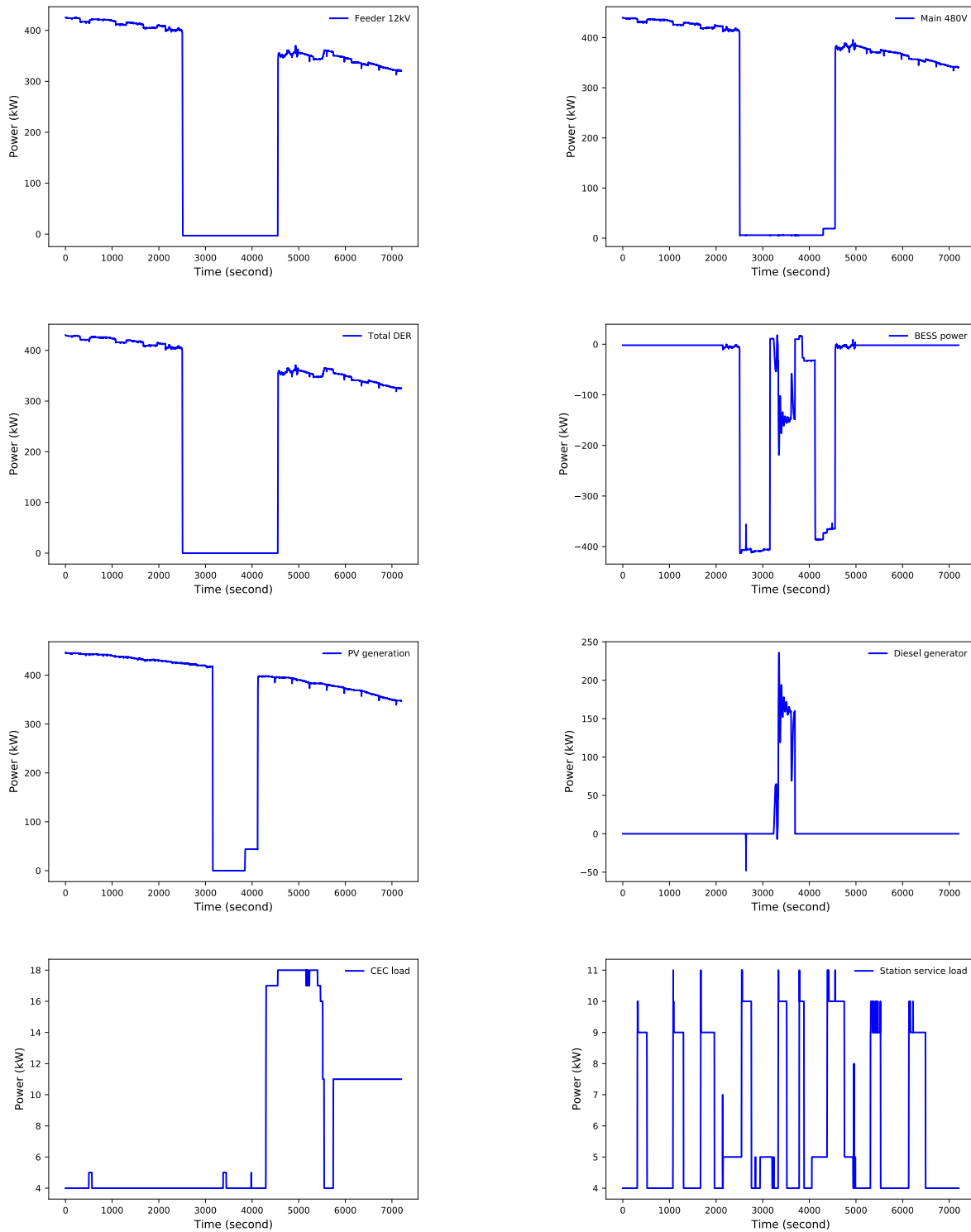


Figure 33: Microgrid operation during the islanded period of the second islanding test on July 26, 2021. Islanding was triggered at 14:41:44 and lasted 34 minutes and 7 seconds.

5.1.3 Third Test

This third test was carried out on September 3, 2021. Islanding was triggered at 14:00:15 and lasted 5 minutes and 17 seconds. Figure 34 illustrates the operation over the entire day, while Figure 35 focuses on the period of islanded operation. As these figures show, the microgrid was islanded seamlessly and the BESS provided power to the loads. The PV inverters and the diesel generator were turned off. The microgrid was then successfully resynchronized with the grid.

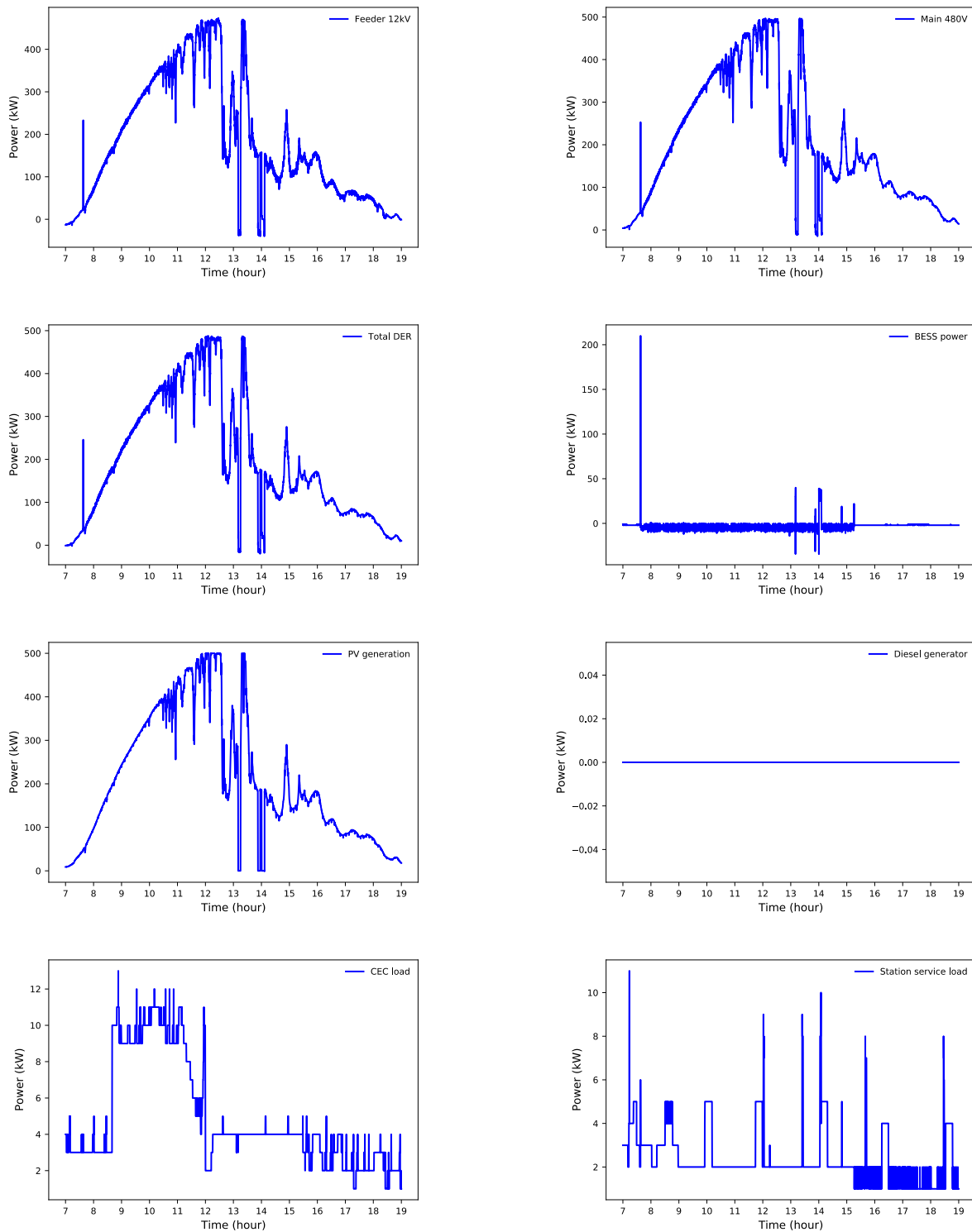


Figure 34: Third islanding test on September 3, 2021. Islanding was triggered at 14:00:15

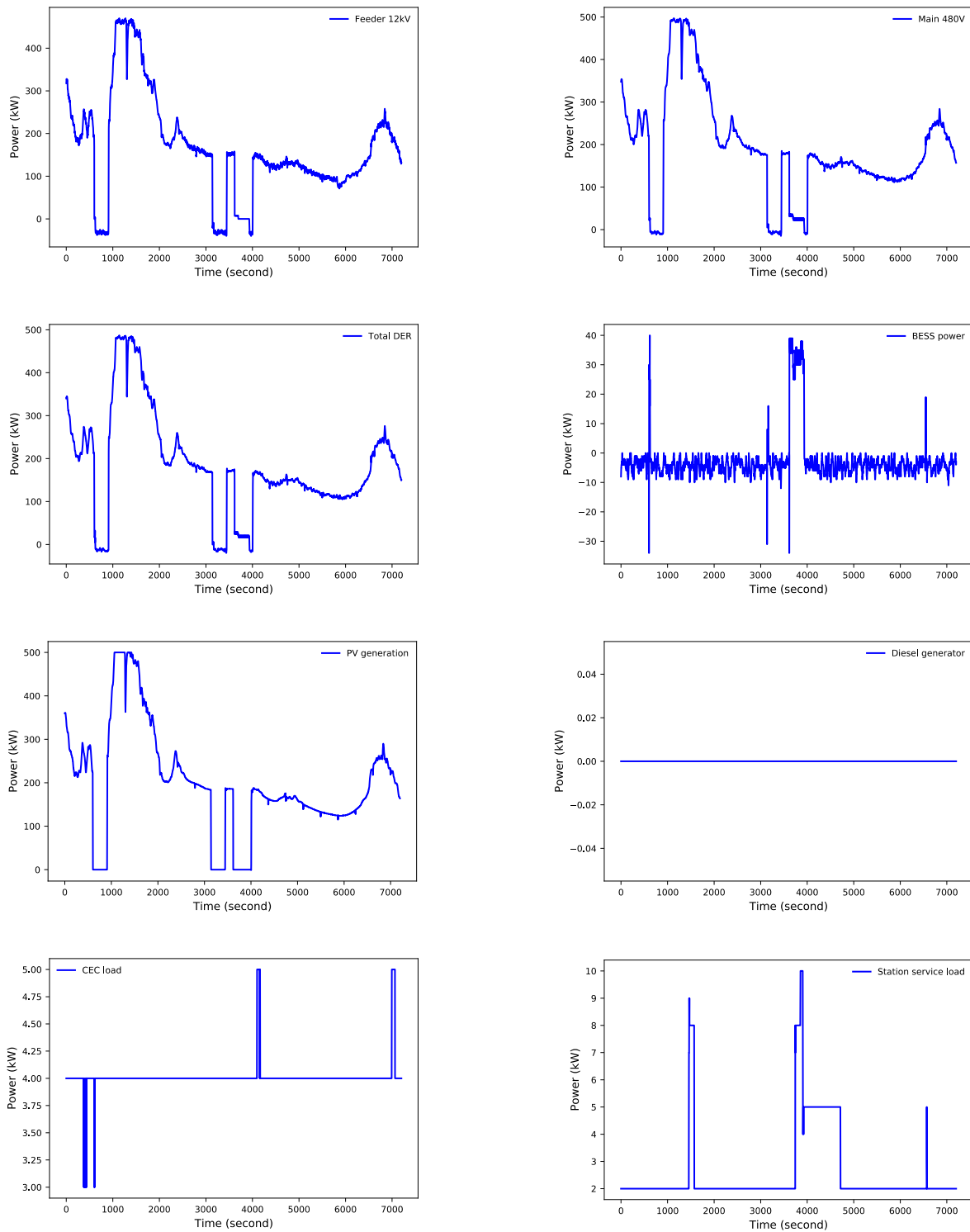


Figure 35: Microgrid operation during the islanded period of the third islanding test on September 3, 2021. Microgrid lasted from second 3615 to second 3932.

5.2 UC2: Renewable Energy Integration

As discussed in Section 4.2, the microgrid can support renewable energy integration by smoothing out the solar generation. This use case was tested over four days. The following data is provided for each day of testing:

- Weather data
- A graph showing the PV generation, the output of the BESS and the net output of the PV + BESS combination for the whole day.
- A graph showing the PV generation, the output of the BESS and the net output of the PV + BESS combination for the period during which abrupt changes happened in the PV generation. During the first day of testing, these abrupt changes were simulated by turning the PV inverters off and on.
- A table summarizing the ramp rates of the PV generation and of the PV + BESS combination over the whole day and during periods of abrupt changes in PV generation. The controller ramp rate used for testing was 4 kW/second.

5.2.1 First Day of Testing Solar Smoothing: Thursday September 2, 2021

Table 14: Weather data for the solar smoothing test on Thursday September 2, 2021

Minimum Temperature	39.0 °F
Mean Temperature	58.8 °F
Maximum Temperature	75.9 °F
Mean sea level pressure	30.07 in
Mean dew point	48.0 °F
Total precipitation	0 in
Visibility	9.5 miles
Snow depth	none
Mean wind speed	4.6 mph
Maximum sustained wind speed	12.77 mph
Maximum wind gust	No data

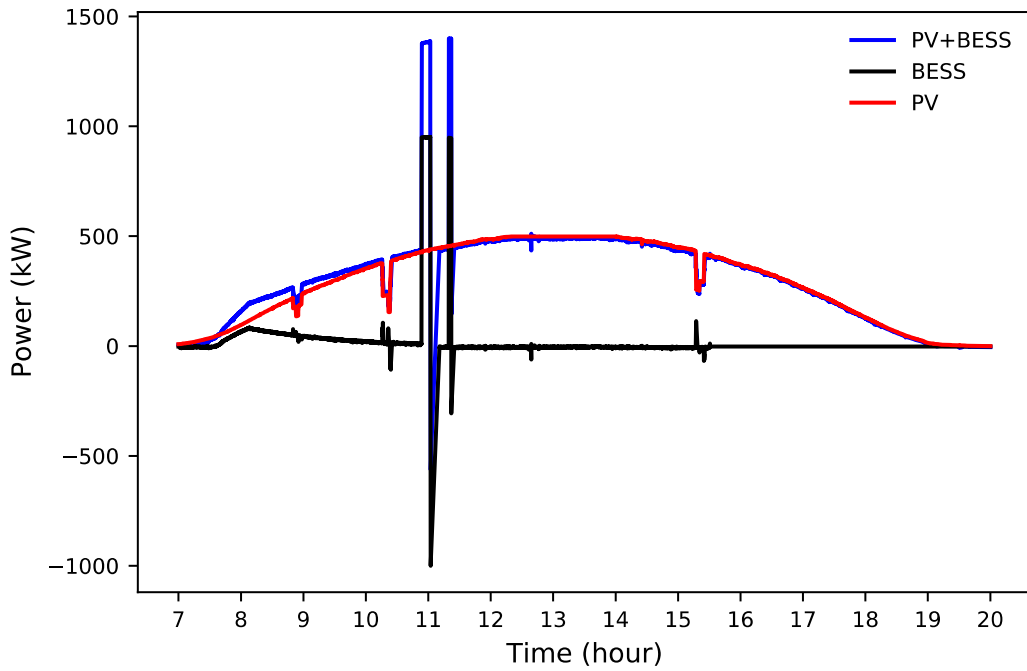


Figure 36: Solar smoothing on Thursday September 2, 2021, from 7am till 8pm. Note that the solar smoothing function was turned off at 5pm because the PUD crew was turning the battery off before they leave work. This was the case until all testing, training and fire safety systems were complete.

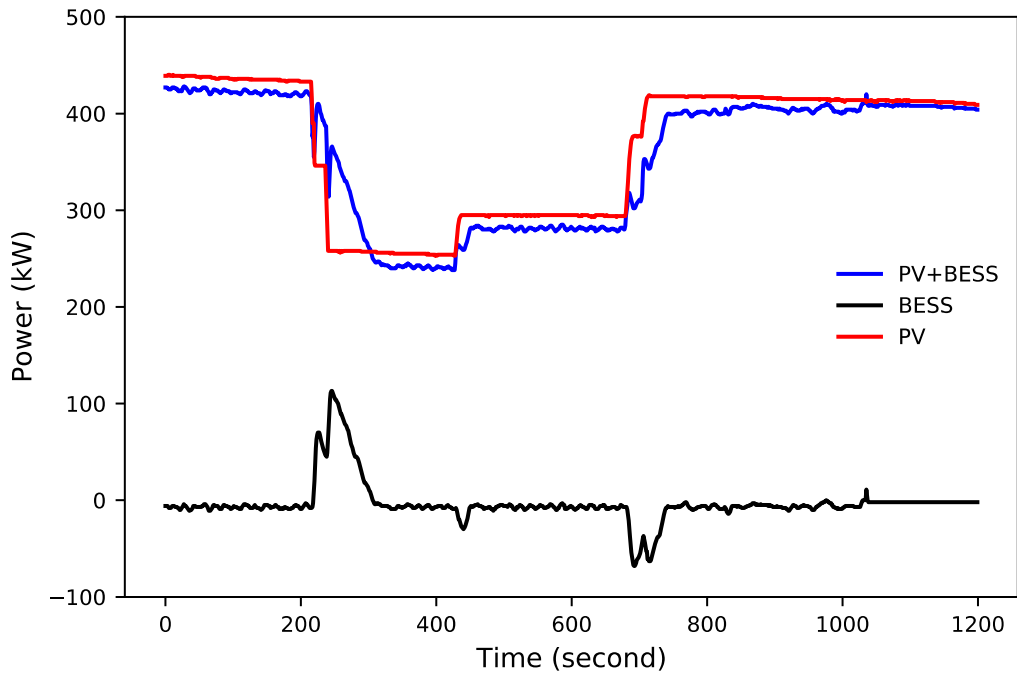


Figure 37: Solar smoothing on Thursday September 2, 2021, over the 20-minute period starting at 3.13pm when the PV generation was turned off and on using solar inverters.

Table 15: Summary of the ramp rates of PV and PV+BESS generation for the 20-minute time period starting at 3.13pm on Thursday September 2, 2021, when the PV generation was turned off and on using the solar inverters.

	PV generation (kW/s)	PV+BESS generation (kW/s)
Maximum ramp rate	41	32
90 th percentile	1	2
75 th percentile	0	1
50 th percentile	0	0
25 th percentile	0	0
Minimum ramp rate	0	0

5.2.2 Second Day of Testing Solar Smoothing: Tuesday September 7, 2021

Table 16: Weather data for the solar smoothing test on Tuesday September 7, 2021

Minimum Temperature	48.2 °F
Mean Temperature	62.2 °F
Maximum Temperature	80.1 °F
Mean sea level pressure	30.09 in
Mean dew point	51.9 °F
Total precipitation	0 in
Visibility	9.6 miles
Snow depth	none
Mean wind speed	5.41 mph
Maximum sustained wind speed	13.81 mph
Maximum wind gust	No data

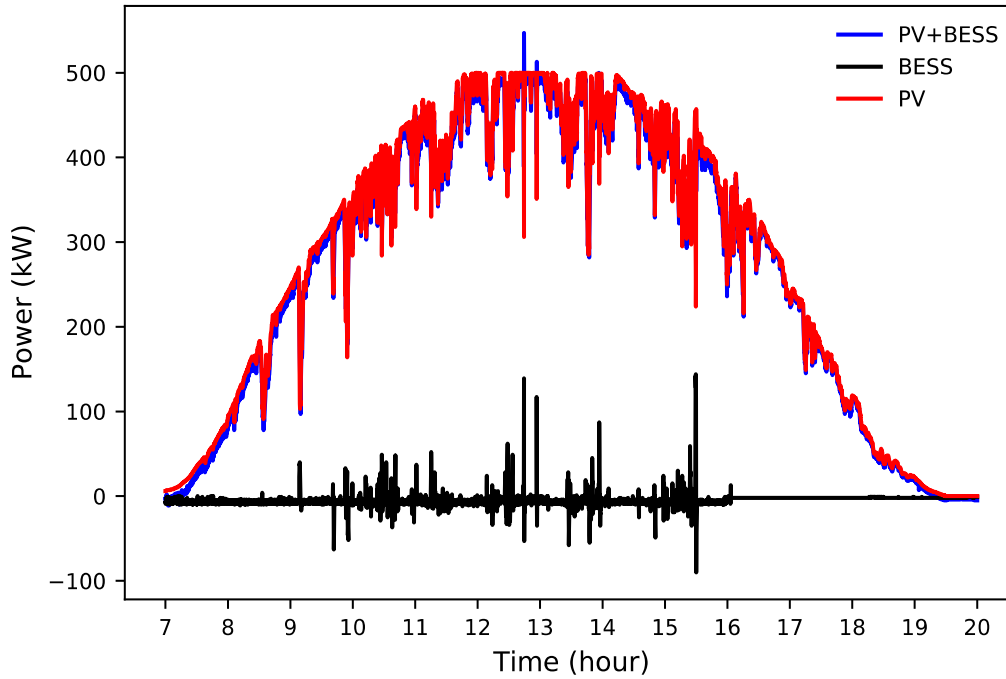


Figure 38: Solar smoothing on September 7, 2021 (Tuesday) from 7am till 8pm.

Table 17: Summary of the ramp rates of PV and PV+BESS generation on September 7, 2021.

	PV generation (kW/s)	PV+BESS generation (kW/s)
Maximum ramp rate	42	34
90 th percentile	2	2
75 th percentile	1	1
50 th percentile	0	0
25 th percentile	0	0
Minimum ramp rate	0	0

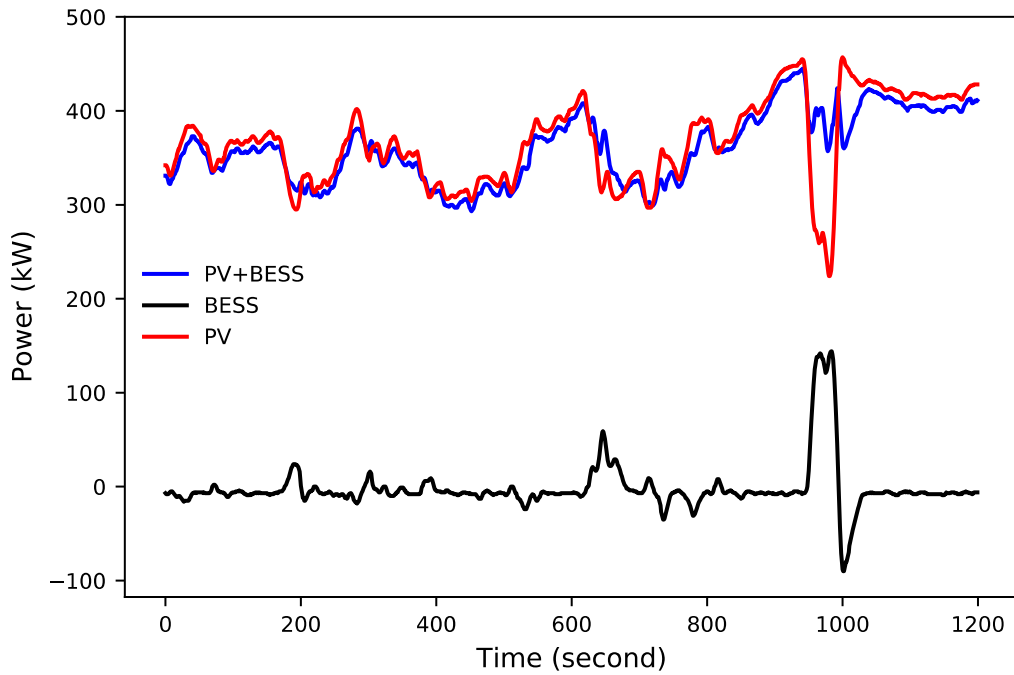


Figure 39: Solar smoothing over a 20-minute period starting at 3.13pm on September 7, 2021.

Table 18: Summary of ramp rates of PV and PV+BESS generation for the 20-minute period starting at 3.13pm on September 7, 2021.

	PV generation (kW/s)	PV+BESS generation (kW/s)
Maximum ramp rate	24	11
90 th percentile	4	3
75 th percentile	2	2
50 th percentile	1	1
25 th percentile	0	0
Minimum ramp rate	0	0

5.2.3 Third Day of Testing Solar Smoothing: Wednesday September 8, 2021

Table 19: Weather data for the solar smoothing test on Wednesday September 8, 2021

Minimum Temperature	59.0 °F
Mean Temperature	66.3 °F
Maximum Temperature	75.9 °F
Mean sea level pressure	29.93 in
Mean dew point	51.6 °F
Total precipitation	0 in
Visibility	10 miles
Snow depth	none
Mean wind speed	5.06 mph
Maximum sustained wind speed	16.11 mph
Maximum wind gust	No data

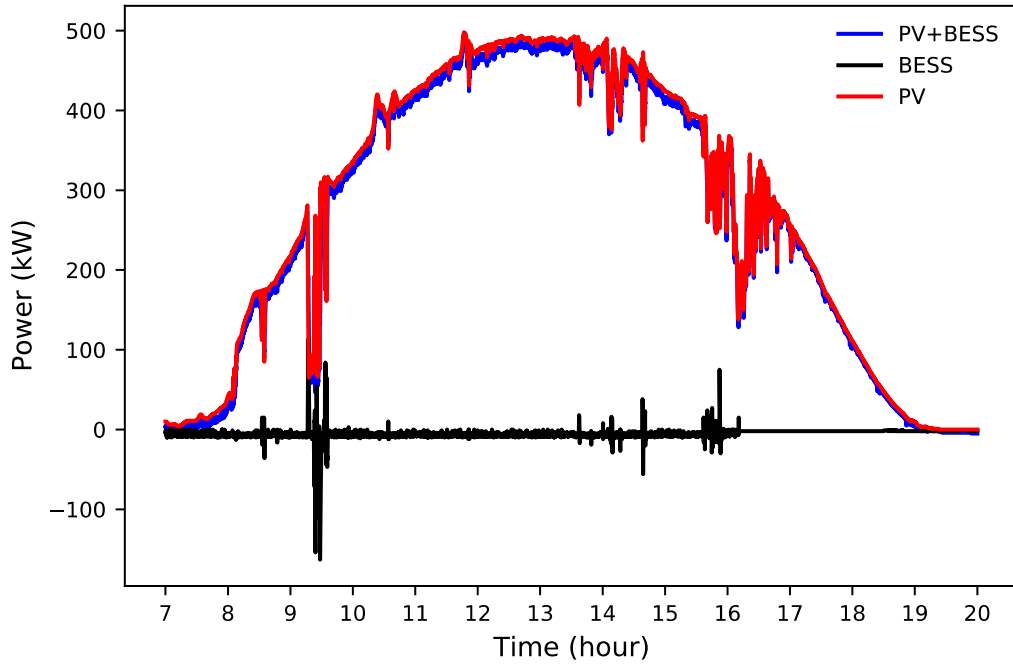


Figure 40: Solar smoothing on Wednesday September 8, 2021, from 7am till 8pm.

Table 20: Summary of ramp rates of PV and PV+BESS generation on September 8, 2021.

	PV generation (kW/s)	PV+BESS generation (kW/s)
Maximum ramp rate	45	26
90 th percentile	1	1
75 th percentile	0	1
50 th percentile	0	0
25 th percentile	0	0
Minimum ramp rate	0	0

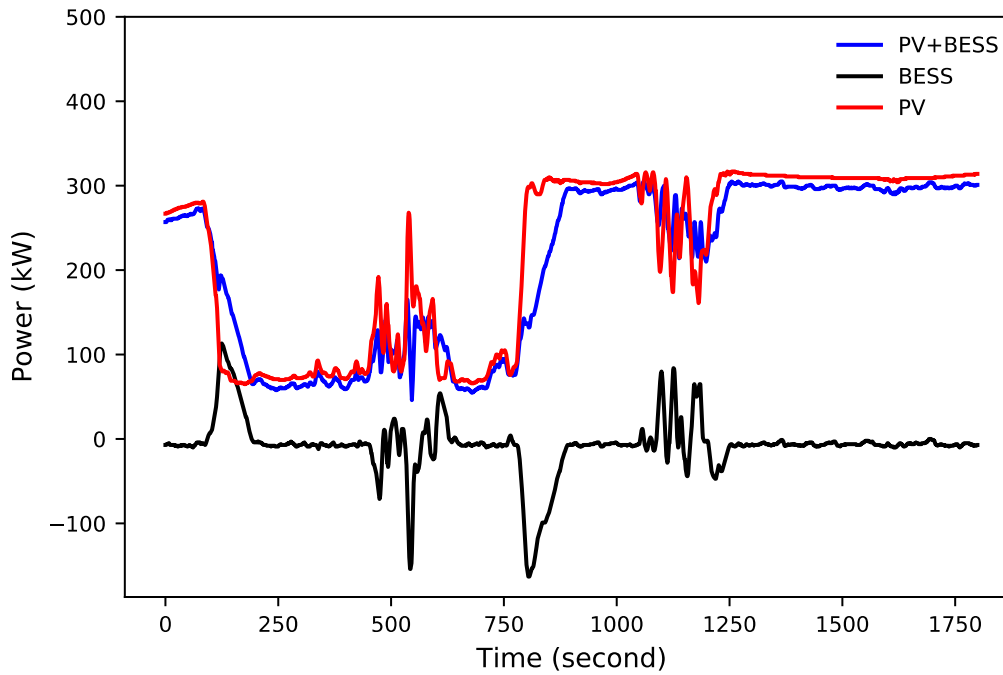


Figure 41: Solar smoothing over a 30-minute period starting at 9.15am on Wednesday September 8, 2021.

Table 21: Summary of ramp rates of PV and PV+BESS generation smoothing over a 30-minute period starting at 9.15am on Wednesday September 8, 2021.

	PV generation (kW/s)	PV+BESS generation (kW/s)
Maximum ramp rate	45	26
90 th percentile	6	4
75 th percentile	2	2
50 th percentile	0	1
25 th percentile	0	0
Minimum ramp rate	0	0

5.2.4 Fourth Day of Testing Solar Smoothing: Monday October 18, 2021

Note that this was the last solar smoothing test that was carried out and the controller was tuned before this test. As shown in Table 22, the solar smoothing function reduces the maximum ramp rate from 30 kW/second to 19 kW/second.

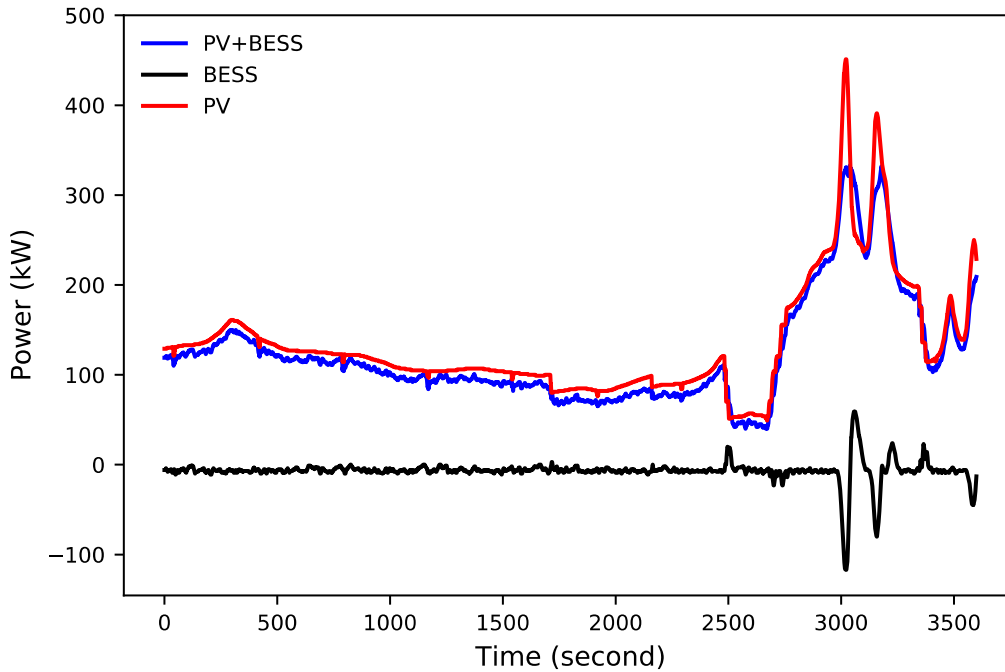


Figure 42: Solar smoothing over a 1-hour period starting at 2 pm on October 18, 2021.

Table 22: Summary of ramp rates of PV and PV+BESS generation smoothing over a 1-hour period starting at 2pm on October 18, 2021.

	PV generation (kW/s)	PV+BESS generation (kW/s)
Maximum ramp rate	30	19
90 th percentile	1	2
75 th percentile	0	1
50 th percentile	0	0
25 th percentile	0	0
Minimum ramp rate	0	0

5.2.5 Conclusion on Solar Smoothing Testing

This report presented solar smoothing tests of the Arlington Microgrid on five days with different PV generation profiles. The ramp rates of the raw PV generation and the PV+BESS presented in tables show that the maximum ramp rate is reduced with solar smoothing. Note that this is not the same as keeping the ramp rate below a certain value.

5.3 UC3: Grid Support and Ancillary Services

As part of the commissioning of the Arlington microgrid, the BESS was integrated into the DERO computer system that Snohomish PUD uses to control its battery energy storage assets. See in Appendix A the site acceptance test relating to this integration.

The BESS must be able to follow a duty cycle that would achieve the desired benefits. As shown in Figure 44, Figure 43, and Figure 45, the battery is able to follow duty cycles of magnitude of 250 kW, 500 kW and 1000 kW.

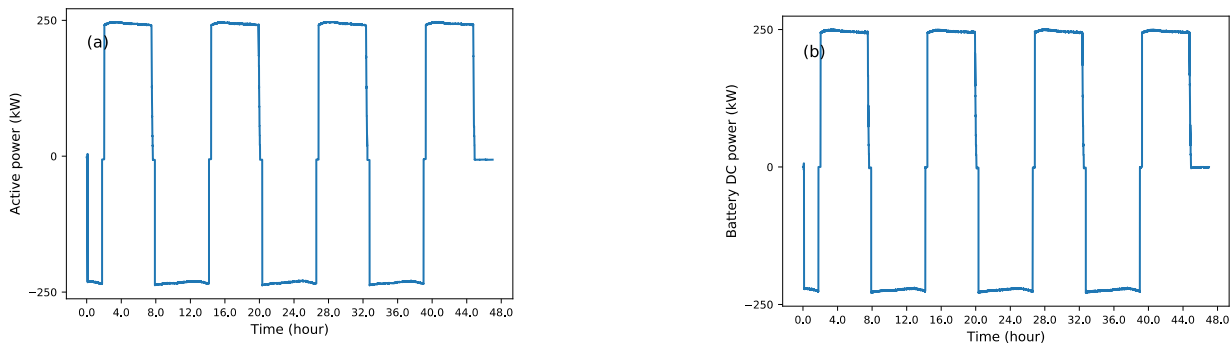


Figure 43: BESS charging and discharging at 250 kW over a day. (a) BESS AC power and (b) BESS DC power

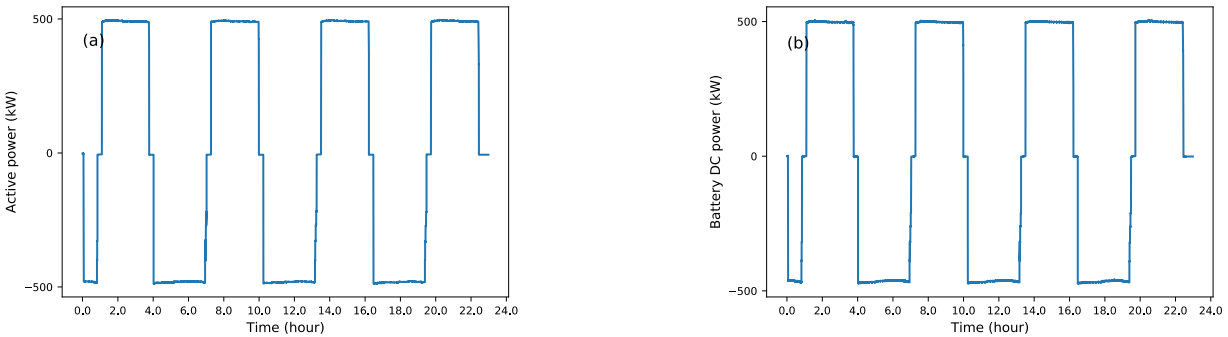


Figure 44: BESS charging and discharging at 500 kW over a day. (a) BESS AC power and (b) BESS DC power

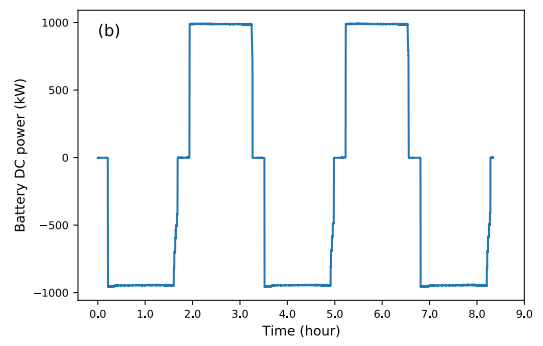
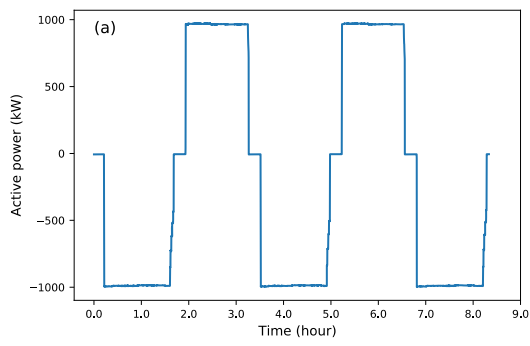


Figure 45: BESS charging and discharging at 1000 kW over a day. (a) BESS AC power and (b) BESS DC power

5.4 UC4: Vehicle-Grid Integration

During the final V2G test that was carried out on January 19, 2022, both EVs were charged and discharged as shown in Figure 46. EV1 had just above 75% SoC while the EV2 had approximately 50% SoC. Figure 48 shows the BESS power and SoC, PV generation, and emergency generator output. The emergency generator was only used for a short period between 9.45am to 10:00 am to charge the BESS when the SoC dropped below 50%. Both the EVs were also discharging during this period. Figure 49, Figure 51 and Figure 50 show these variables over the entire day of testing.

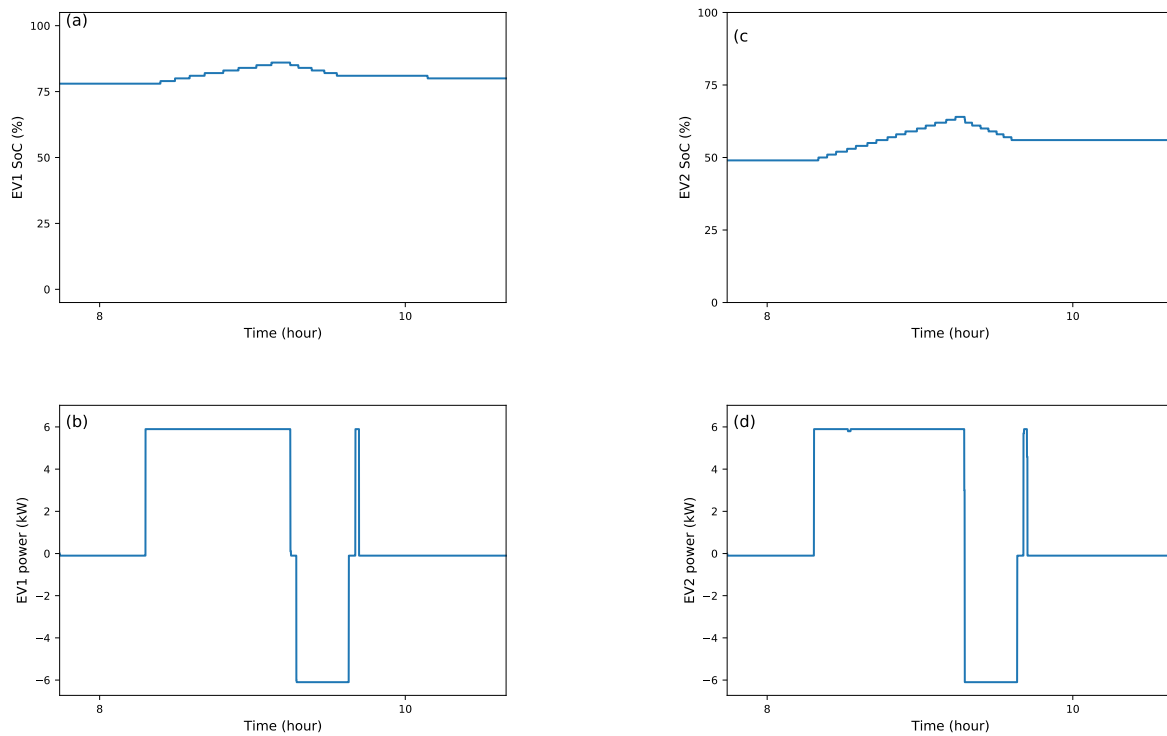


Figure 46: V2G test on January 19, 2022. The SoC and power input/output of the two electric vehicles. Note that the anomalies from measurement error are removed in this figure.

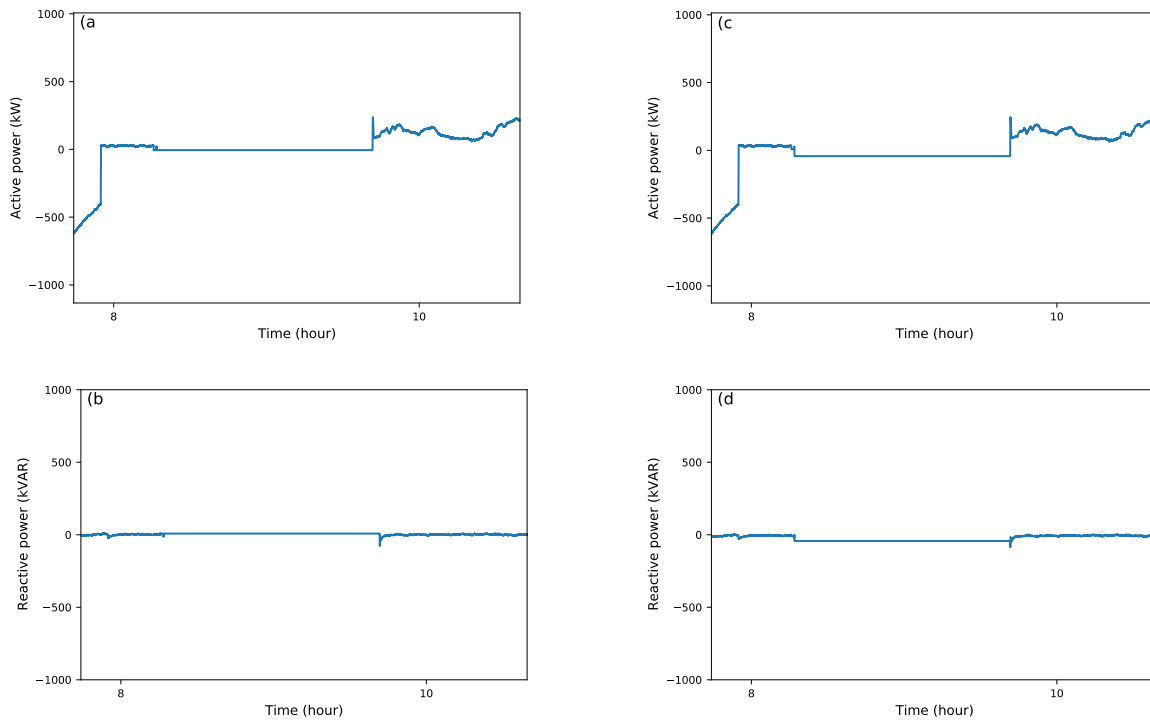


Figure 47: V2G test on January 19, 2022. Active power and reactive power at the outer microgrid (a and b) and inner microgrid (c and d). The outer microgrid includes the data center load.

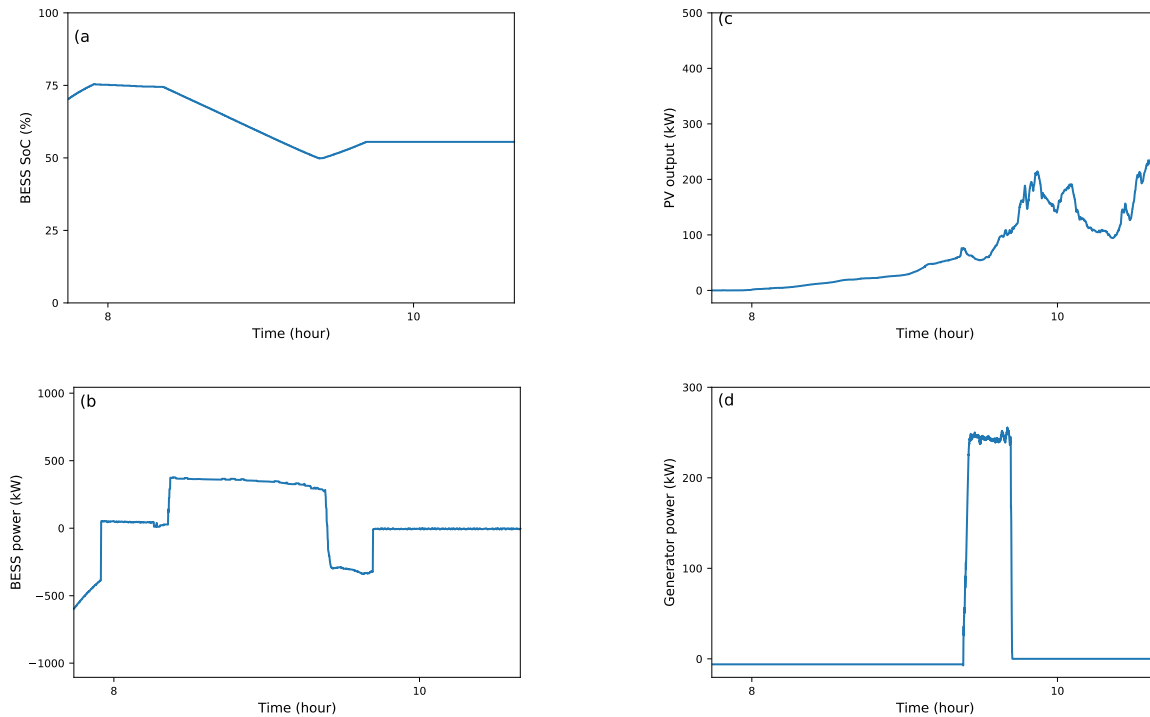


Figure 48: V2G test on January 19, 2022. (a) BESS SoC; (b) BESS power; (c) PV generation; and (d) generator output.

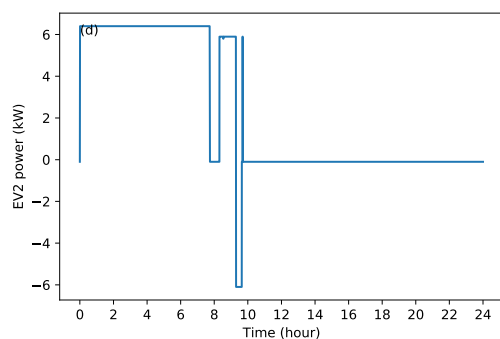
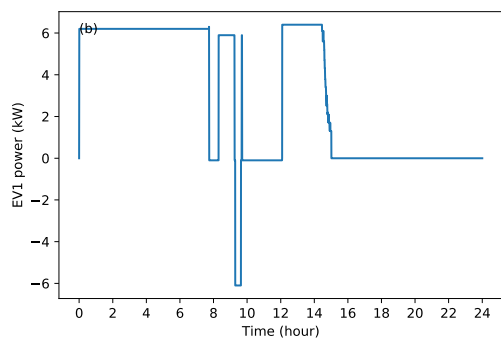
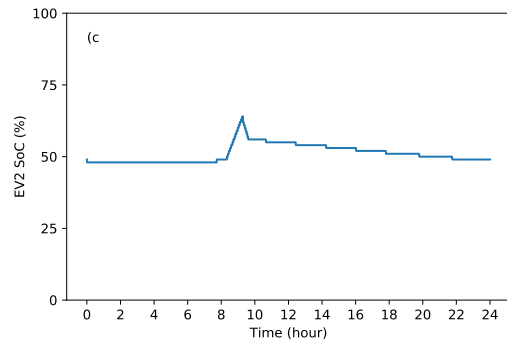
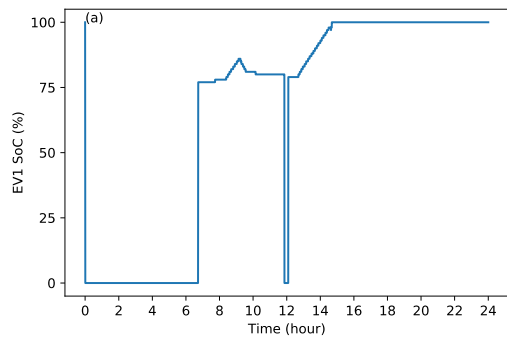


Figure 49: V2G test on January 19, 2022. SoC and power of the two electric vehicles.

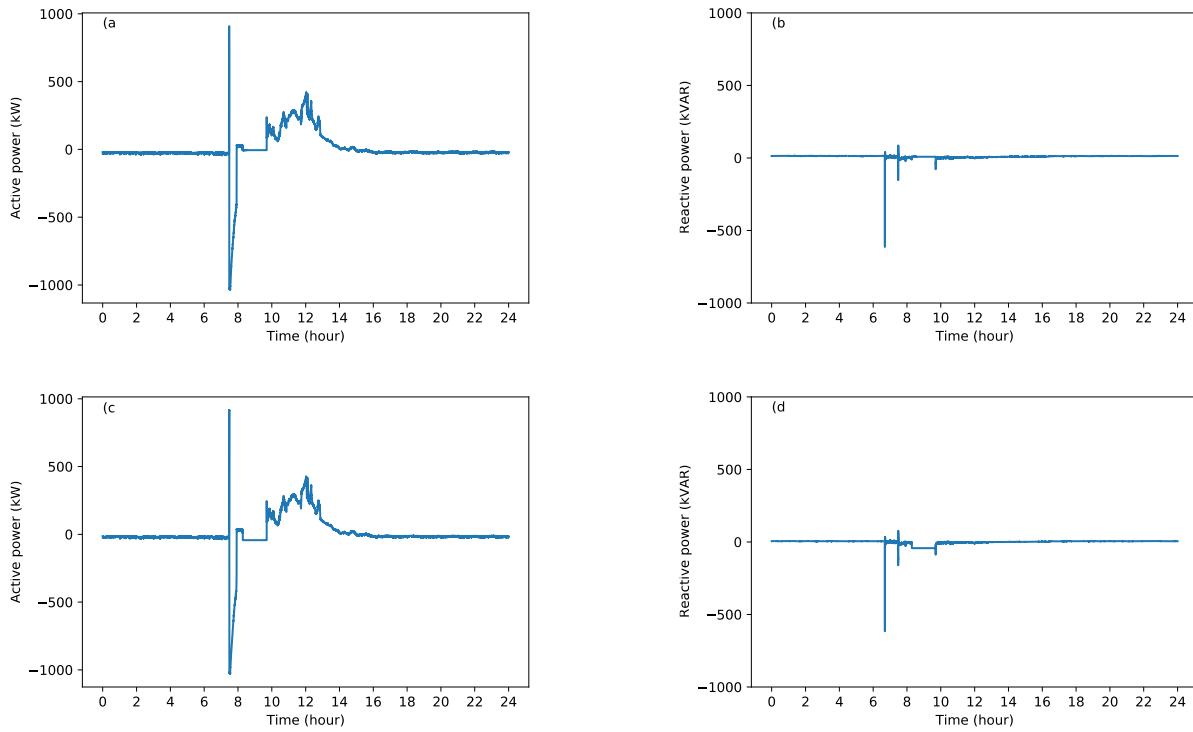


Figure 50: V2G test on January 19, 2022. Active power and reactive power at the outer microgrid (a and b) and inner microgrid (c and d).

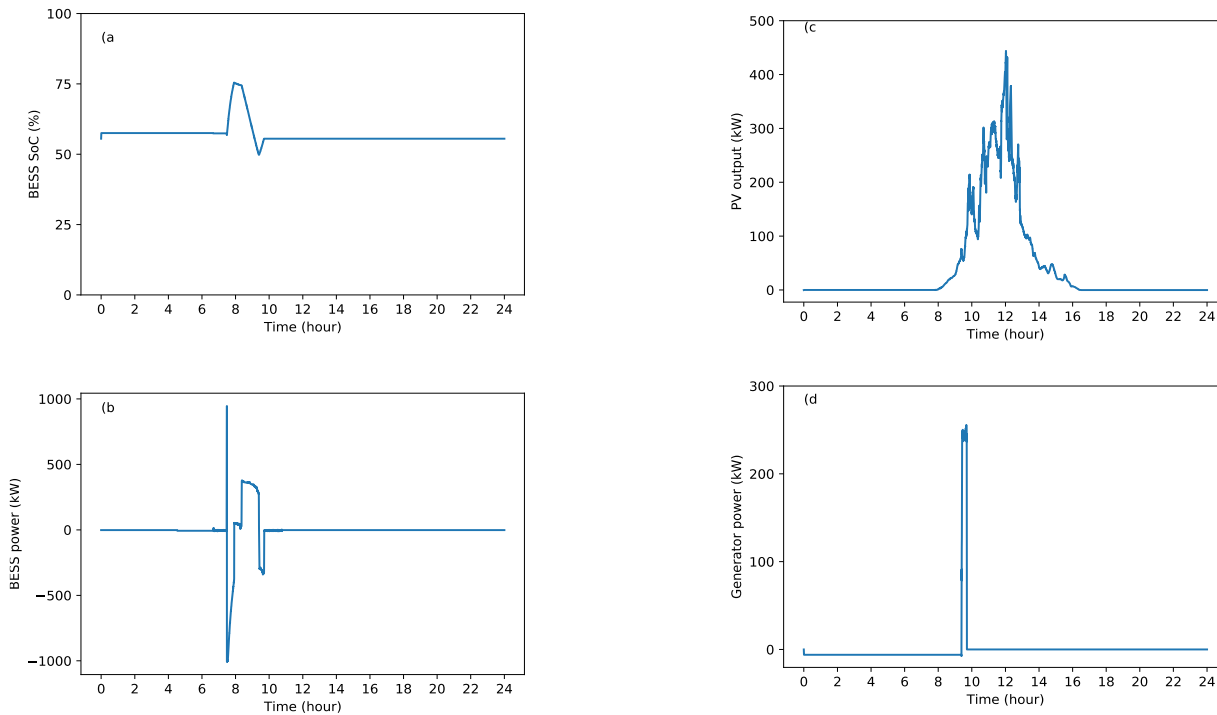


Figure 51: V2G test on January 19, 2022. (a) BESS SoC; (b) BESS power; (c) PV generation; and (d) generator output.

6. Cost Breakdown of the Arlington Microgrid

All costs in \$1,000	Estimated		Actual	
	Utility	Contract	Utility	Contract
Project Development				
Conceptual Engineering	40		50	
Contract development & PM	50	150	100	150
Site/Civil				
Engr. Labor	50	100	50	100
Environmental permitting		40	10	50
Lumped Construction			50	290
Indirects (Const OH & WA Tax)	59	100	75	125
Systems Electrical				
System studies and design	150	557	150	900
Electrical Peripherals	200	450	200	600
Indirects (Const OH & WA Tax)	38	200	38	200
Major Equipment Components				
DER Assets	10	115	10	200
Inverters & trackers		125	5	50
Microgrid & Control Platforms		1500		1555
Batteries		292		300
PCS		200		125
BOS		125		100
BESS Installation & Integration	50	525	750	20
Indirects (Const OH & WA Tax)	97	300	200	150
Communications	50	100	50	100
Indirects (OH & WA Tax)				
IT/Software & SCADA	50	100	50	50
Indirects (OH & WA Tax)				
Other (Analytics)	100	200	50	500
Contingency	532			
Insurance/Misc.				
Administration OH	696		696	
Total Utility Charges	2172		2534	
Total Contract Costs		5179		5565
Total Project Costs	7351		8099	

7. References

- [1] Executive Office of the President, “Economic Benefits of Increasing Electric Grid Resilience to Weather Outages,” 2013. [Online]. Available: [https://www.energy.gov/sites/prod/files/2013/08/f2/Grid Resiliency Report_FINAL.pdf](https://www.energy.gov/sites/prod/files/2013/08/f2/Grid_Resiliency_Report_FINAL.pdf).
- [2] E. L. Geist, “Local tsunami hazards in the Pacific Northwest from Cascadia subduction zone earthquakes.” US Geological Survey, 2005, doi: 10.3133/pp1661b.
- [3] B. Bonlender, “Clean Energy Fund,” 2017. [Online]. Available: <http://www.commerce.wa.gov/wp-content/uploads/2017/04/Commerce-Clean-Energy-Fund-2017.pdf>.
- [4] “Microgrid Portfolio of Activities.” <https://www.energy.gov/oe/services/technology-development/smart-grid/role-microgrids-helping-advance-nation-s-energy-syst-0> (accessed Jan. 26, 2021).
- [5] “Microgrids: An Old Concept Could Be New Again.” <https://www.powermag.com/microgrids-an-old-concept-could-be-new-again/> (accessed Jan. 26, 2021).
- [6] Engerati, “The Tesla microgrid – American Samoa shows the way,” 2016. .
- [7] ABB, “Battery / diesel grid-connected microgrids : a large-scale, industry-based case study of future microgrid capabilities,” 2014.
- [8] H. Gao, Y. Chen, Y. Xu, and C.-C. Liu, “Resilience-Oriented Critical Load Restoration Using Microgrids in Distribution Systems,” *IEEE Trans. Smart Grid*, vol. 7, no. 6, pp. 2837–2848, Nov. 2016, doi: 10.1109/tsg.2016.2550625.
- [9] W. Rickerson, K. Zitelman, and K. Jones, “Valuing Resilience for Microgrids: Challenges, Innovative Approaches, and State Needs,” no. February, 2022, [Online]. Available: <https://pubs.naruc.org/pub/1B571AB6-1866-DAAC-99FB-2509F05E4A67>.
- [10] “Interruption Cost Estimator Calculator.” <https://www.icecalculator.com/build-model?model=interruption> (accessed Jan. 01, 2020).

- [11] “Washington Clean Energy Fund Grid Modernization Projects: Economic Analysis”,
PNNL Report 30594 [Online]:
http://www.pnnl.gov/main/publications/external/technical_reports/PNNL-30594.pdf

**Appendix A: Site Acceptance Test Report on Integration of the Arlington
Microgrid with the DERO Computer System**

Mesa Compliance Test Test Description

Contents

1. Document Purpose	2
2. Test Steps and Validation Approach	2
2.1. Communication Health	2
2.1.1. Zenon Startup.....	2
2.1.2. DERO Startup	2
2.1.3. Signals to be tested after Communication startup procedure	4
2.2. Scheduler Test.....	7
2.2.1. Scheduler Start conditions	7
2.2.2. Step 1 – Add Scheduler for Real power Charge/Discharge	7
2.2.3. Step 2 – Monitoring Scheduler Running.....	10
2.2.4. Step 3 – Add / Edit Scheduler for Real power Charge/Discharge	13
2.2.5. Step 4 – Add / Delete Scheduler for Real power Charge/Discharge	14
2.2.6. Step 5 – Add Scheduler for Smoothing	16
3. Additional Information.....	19
3.1. Listing of related documents	19
4. Revisions	19

PROJECT NAME SnoPUD	BASED ON ,, ,			
PROJECT ID E00025632	EXTERNAL DOCUMENT ID			
CUSTOMER Snohomish PUD	REFERENCE DESIGNATION			
PREPARED 2021-02-01 Carlos Nardi	STATUS Approved	SECURITY LEVEL Internal		
APPROVED 2021-07-25 R.M.Smith	DOCUMENT KIND Certificate of compliance	DCC DCC		
OWNING ORGANIZATION Grid Edge Solutions	DOCUMENT ID	REV. 0	LANG. en	PAGE 1/20

© Hitachi ABB Power Grids 2021. All rights reserved.

1. Document Purpose

The following outline for a MESA compliance test procedure is intended to demonstrate how communications between the DERO System and Hitachi ABB eMESH System can be verified. Key points of the testing will include validation of the communication health between both systems, accuracy of database values and scaling, expected behavior of commands, and functionality for the set-points and the scheduler. This test is intended to be a system wide demonstration, performed at the very end of the commissioning phase after all the independent devices have been integrated and commissioned. The specific information and functions to be tested per this plan draw mainly from the MESA-DER specification.

2. Test Steps and Validation Approach

The following detailed steps are intended to verify communication health/stability of the two systems and provide validation of small signal lists that are considered “critical information” between both systems. A primary focus will be the scheduler, where the main functionality will be tested.

2.1. Communication Health

During this test, the communication will be tested and verified to demonstrate that the system is stable on start / restart conditions. It will also demonstrate that the database is healthy and valid after a reconnection.

2.1.1. Zenon Startup

Start Zenon System and verify the DNP3 communication is online and all signals are valid / have values within the expected range on the DERO screen.

Description / Comments	Passed	Not Passed
System Started	Ok	
Communication Online with Battery Inverter	Ok	
Communication Online with DERO	Ok	

2.1.2. DERO Startup

Start DERO System with Zenon already running and verify the DNP3 communication is online and all signals are valid / have values within the expected range on DERO screen.

Comments	Passed	Not Passed
System Started	Ok	
Communication Online with Zenon	Ok	
Valid data on the Screen	Ok	

STATUS	SECURITY LEVEL	DOCUMENT ID	REV.	LANG.	PAGE
Approved	Internal		0	en	3/20

2.1.3. Signals to be tested after Communication startup procedure

After establishing communication between DERO and Zenon, the following signals need to be verified and/or tested when marked as T (To Be Tested) / V (To Be Verified).

Point Index	Name / Description	State		TBT TBV	Passed	Not Passed
		0	1			
BI1	System Has Priority 1 Alarms	No P1 Alarms Active	Alarm: One or More P1 Alarms Active	T	Ok	
BI2	System Has Priority 2 Alarms	No P2 Alarms Active	Alarm: One or More P2 Alarms Active	T	Ok	
BI3	System Has Priority 3 Alarms	No P3 Alarms Active	Alarm: One or More P3 Alarms Active	T	Ok	
BI10	System Is in Local State	System not in local state	System in local state	T	Ok	
BI12	System Is Starting Up	Not Starting Up	Start command has been received.	T	Ok	
BI13	System Is Stopping	Not Stopping	Emergency stop command has been received.	T	Ok	
BI14	System is Started	Null	Started	T	Ok	
BI15	System is Stopped	Null	Stopped	T	Ok	
BI37	Supports Charge/Discharge Mode	Not Supported	Supported	V	Ok	
BI43	Supports Active Power Smoothing Mode	Not Supported	Supported	V	Ok	
BI70	Oper. Mode - Charge/Discharge Enabled	Disabled	Enabled	T	Ok	
BI76	Oper. Mode - Active Power Smoothing Enabled	Disabled	Enabled	T	Ok	

* Note that the state alarm text might differ slightly from what is written, but is assumed to have the same meaning

Point Index	Name / Description	TBT TBV	Passed	Not Passed
AI17	Storage Effective Actual Energy Capacity. Present actual total energy capacity of the storage system expressed in Storage Capacity Units.	V	Ok	
AI18	Storage Usable Energy Capacity. Usable energy capacity of the storage system expressed in Storage Capacity Units. Not used on DERO	V	-	-
AI32	Maximum Active Generation Power	V	Ok	
AI33	Maximum Active Charging Power	V	Ok	
AI43	System Available Active Generation Power	V	Ok	
AI44	System Available Active Charging Power	V	Ok	
AI45	System Available Reactive Injection Power	V	Ok	
AI46	System Available Reactive Absorption Power	V	Ok	
AI47	System Available Actual State of Charge	V	Ok	
AI48	System Usable State of Charge Not Displayed by DERO	V	-	-
AI68	Active Settings Group	T	Ok	
AI536	System Meter Frequency Not Displayed by DERO	T	-	-
AI537	System Meter Active Power	T	Ok	
AI541	System Meter Reactive Power	T	Ok	
AI545	System Meter Power Factor Not Displayed by DERO	T	-	-
AI546	System Meter Apparent Power Not Displayed by DERO	T	-	-
AI547	System Meter Phase A/B Volts Not Displayed by DERO	T	-	-
AI549	System Meter Phase B/C Volts Not Displayed by DERO	T	-	-
AI551	System Meter Phase C/A Volts Not Displayed by DERO	T	-	-
AI553	System Meter Average Line to Line Voltage	T	Ok	
AI554	System Meter Current A	T	Ok	

	Dero is showing the sum of all phases, the total value is correct.			
AI555	System Meter Current B Dero is showing the sum of all phases, the total value is correct.	T	Ok	
AI556	System Meter Current C Dero is showing the sum of all phases, the total value is correct.	T	Ok	

* These parameters need to be checked for both systems,
as they need to work in the same operational range

2.2. Scheduler Test

The test for the scheduler is the most critical and comprehensive aspect of our testing plan. The test must prove the ability of the system to control the inverter thru a pre-defined and dynamically changed scheduler. The test is composed by DERO system setup scheduler definition and starting the system (if start command available from DERO) and monitor thru time if the system behaves as defined by scheduler settings.

Two different types of schedulers will be tested, Real Power Charge/Discharge and Real Power Smoothing.

2.2.1. Scheduler Start conditions

The conditions below need to match before starting the scheduler test.

Conditions	Passed	Not Passed
Both System Up and Running	Ok	
No Critical or High Priority Alarm	Ok	
Battery Inverter Online	Ok	
System in Remote – (No Local / Lockout Condition)	Ok	
Grid Connected	Ok	

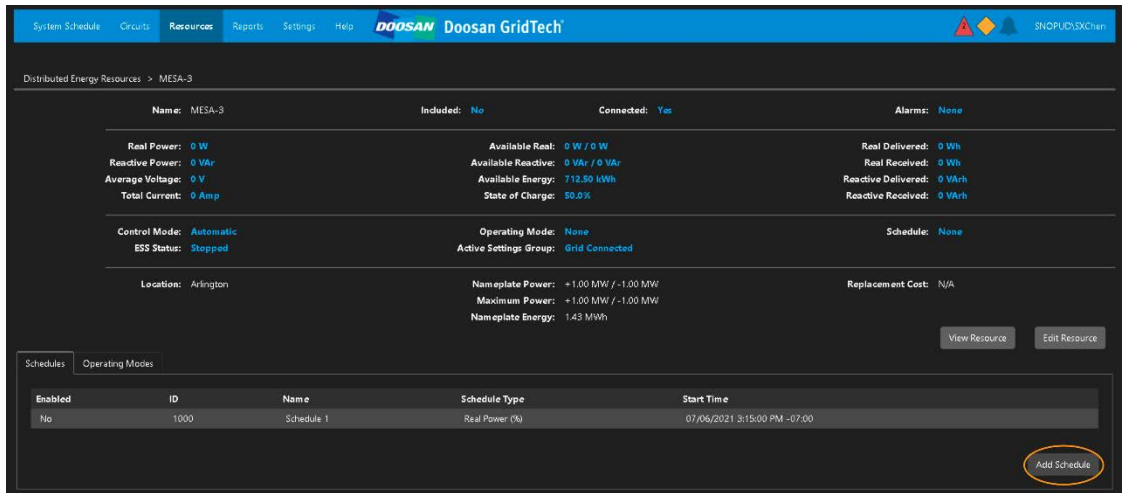
2.2.2. Step 1 – Add Scheduler for Real power Charge/Discharge

In this step the DERO system will setup a new scheduler and write to Zenon based on customer availability.

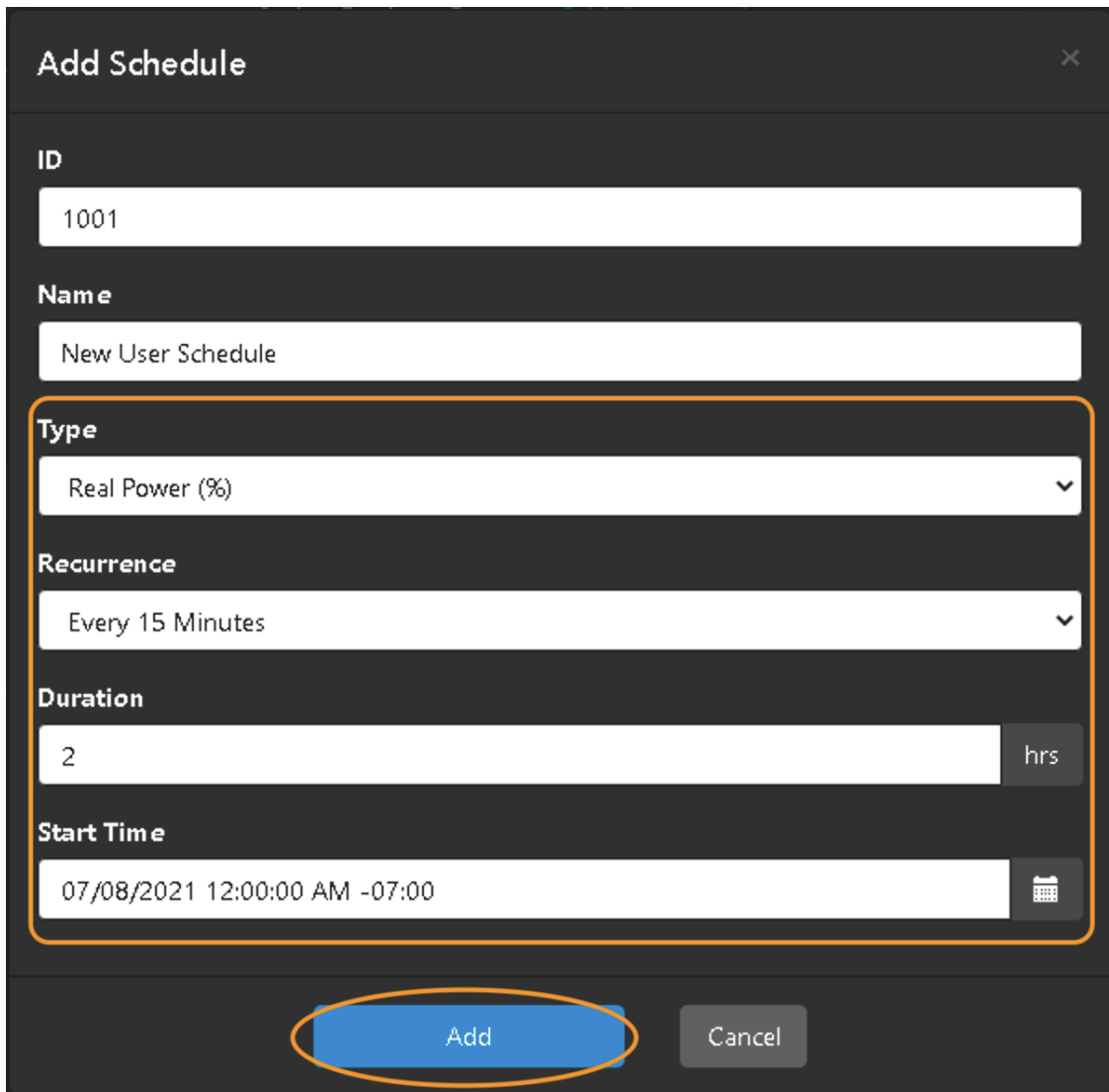
Description	Passed	Not Passed
Create a new Real Power Charge/Discharge Scheduler (2 hours total)	Ok	
Write Scheduler to Zenon	Ok	
Enable Scheduler	Ok	
Check if Scheduler is running as expected on Zenon	Ok	

To add schedule for Real Power Charge/Discharge from DERO:

1. Open DERO web-based user interface and navigate to Resources > MESA-3. Click “Add Schedule”.



- On "Add Schedule" pop-up, choose "Real Power (%)" type, set Recurrence (the interval between schedule setpoints), Duration and Start Time to desired value. Click "Add".



- On schedule detail page, make sure "Enabled" is checked. Enter desired setpoint values. Click "Save" to save the schedule and write the schedule to MESA-3.

System: Schedule Circuits Resources Reports Settings Help **DOOSAN** Doosan GridTech  SNOPLUD.SXchen

Distributed Energy Resources > MESA-3 > New User Schedule

ID: 1001 Start Time: 07/08/2021 12:00:00 AM -07:00 Type: Real Power (%)

Name: New User Schedule Repeat Every: 0 Recurrence: Every 15 Minutes

Priority: 0 Repeat Unit: Never Duration: 2 hrs

Enabled

Set Points and Chart

Time	0:00:00	0:15:00	0:30:00	0:45:00	1:00:00	1:15:00	1:30:00	1:45:00
Value (%)	0	0	0	0	0	0	0	0



Save Delete

STATUS	SECURITY LEVEL	DOCUMENT ID	REV.	LANG.	PAGE
Approved	Internal		0	en	9/20

2.2.3. Step 2 – Monitoring Scheduler Running

The system behavior needs to be verified to certify the scheduler is working properly and sending correct values to the inverter based on the currently defined scheduler parameters. The information from historic databases will be used to compare the behavior of the system against the defined scheduler parameters for a time interval of approximately 1 to 2 hours, dependent upon customer availability.

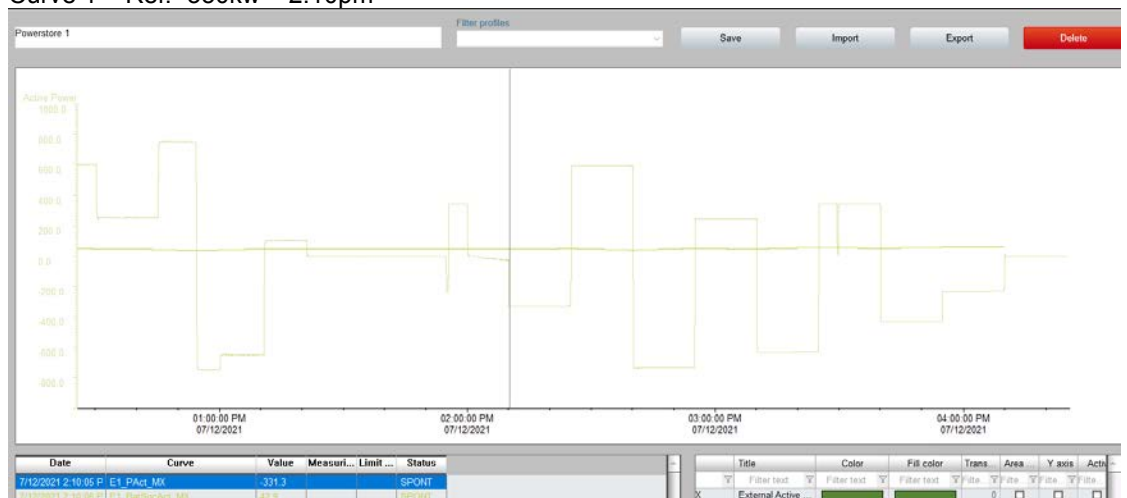
Description	Passed	Not Passed
Scheduler runs as configured	Ok	
Values read from historian matches with scheduler configuration	Ok	
Scheduler end/stop as configured	Ok	
No scheduler is running	Ok	

Additional information from the test:

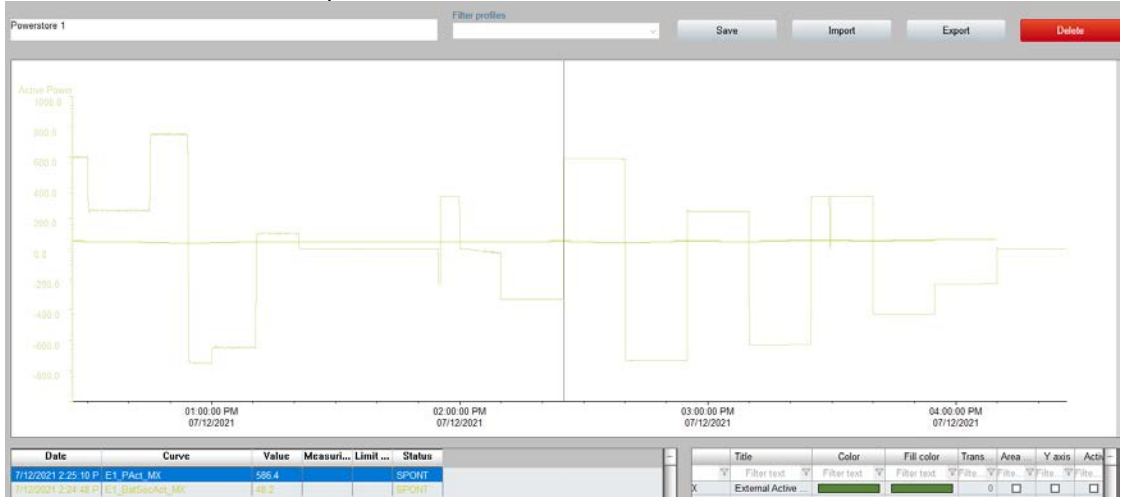
Values received from DERO: 2h schedule with 15min interval starting at 2:10pm.

Name	Value
.RepeatIntervalUnit	0
.NumberOfPoints	9
. Curve_Value	
. Curve_Value[0]	-350
. Curve_Value[1]	600
. Curve_Value[2]	-750
. Curve_Value[3]	250
. Curve_Value[4]	-650
. Curve_Value[5]	350
. Curve_Value[6]	-450
. Curve_Value[7]	-250
. Curve_Value[8]	0
. Curve_Value[9]	0

- Curve 1 – Ref. -350kw – 2:10pm



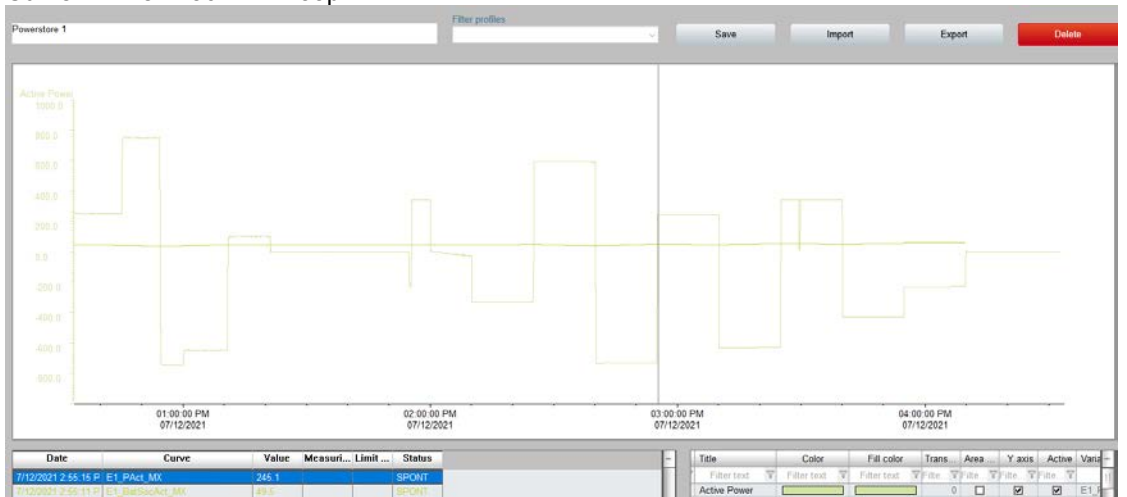
- Curve 2 – Ref. 600kw – 2:25pm



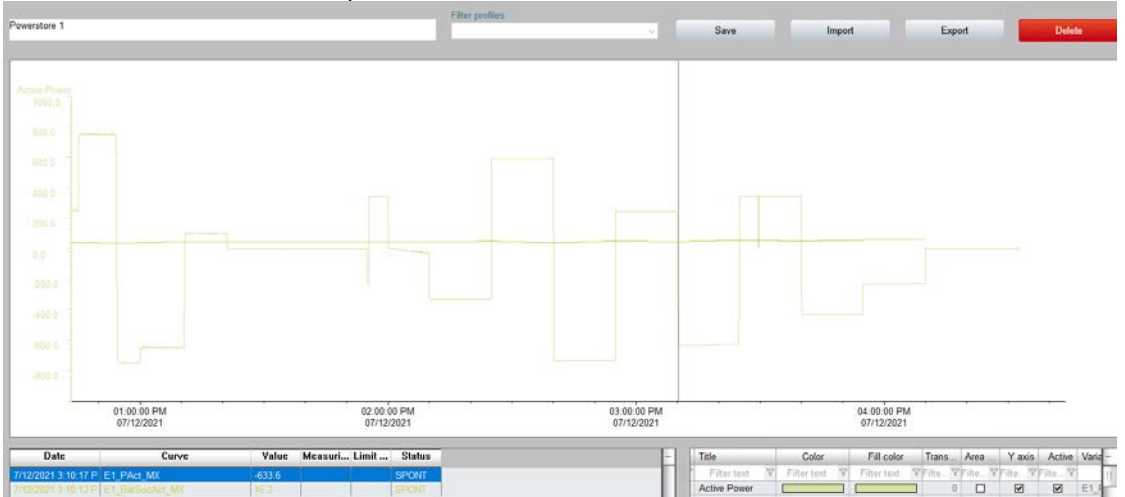
- Curve 3 – Ref. -750kw – 2:40pm



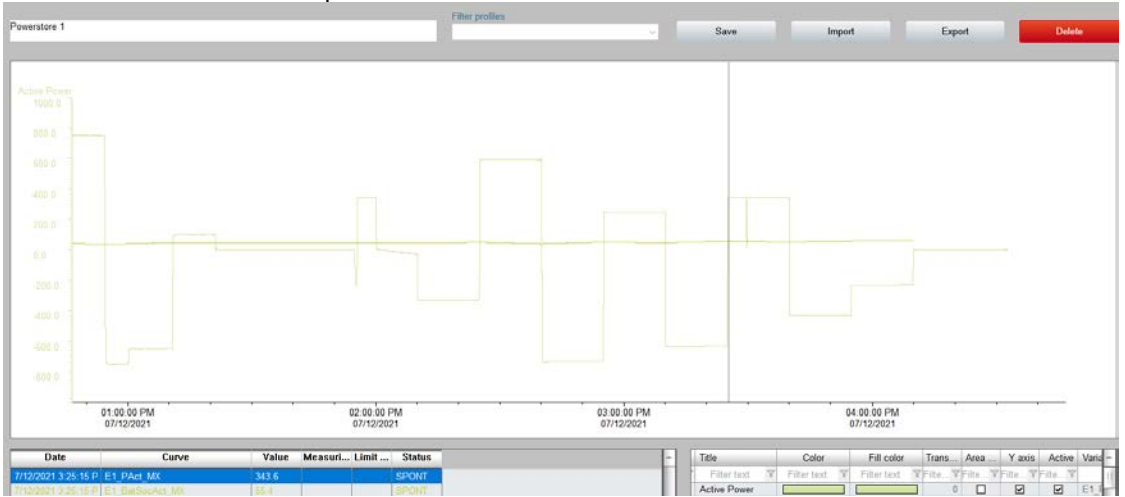
- Curve 4 – Ref. 250kw – 2:55pm



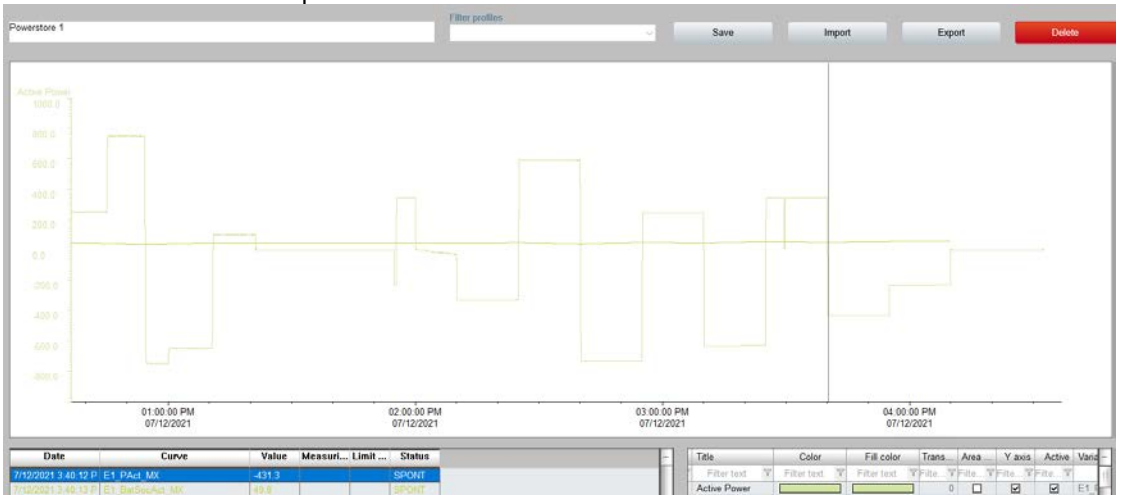
- Curve 53 – Ref. -650kw – 3:10pm



- Curve 6 – Ref. 350kw – 3:25pm



- Curve 7 – Ref. -450 – 3:40pm



- Curve 8 – Ref. -250kw – 3:55pm



- End curve time – 4:10pm



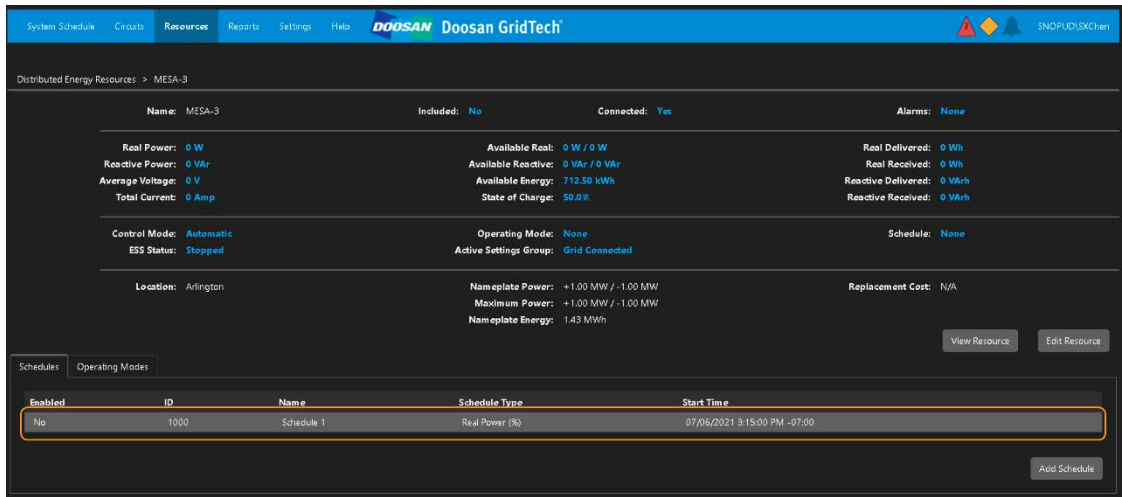
2.2.4. Step 3 – Add / Edit Scheduler for Real power Charge/Discharge

In this step the DERO system will setup a new scheduler and write to Zenon and then this scheduler will be edit and write to Zenon.

Description	Passed	Not Passed
Create a new Real Power Charge/Discharge Scheduler (2 hours total)	Ok	
Write Scheduler to Zenon	Ok	
Edit the Scheduler and write to Zenon	Ok	
Enable Scheduler	Ok	
Check if Scheduler is running as expected on Zenon	Ok	
The historian real power values matches with scheduler configuration	Ok	

To edit an existing schedule from DERO:

4. Open DERO web-based user interface and navigate to Resources > MESA-3. In “Schedules” section, click on the schedule to edit.



- On schedule detail page, edit schedule to desired values. Click “Save” to save the updated schedule and write the schedule to MESA-3.

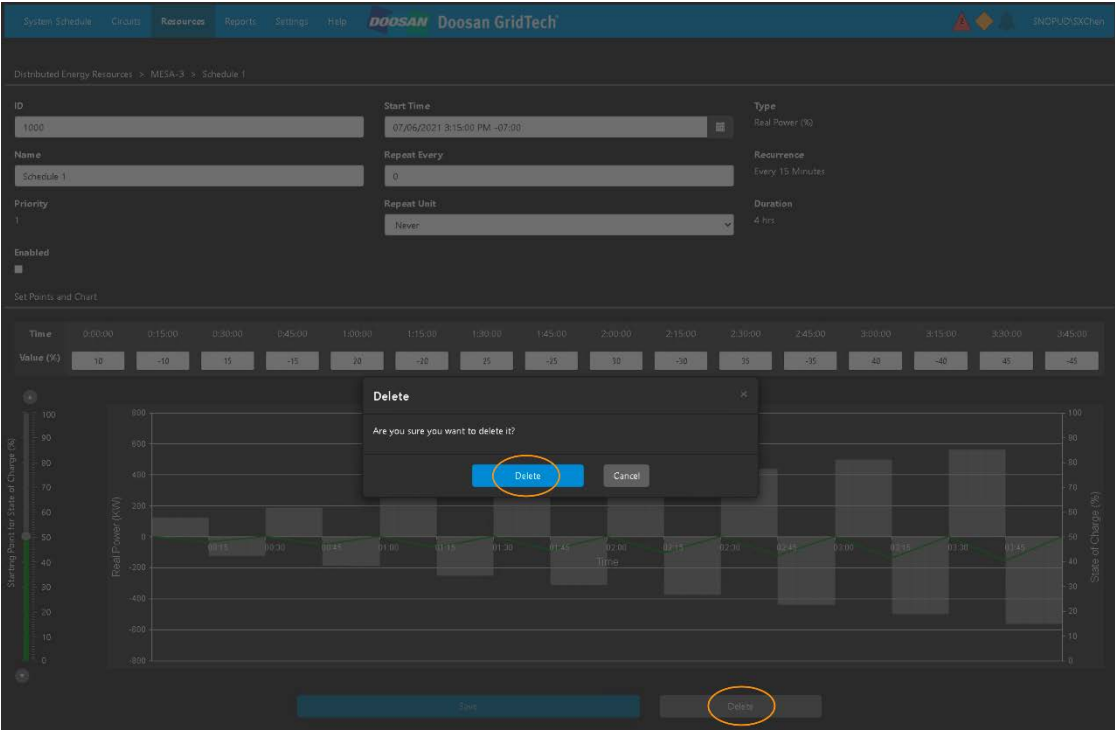
2.2.5. Step 4 – Add / Delete Scheduler for Real power Charge/Discharge

In this step the DERO system will setup a new scheduler and write to Zenon and then this scheduler will be deleted.

Description	Passed	Not Passed
Create a new Real Power Charge/Discharge Scheduler (2 hours total)	Ok	
Write Scheduler to Zenon	Ok	
Delete the scheduler	Ok	
Check if no scheduler is running on Zenon	Ok	

To delete an existing schedule from DERO:

- Follow the steps for editing an existing schedule to open the schedule detail page of the schedule to delete.
- Click “Delete”. On the pop-up window, click “Delete” again to confirm the deletion.



2.2.6. Step 5 – Add Scheduler for Smoothing

In this step the DERO system will setup a new scheduler and write to Zenon based on customer availability.

Description	Passed	Not Passed
Create a new Smoothing Scheduler (2 hours total)	Ok	
Write Scheduler to Zenon	Ok	
Enable Scheduler	Ok	
Check if Scheduler is running as expected on Zenon	Ok	
Check if the Smoothing function is enabled on the Inverter based on scheduler configuration	Ok	
Verify that the function is disable when schedule end.	Ok	

To add schedule for Real Power Smoothing from DERO:

1. Follow the steps for adding Real Power Charge/Discharge schedule.
2. On “Add Schedule” pop-up window, choose “Real Power Smoothing” type.

Add Schedule ✕

ID
1001

Name
New User Schedule

Type
Real Power Smoothing
Real Power (%)
Real Power Smoothing

Duration
12 hrs

Start Time
07/08/2021 12:00:00 AM -07:00

Add **Cancel**

3. Follow the steps to enter setpoint values and save the Real Power Smoothing schedule. Note that setpoint value "1" indicates Real Power Smoothing function will be enabled for the interval; "0" indicates Real Power Smoothing function will be disabled for the interval.

Additional test information:



The Y axis has different scales for each measurement.

This graphs shows the battery response (in green) when a suddenly change occurs on PV (in red), it's possible to note only a small fluctuation on the network(it yellow), when the smoothing function is enabled.

```

MESA_SCHEDULER_ARRAY[2]
  .Identity          1002
  .Priority           1
  .ValidationStatus  7
  .StartDate         18821
  .StartTime         68100000
  .RepeatInterval    0
  .RepeatIntervalUnit
  .NumberOfPoints   9
  .Curve_Value
  .Curve_TimeOffset
  .Status            4
  .RepeatSunday      FALSE
  .RepeatMonday      FALSE
  .RepeatTuesday     FALSE
  .RepeatWednesday  FALSE
  .RepeatThursday    FALSE
  .RepeatFriday      FALSE
  .RepeatSaturday    FALSE
  .SchedulerType     20
  .Type              0
  .Curve_Executed
  .Ready             TRUE
  .Validate           FALSE
  .EndDate           18821
  .EndTime           75300000

```

Schedule details received from DERO (snapshots from internal Zenon logic values)

```

MESA_SCHEDULER_ARRAY
├─ MESA_SCHEDULER_ARRAY[0]
├─ MESA_SCHEDULER_ARRAY[1]
└─ MESA_SCHEDULER_ARRAY[2]
    .Identity                1002
    .Priority                 1
    .ValidationStatus        7
    .StartDate               18821
    .StartTime               68100000
    .RepeatInterval          0
    .RepeatIntervalUnit     0
    .NumberOfPoints         9
    └─ .Curve_Value
        .Curve_Value[0]     1
        .Curve_Value[1]     0
        .Curve_Value[2]     1
        .Curve_Value[3]     0
        .Curve_Value[4]     1
        .Curve_Value[5]     0
        .Curve_Value[6]     1
        .Curve_Value[7]     0
        .Curve_Value[8]     0
        .Curve_Value[9]     0
    
```

Here is possible to verify the configured values for each curve, the interval between curves are 15min, which we can see according to the event list below.

Time received	Identification	
7/13/2021 10:40:00.898 PM	Smoothing Function Enable Feedback	Off
7/13/2021 10:25:00.960 PM	Smoothing Function Enable Feedback	On
7/13/2021 10:10:00.935 PM	Smoothing Function Enable Feedback	Off
7/13/2021 9:55:00.898 PM	Smoothing Function Enable Feedback	On
7/13/2021 9:40:00.962 PM	Smoothing Function Enable Feedback	Off
7/13/2021 9:25:00.926 PM	Smoothing Function Enable Feedback	On
7/13/2021 9:10:00.891 PM	Smoothing Function Enable Feedback	Off
7/13/2021 8:55:00.953 PM	Smoothing Function Enable Feedback	On

Event list showing the function status according to the schedule configuration.

3. Additional Information

3.1. Listing of related documents

Ref #	Document Kind, Title	Document No
1	PDF – Application Note, DNP3 Profile for Communications with Distributed Energy Resources (DERs)	AN2018-001 Version 2019-01-15
2	XLSX – DNP3-Profile-for-DER-Communications	2019-01-15

4. Revisions

Rev.	Page (P) Chapt. (C)	Description	Date Dept./Init.
0		First Draft	2/18/2021

Rev.	Page (P) Chapt. (C)	Description	Date Dept./Init.
1		Edits for basic content	3/8/2021/CN
2		Adapted signal list to match signals available on DERO system, removed start/stop commands and added more detailed scheduler operation.	3/31/2021/CN
3		Document filled with test results and comments.	7/20/2021/CN

STATUS	SECURITY LEVEL	DOCUMENT ID	REV.	LANG.	PAGE
Approved	Internal		0	en	20/20

Appendix B: PNNL Report on Economics of Vehicle-to-Grid Integration



Economic Analysis of Vehicle-to-Grid Tech for Fleets

Application to SnoPUD's Arlington Microgrid

Team: Siddharth Sridhar, Christine Holland, Bowen Huang

Advisors: Di Wu, Ryan Franks, Vilayanur Viswanathan, Charlie Vartanian, Jeremy Twitchell

Thursday, March 17, 2022



PNNL is operated by Battelle for the U.S. Department of Energy



Vehicle-to-Grid (V2G) Technology Overview

❑ What is it?

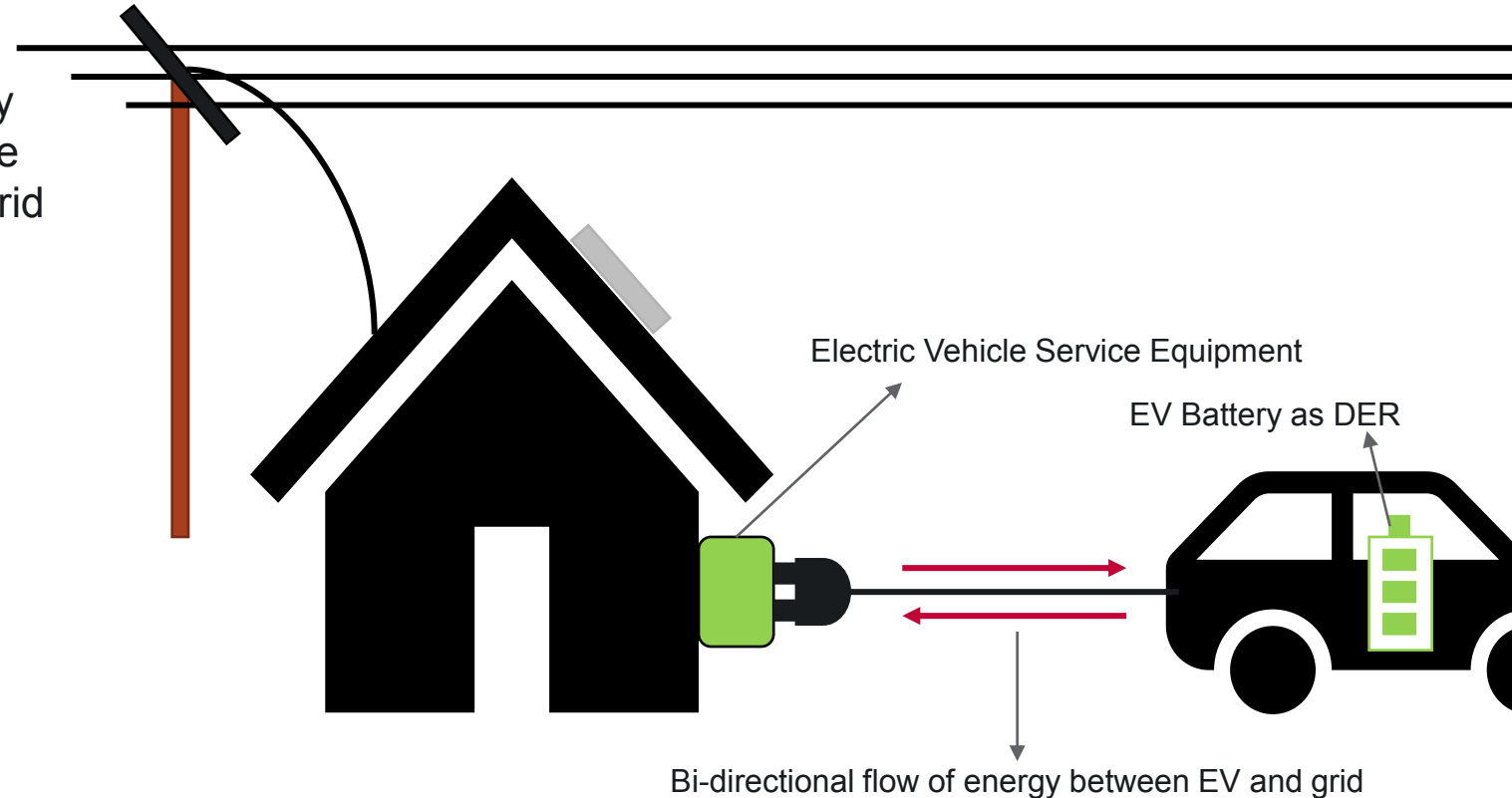
V2G tech enables reverse flow of energy from the Electric Vehicle (EV) back to the grid, in addition to traditional flow from grid to EV.

❑ How does it help the grid?

- Renewable energy integration
- Resilience
- Grid services
- T&D upgrade deferral

❑ What EVs/EVSEs are V2G ready?

- LDV EVs – Nissan Leaf, Ford F150 Lightning, Tesla, Lucid Air
- EV buses – Lion, Blue Bird, Thomas Built
- EVSE – Nuvve, Rhombus, Fermata Energy, Mitsubishi



V2G Pilots in the U.S.

□ V2G using School Bus Fleets

- White Plains School District, NY: ConEdison testing V2G pilot with 5 Lion electric school buses and Nuvve chargers for stress relief
- Beverly Public Schools, MA: Thomas Built school bus used for peak shaving for over 50 hours in summer 2021 by National Grid
- Cajon Valley Union School District, CA: Five Blue Bird buses with Nuvve bi-directional chargers will be used to evaluate additional revenue streams by the school district



□ V2G using Light-Duty Vehicles

- SnoPUD, WA: V2G using Nissan Leaf EVs with Mitsubishi V2G chargers as DER at Arlington Microgrid
- National Grid, RI: Electric Frog's Nissan Leaf used with Fermata Energy V2G chargers for peak shaving
- Roanoke Electric Cooperative, NC: Two Nissan Leaf EVs with Fermata Energy chargers used at utility HQ for peak shaving and back up power

V2G Stakeholders

Priorities

- Sell reasonably-priced EVs with V2G
- Battery cycling for V2G shouldn't degrade EV performance & life
- Leverage V2G for resilient and reliable grid operation, while ensuring energy is economically priced
- EVs ready for primary purpose: moving people & goods
- Compensation for battery degradation & replacement
- Make a profit after infrastructure investment
- Increase adoption of EVs for decarbonization and grid resilience



Challenges and Opportunities

- **Business models** yet to be developed: Driver compensation, discounts on energy, replacement batteries.
- **Regulations** vary by state. Makes nationwide rollout of technology difficult.
- **Fleet participation:** Range anxiety, Guaranteed minimum SOC levels for primary function
- **Battery Degradation:** Who would cover the cost of battery degradation/replacement?
- **Standards:** V2G standards need electric power system & vehicle standards organizations to work together.
- **Incentive schemes:** Clear understanding of location-specific V2G need and economic viability

V2G Economic Evaluation – Research Questions

Stakeholder-specific Questions

- What grid services most benefit from V2G?
- What are the annual benefits to a utility?



Power
Utility

- How is vehicle battery life impacted?
- What is the net long-term benefit to the fleet operator?



Fleet
Operator

- What are the most influential factors that amplify V2G benefits?
- How do these results vary nationally?



Policy
Makers

V2G Economic Evaluation – Fleet Assumptions

Fleet 1: Delivery Vans



- ❑ Rivian delivery van
- ❑ Battery size per EV: 180 kWh
Total fleet: 9 MWh
- ❑ Max power in/out: 11 kW
- ❑ FleetDNA has data for 553 delivery days for 36 vans

Fleet 2: Maintenance Trucks



- ❑ Ford F-150 Lightning
- ❑ Battery size per EV: 170 kWh
Total fleet: 8.5 MWh
- ❑ Max power in/out: 22.5 kW
- ❑ FleetDNA has data for 29 days of operation for 4 trucks

Fleet 3: School Buses



- ❑ Lion-C Electric school bus
- ❑ Battery size per EV: 210 kWh
Total fleet: 10.5 MWh
- ❑ Max power in/out: 19.2 kW
- ❑ FleetDNA has data for 857 school days and 204 bus routes
- ❑ Available 24*7 for 3 months in the summer

Fleet size of 50 vehicles assumed for all fleet types

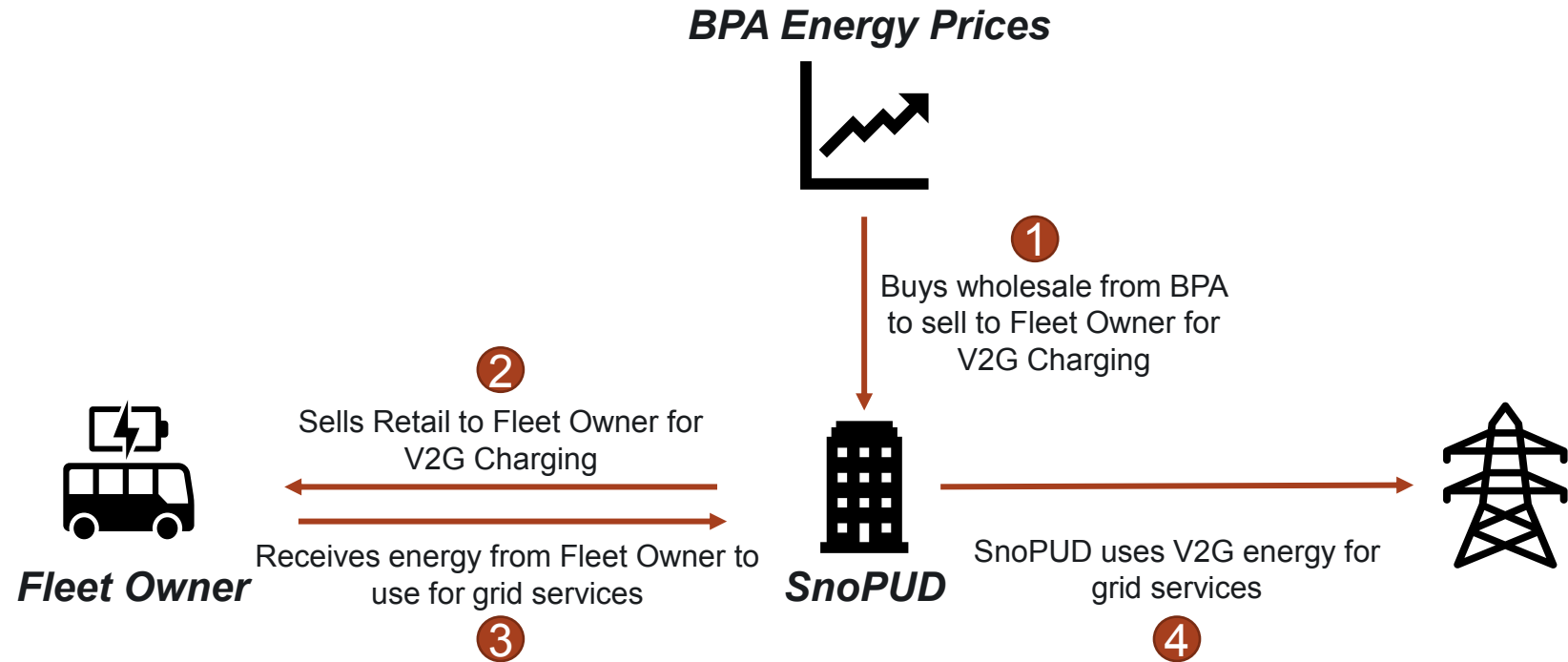
V2G Economic Evaluation – Study Outline

Grid Services Modeled

T&D upgrade deferral	Energy arbitrage
Frequency regulation	Spinning reserve
Capacity adequacy	Demand charge reduction
Balancing charge reduction	Outage mitigation

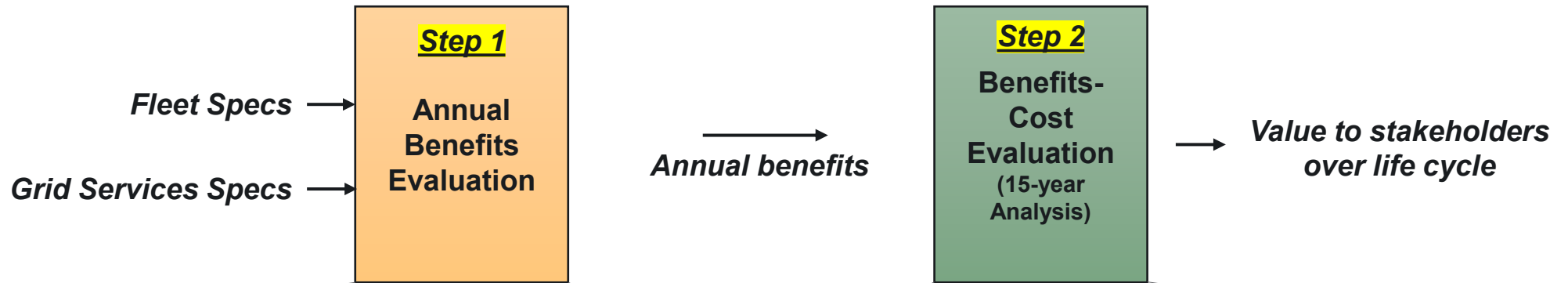
Only highlighted grid services modeled

Market Model



V2G Economic Evaluation – Methodology

Two-step Methodology

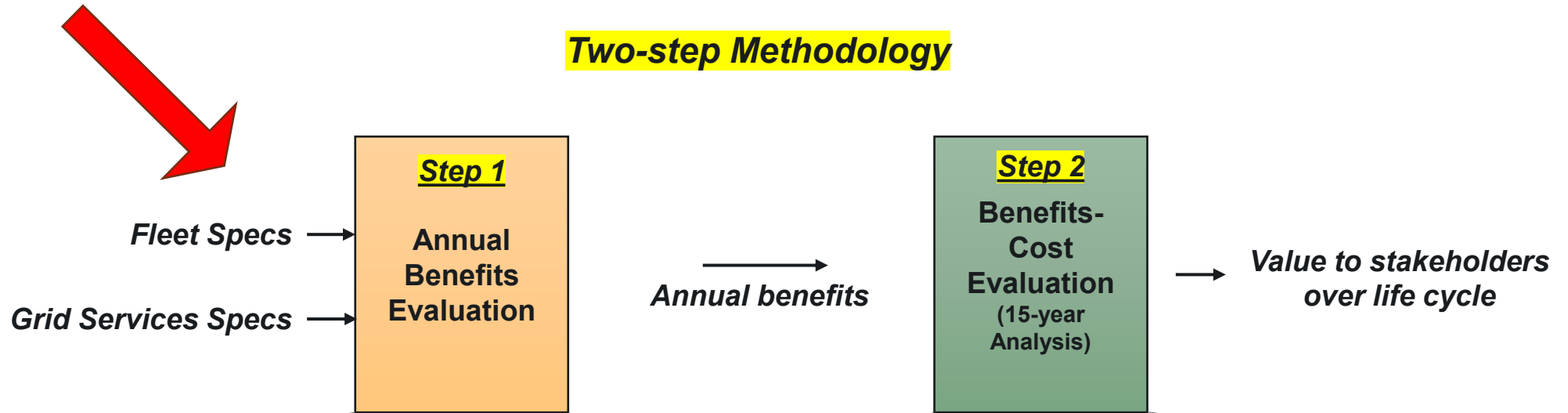


- ❑ Annual benefits evaluated using an optimization model
- ❑ Objective: Maximize utility benefits from grid services
- ❑ Constraints:
 - Battery energy dynamics at EV level
 - Power and energy limits of EV battery
 - Energy and battery balance at fleet level

- ❑ Annual benefits received as input from Step 1
- ❑ Other inputs:
 - Variable and fixed operating costs
 - Battery replacement cost
- ❑ Output:
 - Benefits-cost ratio for all stakeholders
 - Identifying most influential variables that make V2G economically viable

V2G Economic Evaluation – Methodology

Two-step Methodology



- ❑ Annual benefits evaluated using an optimization model
- ❑ Objective: Maximize utility benefits from grid services
- ❑ Constraints:
 - Battery energy dynamics at EV level
 - Power and energy limits of EV battery
 - Energy and battery balance at fleet level

- ❑ Annual benefits received as input from Step 1
- ❑ Other inputs:
 - Variable and fixed operating costs
 - Battery replacement cost
- ❑ Output:
 - Benefits-cost ratio for all stakeholders
 - Identifying most influential variables that make V2G economically viable

Step 1: Annual Benefits Evaluation

Objective Function: Maximize utility benefit from V2G for the four grid services.

$$\text{maximize } \sum_{t=1}^T (\lambda_t p_t + \lambda_t^u r_u + \lambda_t^d r_d + v_t s_t) - \zeta_t L_p$$

Energy arbitrage

λ_t - Energy price at time t

p_t - V2G battery power at time t

Frequency regulation

$\lambda_t^d / \lambda_t^u$ - Regulation down/up price

r_d, r_u - Regulation down/up reserve power

Spinning reserve

v_t - Spinning reserve price at t

s_t - Spinning reserve energy

Demand charge reduction

ζ_t - Demand charge price at t

L_p - System peak load

- Optimization run in 24-hour sliding windows for one year
- Function outputs annual benefit in \$ for every grid service
- Constraints included to determine benefits from a single grid service at a time
- Energy price data for SnoPUD obtained from BPA
- Annual profiles for BPA substation load, AGC signal, & spinning reserve requirement obtained from WECC GridView 2030 case

Step 1: Annual Benefits Evaluation

Constraints

EV battery energy dynamics constraint: $e_i(t + 1) = e_i(t) - d_i^{batt}(t)\Delta T + p_i^{batt}(t)\Delta T$

- Ensures energy is available for primary purpose of fleets: Driving
- Daily driving energy demands pre-computed and included in the constraints

Battery power and energy limits from EV specs: $e_i^{min} \leq e_i(t) \leq e_i^{max}$

- Battery energy limits between 25% to 75%
- EV-specific max/min charge and discharge limits

Battery power and energy limits from EV specs: $d_i^{batt}(t) = \begin{cases} \frac{d_i(t)}{\zeta_i^{b2w}} & \text{if } e_i(t) > 0 \\ 0 & \text{if } e_i(t) = 0 \end{cases} \forall i, t$

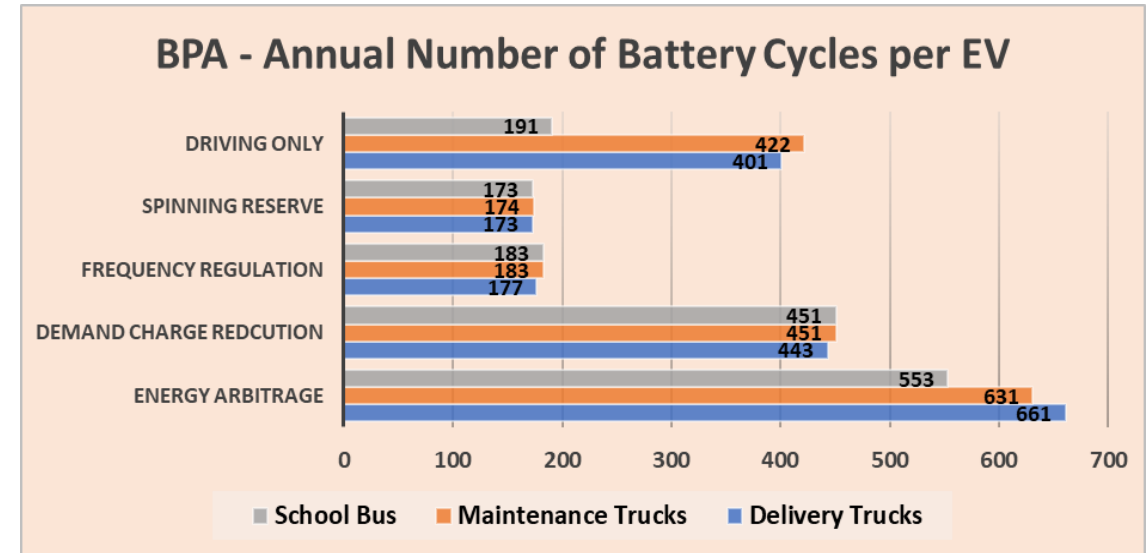
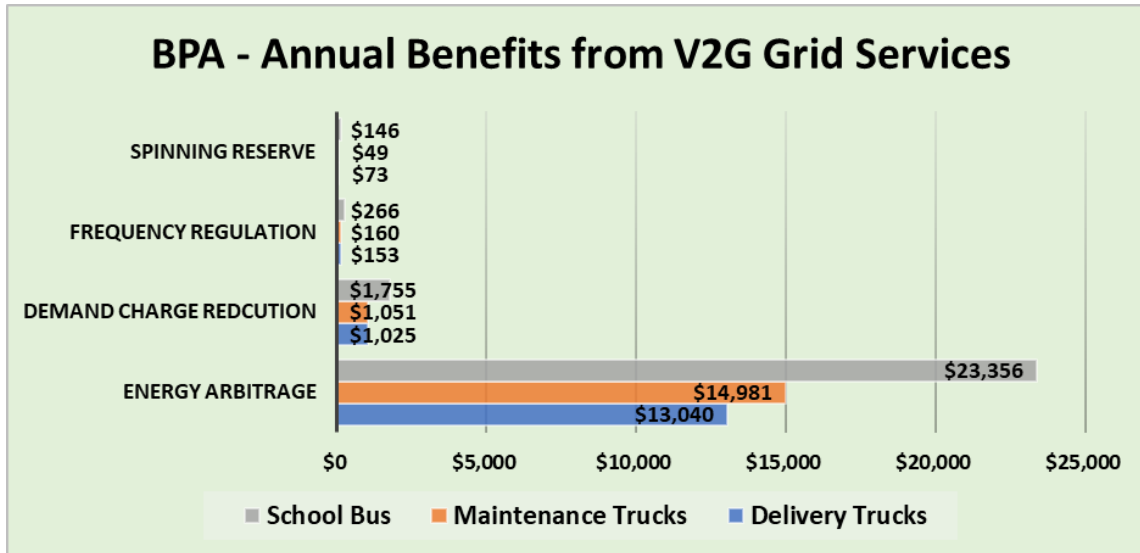
- Battery to wheel losses included in the constraints to determine required SOC

$e_i(t)$ – Battery energy state of EV i at time t
 $p_i^{batt}(t)$ – Battery charging/discharging power at t

$d_i^{batt}(t)$ - Battery energy consumption for driving at time t by EV i
 $d_i(t)$ - Active traction power consumption at the wheels

Step 1: BPA Annual Benefits from Grid Services

Observations for BPA

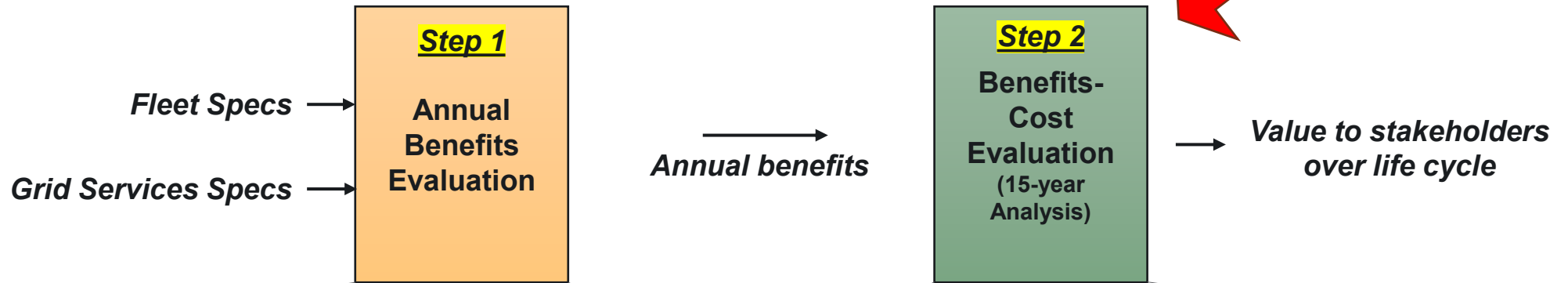


1. Energy arbitrage provides maximum annual benefit to the utility across all fleet types.
2. School bus fleet provides maximum benefit amongst the three fleets. 24*7 availability during summer helps.
3. Spinning reserve returns the least value for BPA. This is due to low price in the region.

4. Energy arbitrage and demand charge reduction cycle the EV battery roughly 2-3 times the number of cycles for driving only.
5. Frequency regulation and spinning reserve cycle EV batteries fewer number of times than driving (50% for maintenance and delivery trucks).

V2G Economic Evaluation – Methodology

Two-step Methodology



- ❑ Annual benefits evaluated using an optimization model
- ❑ Objective: Maximize utility benefits from grid services
- ❑ Constraints:
 - Battery energy dynamics at EV level
 - Power and energy limits of EV battery
 - Energy and battery balance at fleet level

- ❑ Annual benefits received as input from Step 1
- ❑ Other inputs:
 - Variable and fixed operating costs
 - Battery replacement cost
- ❑ Output:
 - Benefits-cost ratio for all stakeholders
 - Identifying most influential variables that make V2G economically viable

Step 2 – Benefits-cost Evaluation

Economic Metrics for Benefit-Cost Evaluation

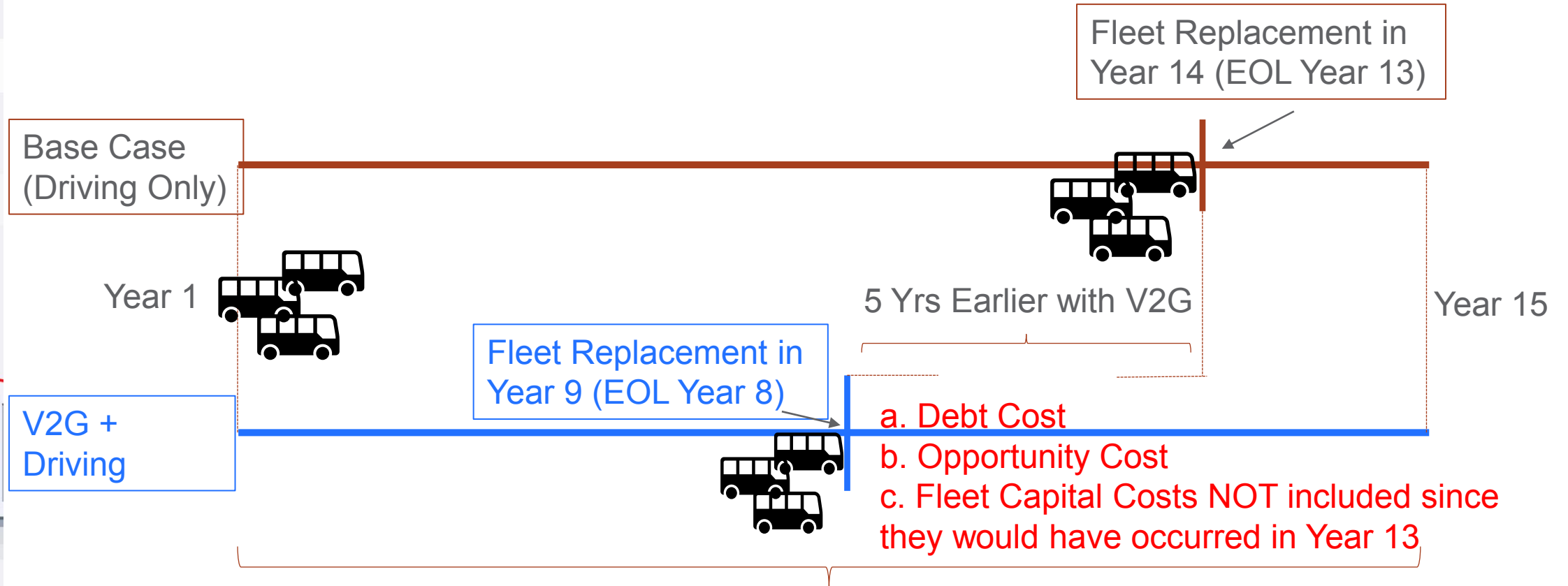
Metric	Perspective	Description
Annualized Net Revenue	Utility	Cost of purchasing from BPA minus revenues from using V2G for various energy services
Annualized Costs	Utility and/or Fleet Owner	The approximate average annual payment necessary for the fleet owner to break even for using V2G in addition to driving.

Assumptions:

- All benefits from V2G go to SnoPUD
- All costs (except fuel charges) are accrued to fleet owner (charger upgrades, additional wear and tear on battery)

Step 2 – Benefits-cost Evaluation

Overview of Costs with & without V2G – Example Scenario



15 Years – All Marginal Operational Costs associated w V2G

Step 2 – Benefits-cost Evaluation

Input Assumptions

Vehicle	Energy Service	Annual Cash Flow - V2G only*		
		Revenue	Charging Cost	Net Revenue
Bus	Energy arbitrage	\$357,854	\$334,498	\$23,356
	Demand charge reduction	\$26,890	\$25,135	\$1,755
	Frequency regulation	\$4,076	\$3,810	\$266
	Spinning Reserve	\$2,237	\$2,091	\$146
Van	Energy arbitrage	\$658,064	\$643,083	\$14,981
	Demand charge reduction	\$46,167	\$45,116	\$1,051
	Frequency regulation	\$7,028	\$6,868	\$160
	Spinning Reserve	\$2,152	\$2,103	\$49
Truck	Energy arbitrage	\$358,147	\$345,107	\$13,040
	Demand charge reduction	\$28,152	\$27,127	\$1,025
	Frequency regulation	\$4,202	\$4,049	\$153
	Spinning Reserve	\$2,005	\$1,932	\$73

*One year only (\$2020). Revenues and costs decline according to degradation rates.

Cost for a 50 Vehicle Fleet (\$2020)	
Bus	\$12,500,000
Van	\$3,500,000
Truck	\$2,083,450

Other Assumptions	
Federal Tax Rate	0.21
Utility Tax Rate	0.039
% Financed with Equity	0.2
% Financed with Debt	0.8
Discount Rate	0.045
Inflation Rate	0.02
Annual Labor Fee Interactive Controllers and Software(40 hrs @\$200/hr)	\$8,000
Variable O&M for Battery Usage (\$/kwh)	\$0.00052

Step 2 – Benefits-cost Evaluation

Cycles and Battery Life

		Annual Cycles With V2G only			
	Cycles Without V2G	Energy arbitrage	Demand charge reduction	Frequency regulation	Spinning Reserve
Bus	191	582	475	192	182
Van	422	664	475	192	183
Truck	401	696	466	190	182

Battery Life: Driving + V2G					
	Battery Life from Driving Only	Energy arbitrage	Demand charge reduction	Frequency regulation	Spinning Reserve
Bus	13	9.15	10.62	13	13
Van	13	6.51	7.88	11.51	11.69
Truck	13	6.44	8.15	11.96	12.13

Step 2 – Benefits-cost Evaluation

Implications for Early Fleet Replacement – Comparison between Arbitrage and Frequency Regulation

Buses Used for Arbitrage		
Battery Life	9 Yrs	
Fleet Replacement Cost in 2031	\$15,237,430	
Present Value	% of Cost	
Foregone Interest on alternative use of equity (4 Yrs)	-\$2,543,513	25%
Debt on Earlier Loan (4 Yrs)	-\$4,326,465	42%
Operating Cost (includes taxes)	-\$3,487,278	34%
Total Costs	-\$10,357,255	

Buses Used for Frequency Regulation		
Battery Life	13 Yrs	
Fleet Replacement Cost in 2035	Net zero	
Present Value	% of Cost	
Foregone Interest on alternative use of equity (4 Yrs)	\$0	0%
Debt on Earlier Loan (4 Yrs)	\$0	0%
Operating Cost (includes taxes)	-\$127,178	100%
Total Costs	-\$127,178	

Results

V2G Economic Analysis			
Vehicle	Service	Required Approximate Annualized Recovery Cost to Fleet Owner (Does not include purchase price of electricity)	Annualized Net Revenue to SnoPUD (includes purchase of electricity)
Bus	Frequency Regulation	\$8,087.24	\$262.18
Bus	Spinning Reserve	\$7,966.01	\$144.07
Bus	Demand Charge Reduction	\$293,469.14	\$1,729.78
Bus	Arbitrage	\$634,715.48	\$23,020.31
Truck	Spinning Reserve	\$30,734.78	\$71.86
Truck	Frequency Regulation	\$30,846.22	\$150.80
Truck	Demand Charge Reduction	\$143,702.08	\$1,010.27
Truck	Arbitrage	\$241,525.49	\$12,852.58
Van	Frequency Regulation	\$46,609.09	\$157.70
Van	Spinning Reserve	\$46,270.00	\$48.66
Van	Demand Charge Reduction	\$199,823.86	\$1,035.89
Van	Arbitrage	\$320,706.93	\$14,765.68

Key Learnings - Economic Considerations

- ❑ Number of cycles drives early replacement cost, the largest part of overall cost due to high fleet replacement cost.
- ❑ Arbitrage consistently has the highest number of cycles and correspondingly highest costs.
- ❑ Frequency regulation and spinning reserve have the lowest cycles and lowest costs.
- ❑ Replacement cost technologies – battery pack replacement should be investigated. [Currently, we're assuming the full value of the vehicle]

Appendix C: PNNL Report on Standards for Vehicle-to-Grid Integration

PNNL- 32661

Evaluation of the Arlington Microgrid Project's V2G Technical Specification vs V2G Standards

March 2022

Siddharth Sridhar, Senior Research Scientist/Engineer
Hawk Asgeirsson, Consultant
Ryan Franks, Senior Engineer
Charlie Vartanian, Adviser

Pacific Northwest National
Laboratory

DISCLAIMER

This report was prepared as an account of work sponsored by an agency of the United States Government. Neither the United States Government nor any agency thereof, nor Battelle Memorial Institute, nor any of their employees, makes **any warranty, express or implied, or assumes any legal liability or responsibility for the accuracy, completeness, or usefulness of any information, apparatus, product, or process disclosed, or represents that its use would not infringe privately owned rights**. Reference herein to any specific commercial product, process, or service by trade name, trademark, manufacturer, or otherwise does not necessarily constitute or imply its endorsement, recommendation, or favoring by the United States Government or any agency thereof, or Battelle Memorial Institute. The views and opinions of authors expressed herein do not necessarily state or reflect those of the United States Government or any agency thereof.

PACIFIC NORTHWEST NATIONAL LABORATORY
operated by
BATTELLE
for the
UNITED STATES DEPARTMENT OF ENERGY
under Contract DE-AC05-76RL01830

Printed in the United States of America

Available to DOE and DOE contractors from the
Office of Scientific and Technical Information,
P.O. Box 62, Oak Ridge, TN 37831-0062;
ph: (865) 576-8401
fax: (865) 576-5728
email: reports@adonis.osti.gov

Available to the public from the National Technical Information Service
5301 Shawnee Rd., Alexandria, VA 22312
ph: (800) 553-NTIS (6847)
email: orders@ntis.gov <<https://www.ntis.gov/about>>
Online ordering: <http://www.ntis.gov>

Evaluation of the Arlington Microgrid Project's V2G Technical Specification vs V2G Standards

March 2022

Siddharth Sridhar, Senior Research Scientist/Engineer
Hawk Asgeirsson, Consultant
Ryan Franks, Senior Engineer
Charlie Vartanian, Adviser

Pacific Northwest National Laboratory

Prepared for
the Snohomish Public Utility District

Pacific Northwest National Laboratory
Richland, Washington 99354

Abstract

This report presents a summary-level comparison between 1) technical specification for the Arlington Microgrid's V2G (Vehicle-to-Grid) setup versus 2) V2G-related standards by the Institute of Electrical and Electronics Engineers and the Society of Automotive Engineers. This case study will inform future efforts to define and specify technical capabilities for V2G products and projects. The use of industry published standards, as they become available and where appropriate, lessens the need for custom case-by-case engineering and thus will lower barriers to designing and implementing future V2G-capable products and projects.

Summary

This report presents a summary-level comparison between 1) technical specification for the Arlington Microgrid's V2G (Vehicle to Grid) setup versus 2) V2G-related standards by the Institute of Electrical and Electronics Engineers (IEEE) and the Society of Automotive Engineers (SAE).

The first part of the report describes a specific V2G demonstration project that provided a basis for investigating how evolving technical standards can be applied to add efficiencies to the development and deployment of V2G products and projects. This case study maps the technical requirements documentation for the Arlington microgrid as a basis to identify those requirements that map to technical standards. Many of the standards cited did not exist when the Arlington Microgrid's V2G scope was developed. This comparison is not a critique of this prior specification; rather the intent is to inform future V2G product and project development and deployment.

The second part of this report focuses on relatively recent industry efforts to develop technical standards that can be applied to V2G products and their application. A major challenge is the need to coordinate efforts across different industries that do not typically interact for development of their respective standards. Specifically, the power industry and one of their major standards developing organization (SDO), the IEEE, and the automotive industry and their major SDO, the SAE. This section summarizes efforts by PNNL staff to coordinate across these two industries in regard to developing new V2G standards. This second part of the report concludes with general observations on the benefits from using technical standards.

Acknowledgments

This project was supported by funding from the Department of Energy, Office of Electricity, Energy Storage Program. The authors of this report would like to thank Imre Gyuk (DOE) and Vince Sprinkle (PNNL). The authors also thank Scott Gibson for coordinating information exchange between the Snohomish Public Utility District's Arlington Microgrid Project and PNNL staff.

Acronyms and Abbreviations

AC	alternating current
AMG	Arlington microgrid
C&S	codes and standards
CCS	combined charging system
CSA	Canadian Standards Association
DC	direct current
DER	distributed energy resource
DOE	Department of Energy
EPS	electric power system
EV	electric vehicle
EVSE	electric vehicle supply equipment
IEC	International Electrotechnical Commission
IEEE	Institute of Electrical and Electronics Engineers
OE	Office of Electricity
PNNL	Pacific Northwest National Laboratory
SAE	Society of Automotive Engineers
SDO	standards development organization
SnoPUD	Snohomish Public Utility District
UL	Underwriters Laboratories
V2G	Vehicle to Grid

Contents

Abstract.....	ii
Summary	iii
Acknowledgments.....	iv
Acronyms and Abbreviations.....	v
Contents	vi
1.0 Introduction	1
2.0 Impact of C&S Development and Adoption.....	3
3.0 Arlington V2G Technical Specification Mapped to Standards	6
4.0 Coordination Efforts Across IEEE and SAE	9
4.1 North American Charging Standards.....	9
4.2 Fleet V2G in North America	12
4.3 Communication to Manage V2G EVs and DERs.....	12
5.0 Conclusions.....	13
6.0 References.....	14
Appendix A – Standards	A.1

Figures

Figure 1. Nissan Leaf EVs Plugged-in at the AMG.....	2
Figure 2. Closing C&S Gaps Decreases Time for a Project to Return a Net Benefit.....	3
Figure 3. Electrical Ratings Specified by SAE J1772 Electric Vehicle and Plug in Hybrid Electric Vehicle Conductive Charge Coupler.....	10
Figure 4. Configuration Diagram for V2G-AC Operation.....	10
Figure 5. Configuration Diagram for V2G-DC Operation	10
Figure 6. System Diagram for EV and Charging Station.....	11
Figure 7. SAE J372 Charging Station System Diagram for V2G-AC	11

Tables

Table 1. Selected Performance Capabilities, Associated Specifications, and Standards.....	6
---	---

1.0 Introduction

With the decreased cost of battery-based energy storage (ES) technologies over the past decade, ES is now viewed as an important element of power grids. In fact, the global adoption of ES in grid space is becoming reality for supporting the increased adoption of renewable energy sources, in addition to offering more capabilities through grid services. As identified in the recent Department of Energy (DOE) ES program planning report, the deployment of ES is expected to increase significantly in the next several years. In part due to similar improvements in the economics, adoption of electric vehicles (EVs) is also accelerating in North America [1].

With this growth in adoption, there is also an interest in tapping into the ability of EVs to offer grid service capabilities like stationary ES units. However, for both stationary and mobile applications, the costs must still be offset by higher value returns. On the one hand, the increased deployments of ES bring several benefits to future power grids. On the other hand, there are several challenges that need to be addressed to support the effective deployment of ES in the future. This report focuses on one such challenge, the codes and standards (C&S) associated with ES implementations, particularly Vehicle-to-Grid (V2G) implementations.

The activity presented in this report was supported by two different programs, the DOE Office of Electricity's (OE's) ES C&S program and the Washington State Clean Energy Fund.

DOE OE ES C&S Program. The PNNL ES Program supports the DOE OE's Advanced Grid Research and Development mission by accelerating discovery and innovation of next-generation storage technologies and tools. The research objectives of the program are focused on enabling greater deployment of ES to improve the resiliency, reliability, and efficiency of the electric grid and supports the four principal challenges identified in the 2013 DOE strategic plan for Grid Energy Storage: cost competitive ES technology, validated reliability and safety, equitable regulatory environment, and industry acceptance [2]. Projects are planned and implemented with industry stakeholders from federal, state, and local governments, electric utilities, developers, national laboratories, and universities to ensure research and development efforts are impactful to public, private, local, and national needs.

The program is designed to advance a portfolio of ES technologies, such as advanced sodium batteries, flow batteries, and power electronics, which have the potential for reduced cost, higher energy and power density, and increased safety and reliability. The program also supports the development of next-generation analysis tools that can determine the size, duration, and location of ES for optimal economic dispatch, and validates these tools with data from regionally deployed ES systems. The program works with the stakeholder community to disseminate technical information through peer-reviewed scientific publications, web-based databases, and safety- and performance-based standards bodies.

For ES systems to be ubiquitously accepted the technology must be demonstrably safe and reliable. This activity is focused on using a scientifically derived knowledge base to develop protocols, improve understanding, and engineer new, safer, and more reliable systems.

Washington State Clean Energy Fund. The program funds development, demonstration, and deployment of clean energy technology. Established in 2013, Gov. Inslee has continued to champion the fund and the legislature again invested capital budget in these grant programs. Program development and deployment is currently underway. The Snohomish Public Utility District's (SnoPUD) Arlington microgrid (AMG), developed through support from the Clean

Energy Fund, features a 1 MW/1.4 MWh lithium-ion battery ES system, a 500 kW alternating current (AC) solar array with smart inverters, and V2G systems shown in Figure 1 [3]. The AMG, designed to operate independently when disconnected from the grid, will help address multiple research questions: (1) how the AMG will be used to demonstrate the applicability of microgrids for disaster recovery, grid resiliency, renewable energy integration and grid support; and (2) how the AMG will support research that demonstrates intelligent solar photovoltaic controllers and V2G systems and their benefit to the grid. PNNL's engagement with the AMG is centered around two key research topics associated with V2G systems: an assessment of the AMG's V2G equipment standards in comparison to current industry standards and an economic assessment of V2G systems to determine potential for long-term benefits to stakeholders.



Figure 1. Nissan Leaf EVs Plugged-in at the AMG

The rest of this report describes the importance of C&S to reducing the cost and complexity of engineering projects in Section 2.0, compares the specifications of the AMG's V2G capability to existing standards in Section 3.0, and highlights coordination efforts between standards development organizations (SDOs) across the energy systems and automotive industries in Section 4.0.

2.0 Impact of C&S Development and Adoption

Gaps in C&S development can lead to a variety of impacts:

- Poorly written requirements can lead to unenforceable code.
- C&S can be overly restrictive for newer technologies that have yet to demonstrate a history or dataset of safe performance.
- Industries or manufacturers seeking to obtain exemptions from the code can erode adoption as jurisdictions amend certain sections or, in some cases, the entire code.
- Providers of risk management tools have difficulty pricing and providing their products, including warranties and performance bonds.
- Financial providers charge risk-premium cost adders or are unable to provide financing at all.

On the other side, C&S with requirements having consensus from stakeholders can:

- Foster the deployment and effective use of products and technologies.
- Lower barriers to adoption.
- Improve safety and reliability.
- Assist in creating markets and establishing customer and user trust.

Gaps in V2G C&S increase the cost, the negative slope of the net cost portion of the graph in Figure 2, and increase the time needed to deploy V2G projects. In Figure 2, the curves from A to C correspond to an environment where C&S are well developed to a less-developed C&S environment resulting in relatively more time for a deployed project to reach net positive economic benefit. The negative-to-positive change in slope corresponds to robust C&S versus weaker C&S being available to all stakeholders, with projects going into service and delivering net positive returns sooner versus later, respectively.

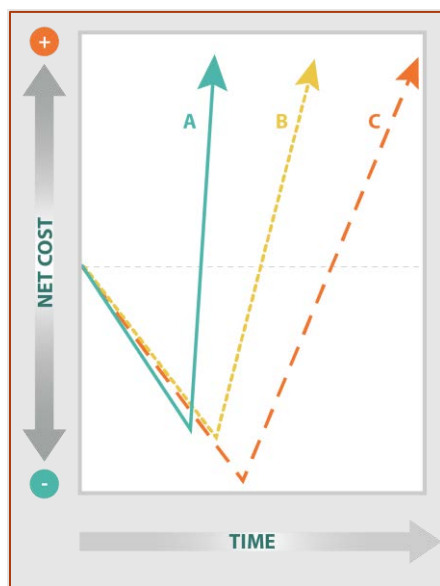


Figure 2. Closing C&S Gaps Decreases Time for a Project to Return a Net Benefit

Impacts due to gaps in C&S affect all phases of a V2G project's lifecycle, from design, financing, permitting, construction, commissioning, operation, and decommissioning. In addition, C&S are developed to address problematic, unclear, or conflicting requirements and fill gaps as V2G technologies, components, and use cases evolve and mature. V2G products and projects, in some respects, face an adoption curve similar to stationary ES. A prior DOE-sponsored project gathered input from traditional risk products and finance providers serving more established technologies (e.g., wind, gas generation) to inform industry on lowering barriers to ES projects achieving bankability and getting financed. The resulting report, published in 2019, is a "best practice guide" that includes guidance on how ES C&S can help facilitate the use of risk and financial tools needed for the development of larger ESS projects [4].

C&S will enable V2G by helping overcome technology hurdles including aggregation of loads, data commonality, establishing levels of critical information exchange, cybersecurity, electrical and fire safety, and interoperability.

One aspect of V2G development that is unique is that it involves the close cooperation between several industries that do not have a long history of interaction, including electrical equipment manufacturers making electric vehicle supply equipment (EVSE), vehicle original equipment manufacturers and some vehicle component suppliers, and various electrical load-serving entities (e.g., utilities, cooperatives, and municipal power systems), plus digital payment and communication network providers in many instances. Furthermore, many of these stakeholders operate globally but must adhere to local, regional, and national regulations. To have efficiency in design and production, cooperation is needed across industries, regions, and nations.

While not mutually exclusive and completely exhaustive, there are three types of V2G interactions and business cases that cover most scenarios: independent and privately owned EVSE, networked EVSE charging infrastructure (including commercial fleets), and utility-owned EVSE. Those three areas may operate differently and have different levels of information exchange and operations. For instance, networked charging infrastructure could operate as a load and demand resource and respond to grid signals to provide ancillary services across different geographic areas. Utilities may also perform these grid services with their EVSE but may have stricter control measures in place to achieve operational objectives.

Regarding safety, codes including the National Electric Code (National Fire Protection Association NFPA 70), National Electrical Safety Code IEEE C1, National Fire Code (NFPA 1), and International Fire Code must adapt to V2G and call upon relevant standards. The most important life safety issues are the prevention of back feed electricity to the premise or distribution circuits and safety regarding the interaction of electricity and water or other environmental factors (i.e., many V2G charging locations are located outdoors). In addition to the development of code language that enables V2G, local authorities having jurisdiction must proactively adopt the model codes listed above for them to be enforceable compliance requirements. Model codes are typically adopted on 3-year code cycles, meaning that from the initiation of a change in language, it can be 3 to 6 years, or historically more, for such changes to become true compliance requirements.

When available and adopted, robust C&S can reduce soft cost components by streamlining all stages of a product or project lifecycle. This cost reduction is among the benefits motivating SDO communities, their customers, and members, including Underwriter Laboratories (UL), Canadian Standards Association (CSA), International Electrotechnical Commission (IEC), Society of Automotive Engineers (SAE), and Institute of Electrical and Electronics Engineers (IEEE) to close

gaps in C&S for ES by updating existing C&S and developing new C&S. Several examples of C&S published or in development include:

- CSA C22.2-340 “Battery Management Systems”
- IEC 61851 Suite “Electric vehicle conductive charging system”
- IEC Joint Working Group (TC 69 WG 15) “Distributed energy storage systems based on Electrically Chargeable Vehicles”
- IEEE 1547 “Standard for Interconnection and Interoperability of Distributed Energy Resources with Associated Electric Power Systems Interfaces”
- IEEE 1547.1 “Standard Conformance Test Procedures for Equipment Interconnecting Distributed Energy Resources with Electric Power Systems and Associated Interfaces”
- IEEE P2686 “Recommended Practice for Battery Management Systems in Energy Storage Applications “ IEEE P1547.9 “Guide to Using IEEE 1547 for Interconnection of Energy Storage Distributed Energy Resources with Electric Power Systems”
- IEEE P2688 “Recommended Practice for Energy Storage Management Systems in Energy Storage Applications”
- SAE J3072 “Interconnection Requirements for Onboard, Utility-Interactive Inverter Systems
- SAE J2836/3 “Use Cases for Plug-in Vehicle Communication as a Distributed Energy Resource”
- UL 1741 “Inverters, Converters, Controllers, and Interconnection System Equipment for Use with Distributed Energy Resources”
- UL 2202 “Standard for Electric Vehicle (EV) Charging System Equipment”
- UL 2594 “Standard for Electric Vehicle Supply Equipment”
- UL 9741 “Outline of Investigation for Electric Vehicle Power Export Equipment”

In addition, communication protocols in use for V2G include:

- IEEE 2030.5/SAE J2847/3 “Communication for Plug-in Vehicles as a Distributed Energy Resource”
- OCPP “Open Charge Point Protocol”
- OpenADR
- ISO 15118 “Vehicle to grid communication interface”

3.0 Arlington V2G Technical Specification Mapped to Standards

As discussed in Section 2.0, availability and use of technical standards add efficiency to projects. For relatively mature power equipment and systems, the power industry has well-established practices for applying standards where appropriate to help assure that projects deliver minimum acceptable performance, reliability, and safety. The complimentary outcome of higher project efficiency (reduced time and cost to design and build) is relative to projects for which each capability or characteristic is custom defined in the buyer’s procurement specification, and then custom designed in the seller’s engineered and built solution.

At present, V2G products and their application are not at the mature stage of industry adoption and use; thus, there are not yet comprehensive and universally-adopted industry standards and standardization (e.g., formalized best practices per industry experience) to support early V2G projects. SnoPUD’s project is a useful early reference point. For this report, PNNL staff reviewed SnoPUD’s procurement specification and the seller’s product specification [5]. The result of the review is Table 1, which maps core equipment performance requirements, typically specified for a power equipment purchase, versus potentially applicable existing technical standards.

Table 1. Selected Performance Capabilities, Associated Specifications, and Standards

	Equipment Performance Requirement	Project or Product Specifications	Potentially Applicable Standards
Power Ratings & Interfaces	Power Rating, KVA	“CHAdeMO 1.0 and CCS level 2 DC charging standards”	SAE has standards that set power capacity for various defined charging levels. See Section 3.0.
	Ampacity, A Voltage, V		For AC voltages, ANSI C84.1 for nominal and allowable ranges. Can apply to both charging (AC supply to load) and discharging (AC output by resource). [6]
Interoperability Capabilities & Interfaces	Communication Transport Layer(s)		IEEE 1547 for discharging (resource). 1547 cites TCP/IP over ethernet and RS-485
	Communication Protocol(s)		IEEE 1547 for discharging (resource). 1547 cites Modbus, SEP32 (IEEE 2030.5), and DNP 3 (IEEE 1815)
	Minimum/Required Information Content	“The V2G Solution must support communication standards, such as IPv6, 802.15.4e and 802.15.4g.”	MESA-Device, Sunspec Modbus models
	Cyber security	IEEE 1686-2007 Security for Intelligent Electronic Devices (IEDs)	None in addition to the spec’s list

	Equipment Performance Requirement	Project or Product Specifications	Potentially Applicable Standards
		NERC CIP 002-009 Cyber Standards for the bulk power system	
		NIST Special Security Publication SP 800-53 & NIST SP 800-82. Cyber Security Standards and guidelines for Federal Information Systems for application in Bulk Power System	
		FIPS140-2 Security Requirements for Cryptographic Modules	
Interconnection Requirements	General	“Operation of the V2G charger(s) shall not interfere with the facility’s overall compliance with Interconnection Requirements at the PCC”	
	Anti-Islanding		IEEE1547 for discharging (resource)
	VAR capacity and voltage control modes Grid Disturbance Ride Through		IEEE1547 for discharging (resource) IEEE1547 for discharging (resource)
Power Quality	Harmonic Limits	“Operation of the V2G charger(s) shall not cause degradation of power quality when operating (e.g., measurable harmonic injection must be within IEEE 519 limits)”	IEEE 519 for charging (load) IEEE 1547 for discharge (resource). 1547 references and extends 519.
	Maximum temporary overvoltage or undervoltage		IEEE 1547 for discharge (imparted by resource) Information Technology Industry Council voltage curve for charging (load withstand capability)
Other	Fire Safety		UL 9540 and UL 9540A, if the V2G charger has integrated stationary storage
	Grounding		IEEE 142 [7]
	Metering		IEEE 1377 [8]
	Arcflash and associated energy and PPE levels Recovery, Reuse or Recycling at end of life		IEEE 1584 [9] NFPA 70E Unknown, possible industry gap

(Bold italicized standards were in the project or product specification)

Table 1 is a subset of the full specification. There is potential to further expand this mapping of existing standards versus V2G product and project requirements. Using available standards will 1) further add efficiencies and streamline the design, purchase, and deployment of early V2G equipment and projects; and 2) inform SDOs as they evaluate the need for and develop V2G-specific standards.

While none of the cited standards in the table are specific to V2G, it is useful to note that many existing and established standards as listed above can be applied to V2G products and projects now. Thus, in the interim, while best practices are being identified and documented for future standardization of V2G equipment and application, there are existing general standards that can be applied to improve the efficiency and success of V2G projects. One active example of leveraging existing grid (IEEE) standards for V2G is SAE's work to coordinate their industry's V2G-related standards with relevant IEEE Standards, for both onboard and outboard charging equipment. This is discussed further in Section 4.0.

4.0 Coordination Efforts Across IEEE and SAE

For V2G to be readily available and accepted by regulatory organizations, SDOs that develop standards for the electric power system (EPS) and automobile need to coordinate standards development. The IEEE develops standards for the EPS and SAE develops standards for the automobile. These two SDOs are coordinating in their various working groups to make sure that standards pertaining to V2G are harmonized. This coordination allows standard setting organization such as UL to develop testing and safety standards that allows V2G products to be tested and listed and then connected as a distributed energy resource (DER) to the EPS. UL is developing the UL 1741 SC standard for V2G-AC-enabled EVSE. Members of the IEEE and SAE working groups, who worked on the V2G standards development, are working together with UL to develop this standard [9]. Once UL 1741 SC is published, V2G-AC-enabled products that comply with industry standards can be produced, eliminating the need for customization.

4.1 North American Charging Standards

Three light and medium-duty electric vehicle automotive charging connectors/couplers standards exist in North America: The Tesla connector (exclusively for Tesla vehicles), CHAdeMO, and combined charging system (CCS). There are other EV charging standards for transportation buses and medium/heavy-duty trucks that are evolving that are discussed in Section 4.2. The Tesla, CHAdeMO, and CCS couplers can be used to charge EVs at 120 volts directly from a typical 120-volt outlet that is limited to 15 or 20 amps. For higher charge rates or bidirectional operation, EVSE is required by standards.

The Tesla connector is presently not V2G-enabled. The CHAdeMO standard, used currently in North America by Mitsubishi and Nissan, has the capability for bidirectional energy flow and is used for this purpose in Japan. But the bidirectional capability has not been deployed in North America beyond testing scenarios. In fact, Nissan will void automobile warranty if it is used for V2G. However, the CHAdeMO standard connector is being phased out in North America. This means that all future non-Tesla mass manufactured light-duty EVs sold will use the CCS standard. Nissan announced in 2020 that they will abandon the CHAdeMO charger in favor of the CCS standard in future EV products, starting with their Ariya EV arriving in 2022 [10]. At the time of writing of this report, Mitsubishi is the only EV original equipment manufacturer outlier. Electrify America has also announced they will no longer include the CHAdeMO standard on their charging stations starting in January 2022 [11].

The CCS charge coupler is defined by the SAE J1772 Standard that specifies the general physical, electric, functional, and performance requirements to facilitate conductive charging of EVs in North America [12]. The electrical ratings for the SAE J1772 are provided in Figure 3.

Charge Method	Voltage (AC V)	Phase	Max. Current (A, continuous)	Branch Circuit Breaker Rating (A)	Max. Power (kW)
AC Level 1	120	1-phase	12	15 (min.)	1.44
			16	20	1.92
AC Level 2	208 to 240	1-phase	≤ 80	Per NEC 625	Up to 19.2

Charge Method	EVSE DC Output Voltage (DC V)	Max. Current (A)	Max. Power (kW)
DC Level 1	50 to 1000	80	80
DC Level 2	50 to 1000	400	400

Figure 3. Electrical Ratings Specified by SAE J1772 Electric Vehicle and Plug in Hybrid Electric Vehicle Conductive Charge Coupler

The SAE J3072 Standard establishes the requirements for an EV-integrated inverter system that connects to the EPS through a conductively coupled EVSE [13]. This standard also defines the communication between the EV and EVSE, required for the onboard inverter function to be configured and authorized by the EVSE for discharging at a site. Figure 4 and Figure 5 show pictorial representations of V2G-AC and V2G-direct current (DC) configurations [14]. The main difference between V2G-AC and V2G-DC is the location of the inverter that connects to the EPS.

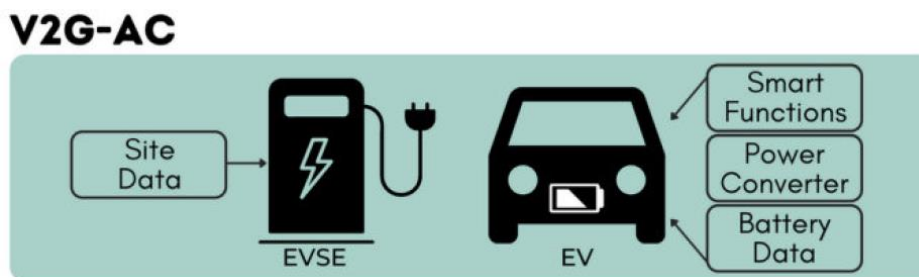


Figure 4. Configuration Diagram for V2G-AC Operation

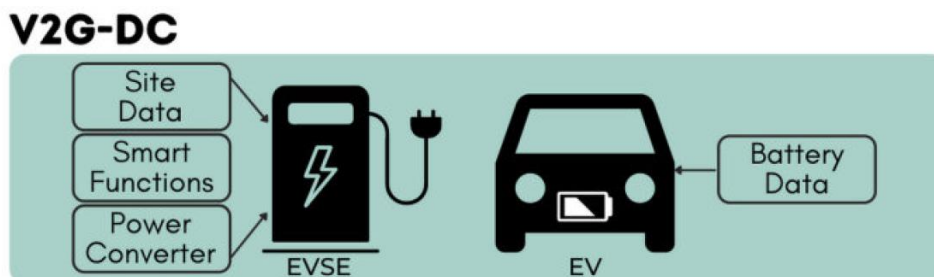


Figure 5. Configuration Diagram for V2G-DC Operation

In 2021 SAE J3072 was updated to include the requirements that an EV with bidirectional onboard inverter must meet in IEEE 1547-2018 and IEEE 1547.1-2020. The update also specifies that a charging station will be the DER management entity to facilitate bidirectional operation between the EPS and the EV. The V2G-AC charging station will act as a gateway between the EPS and EV to authorize operation of an EV with an onboard grid interactive inverter that complies to IEEE 1547. With this recent update of SAE J3072, an EV with an onboard bidirectional inverter and a bidirectional charging station will comply to IEEE 1547-2018

and be compliant to IEEE interconnection standards to perform V2G-AC operation. See Figure 6 and Figure 7 for system diagrams.

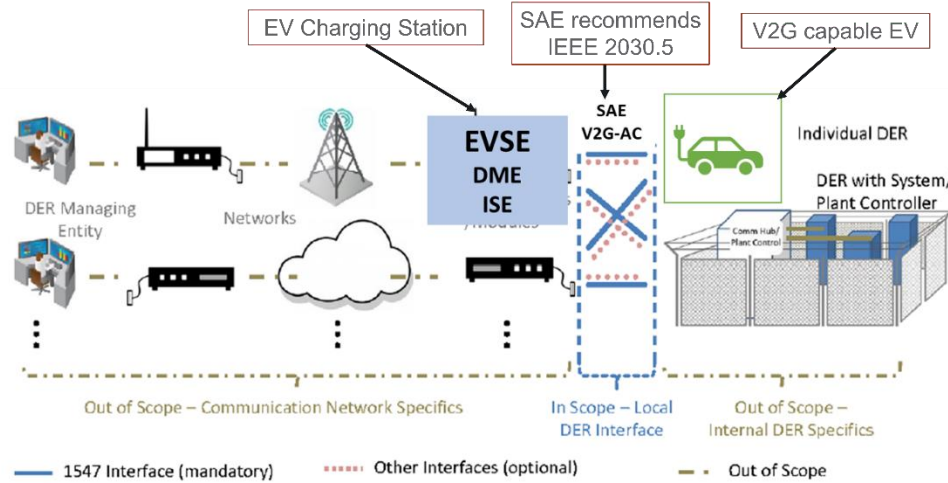


Figure 6. System Diagram for EV and Charging Station

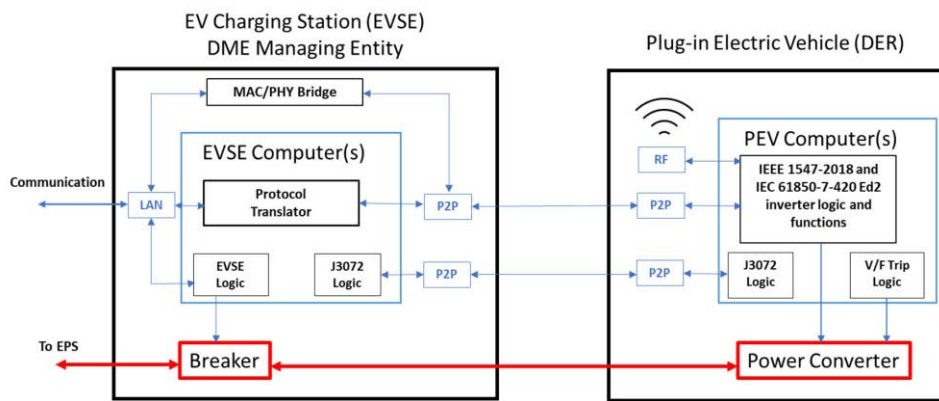


Figure 7. SAE J3072 Charging Station System Diagram for V2G-AC

It should be noted that for automobiles to be V2G-AC capable, the onboard EV grid interactive inverter must be compliant to SAE J3072, and in turn IEEE 1547, to be able to operate as V2G-AC EV. As of this report there are no mass-produced automobiles available for purchase with that capability.

For a charging station, or EVSE, to be installed in public facilities for bidirectional operation it needs to be tested and listed. There is a UL working group, that includes representatives from IEEE and SAE that were involved in developing V2G standards, who are in the process of updating UL 1741 Interconnection Standard to incorporate SAE J3072 requirements such that V2G-AC grid interactive charging stations can be approved for public use. The updated standard will be designated as UL 1741 SC and is expected to be published in 2022.

With this recent development and the coordination of SDOs, any EV with an onboard bidirectional inverter that is compliant to SAE J3072 and in turn IEEE 1547 will be able to connect to all charging stations that are UL 1741 SC listed and interact with the EPS and perform V2G-AC operation. Grid connected V2G-DC can be accepted with today's standards if the off-board EV charger that contains the inverter is listed to UL 1741 and is accepted by the

local electric utility as a functioning DER. Most DC charging of EVs is performed at DC fast charging stations (gas station model) and is not conducive for V2G-DC operation.

4.2 Fleet V2G in North America

Today, most electric fleet vehicles and electric school buses use the SAE J1772 coupler for charging. The choice of AC or DC charging is dependent on manufacturing offering and customer requirements. If the fleet EVs incorporate SAE J3072 requirements for bidirectional operation, they will be able to perform V2G-AC with a charging station that is compliant to UL 1741 SC. For DC charging, if the grid connected inverter is compliant to UL 1741, it has the capability to perform V2G-DC operation. In general, DC charging is not conducive to V2G-DC because the aim of DC charging is quick or fast charging to allow EVs to continue their operation, such as transit buses and fleet vehicles that have long operation periods. There is another SAE standard that can be used by medium-duty EVs that incorporates three-phase 480 V_{ac} or DC. That standard is SAE J3068, also referred to as Type B1, and it is required to meet the new SAE J3072 requirements. The SAE J3068 system is not widely used because the SAE J1772 CCS coupler rating overlaps many of the SAE J3068 ratings.

For electric transit buses there is an SAE J3105 recommended practice for automated connection devices that mate chargers with electric buses. The SAE J3105 is for roof-mounted charging, usually with a vehicle-mounted pantograph. Transit buses can incorporate opportunity charging during their route or at a bus depot. The SAE J3105 recommended practice does not incorporate V2G functionality.

Another standard that is in the early draft phase is SAE J3271 Megawatt Charging System Standard. This standard is expected to be developed over the next two years and to be published in early 2025. This proposed standard is geared to high-power charging, up to 1,500 V_{DC} at 3,000 A, of heavy-duty vehicles, ships, airplanes, farm equipment, and any equipment requiring very high charge rates that do not currently exist. This standard will incorporate V2G functionality.

4.3 Communication to Manage V2G EVs and DERs

Electric utility communication and cybersecurity for EVs is still evolving and is very dependent on utility requirements, end-use systems, and equipment manufacturers. For large DER systems that have a single point of interconnection, utilities generally use their preferred communication standard that are often DNP3 or IEC 61850. The challenge going forward is how to manage many dispersed small DER/EV systems and aggregators. There are many options in this space such as OpenADR and IEEE 2030.5 Standard for Smart Energy Profile Application Protocol. There is growing interest by electric utilities to use IEEE 2030.5 to communicate with DER and EV systems and potential aggregators who are participating in the energy markets.

5.0 Conclusions

This adequacy assessment provided in this report is a baseline from which to evaluate market-specific needs in terms of further development of C&S and to support the adoption and use of ES technologies, products, and systems. There remain significant challenges and opportunities in all markets for development and application of C&S specific to stationary and mobile ES systems. Collaborative efforts between SDOs from both the power and automotive industries are critical to overcome these challenges. Current progress between these SDOs shows promise toward the development of effective C&S that enable seamless integration and interaction between EVs and the EPS.

6.0 References

- [1] U. D. o. Energy, "Energy storage program planning document," 2011.
- [2] U. D. o. Energy, "Grid Energy Storage," 2013.
- [3] S. Gibson and A. Swaney, "Lessons from the Microgrid," *T&D World*, September 2019.
- [4] R. Baxter, "Energy Storage Best Practice Guide," 2019.
- [5] S. P. U. District, *Request for Proposal No. DOC1351248316 Equipment and Support Services for Implementing the Vehicle to Grid (V2G) Demonstration Project at the Arlington Microgrid*, 2018.
- [6] IEEE, "IEEE 142-2007 - IEEE Recommended Practice for Grounding of Industrial and Commercial Power Systems," IEEE, 2007.
- [7] IEEE, "IEEE Standard for Utility Industry Metering Communication Protocol Application Layer (End Device Data Tables)," IEEE, 2012.
- [8] IEEE, "IEEE Guide for Performing Arc-Flash Hazard Calculations," IEEE, 2018.
- [9] U. Laboratories, "Inverters, Converters, Controllers and Interconnection System Equipment for Use With Distributed Energy Resources," Underwriters Laboratories, 2021.
- [10] Nissan, "2023 Nissan Ariya," Nissan, 2022. [Online].
- [11] E. America, "National ZEV Investment Plan:," 2021.
- [12] S. o. A. Engineers, "SAE Electric Vehicle and Plug in Hybrid Electric Vehicle Conductive Charge Coupler," 2017.
- [13] U.-I. I. S. Interconnection Requirements for Onboard, "Society of Automative Engineers," 2021.
- [14] M. Mafazy, "Paving the Way: Vehicle-to-Grid Standards for Electric Vehicles," Interstate Renewable Energy Council, 2022.

Appendix A – Standards

The references below include standards cited in the report, as well as other standards and industry references and industry specifications that may be useful to the reader.

1. IEC Standard TS 62933-3-1. Electrical Energy Storage (EES) systems – Part 3-1: Planning and performance assessment of ESS systems – General specification. International Electrotechnical Commission.
2. IEC Standard 62933-2-1. Electrical energy storage (EES) systems – Part 2-1: Unit parameters and testing methods – General specification, Ed. 1.0, 2017-12.
3. IEC Standard 62933-2-2. Electric Energy Storage Systems – Part 2-2: Unit parameters and testing methods – Applications and Performance testing. International Electrotechnical Commission.
4. IEC Standard TS 62933-3-1. Electrical Energy Storage (EES) systems – Part 3-1: Planning and performance assessment of electrical energy storage systems – General specification. , International Electrotechnical Commission.
5. IEC Standard 62933-1. Electric Energy Storage Systems – Part 1: Vocabulary. International Electrotechnical Commission.
6. IEC Standard TS 62933-5-1:2017. Technical Specifications – Electrical energy storage (EES) systems – Part 5-1: Safety considerations for grid-integrated EES systems – General specification. International Electrotechnical Commission.
7. IEC 62933-5-2: 2020 PRV (Pre-release version). Electrical energy storage (EES) systems – Part 5-2: Safety requirements for grid-integrated EES systems – Electrochemical based systems. International Standard, International Electrotechnical Commission.
8. IEC Standard TR 62933-4-200/Ed.1. Greenhouse gas (GHG) emission reduction by electrical energy storage (EES) systems. International Electrotechnical Commission.
9. IEEE Standard 1679. IEEE Recommended Practice for the Characterization and Evaluation of Emerging Energy Storage Technologies in Stationary Applications. 2010. <https://standards.ieee.org/standard/1679-2010.html>
10. IEEE Draft Standard P2868, approved project scope (PAR). IEEE Recommended Practice for Battery Management Systems in Energy Storage Applications. , September 27, 2018. <https://standards.ieee.org/project/2868.html>
11. MESA-ESS(DER) draft specification, Modular Energy Systems Architecture (MESA) Alliance. December 2018. <http://mesastandards.org/mesa-downloads/>
12. MESA-Device specification, Modular Energy Systems Architecture (MESA) Alliance. <http://mesastandards.org/mesa-device/>
13. Conover D, et al. Protocol for Uniformly Measuring and Expressing the Performance of Energy Storage Systems. Pacific Northwest National Laboratory and Sandia National Laboratory for the U.S. Dept. of Energy Office of Electricity. PNNL-22010 Rev. 2 / SAND2016-3078 R. April 2016.
14. Mongird K, et al. Energy Storage Technology and Cost Characterization Report. Pacific Northwest National Laboratory for the U.S. Dept. of Energy. PNNL-28866. July 2019, <https://energystorage.pnnl.gov/pdf/PNNL-28866.pdf>

15. Westlake B and Thompson J. Energy Storage Integration Council (ESIC) Energy Storage Test Manual. 3003013530, Technical Update. December 2019.
16. Kaun B, et al. ESIC Energy Storage Technical Specification Template v3.0. EPRI Product 3002013531.
17. Bhattari, B., Franks, R., and Vartanian, C., Energy Storage Codes and Standards Adequacy Assessment, Pacific Northwest National Laboratory. PNNL – 32049. October 2021.

Pacific Northwest National Laboratory

902 Battelle Boulevard
P.O. Box 999
Richland, WA 99354
1-888-375-PNNL (7665)

www.pnnl.gov

Appendix D: CIGRE Paper on V2G

C6 - Active Distribution Systems and Distributed Energy Resources
PS 3 - Aggregated DER for enhancing resilience, reliability, and energy security
of distribution systems

A microgrid platform for V2G: Lessons learned from the Arlington Microgrid

J. GLASSMIRE*¹, S. GIBSON², R. SMITH¹, C. KEERTHISINGHE³

¹ Hitachi Energy, ² Snohomish County Public Utility District, ³ University of Washington
United States

john.glassmire@hitachienergy.com

SUMMARY

One electric utility in the US Pacific Northwest, in a look toward the long-term needs of the region, has developed a state-of-the-art microgrid combining community solar photovoltaic generation, an advanced grid-forming battery energy storage system (BESS), and vehicle-to-grid (V2G) technology. This microgrid demonstrates the promise of an increasingly electrified future—from grid resiliency to V2G integration to an ability to run on 100% renewable power. Commissioned in 2022, the project represents a critical milestone in Snohomish County Public Utility District's (PUD) journey to maximize the value of grid edge technologies across their service territory.

One primary challenge that the microgrid addresses is the challenge of V2G integration and interoperability. Microgrid approaches can reduce the complexity and streamline the two-way service between the vehicle and grid. They also offer reinforcing benefits, where the vehicles can act as distributed energy resources (DER) for the microgrid and beyond, and the microgrid can serve as a resilient hub for ensuring power for the electric vehicles. The paper provides insight into strategies used, as well as showcases the benefits to the vehicle fleet, the microgrid, and the utility network. Lessons learned from the implementation are distilled and highlighted. The paper also presents the architecture and demonstrates measurable impacts with measured data.

In addition to the hardened V2G infrastructure, the microgrid host two facilities critical to the PUD operations, including a new utility office. Both facilities benefit from failsafe and secure power provided by the microgrid, enabling the PUD to meet critical objectives for disaster response. This capability allows the site to act as an emergency operations center and critical response hub during disaster events, providing utility resiliency against earthquakes that are common in the area, as well as risk reduction against increasingly severe weather events that are expected due to climate change.

Interoperability of components was a key factor in the microgrid design. A central strategy to address this has been compliance with the Modular Energy Storage Architecture (MESA) open standard to streamline physical, electrical, and communication interconnection of energy storage systems. MESA seeks to accelerate the interoperability of distributed energy resources, with a focus on utility-scale energy storage. The MESA-compliant BESS in the Arlington Microgrid complies with IEEE 1547 and California Rule 21 as well as additional market-based functions to ensure safe, reliable, and efficient operations for the utilities grid.

Microgrid projects like the Arlington Microgrid are helping to demonstrate the symbiotic benefits of pairing electric vehicles and locally generated solar. A microgrid also addresses the inter-related

dependencies between transportation, integrated vehicle charging solutions, and the increasingly renewable backbone of the electric grid. For example, it allows clean solar energy stored in electric vehicles to provide ancillary and energy services necessary to integrate high penetrations of solar. A successful microgrid, much like energy storage investments, bundles together a range of values at the grid edge. This paper illustrates how the value of each asset stacks into a successful business case for the utility, by providing critical backup power from hybrid operation of solar, BESS, and V2G; using the BESS to stabilize the network and manage peak demands; and providing a platform for renewables and electric vehicles.

KEYWORDS

Microgrid - Vehicle to Grid - V2G - Reliability - Resiliency - Battery - BESS - Community Solar - Hybrid - Grid Edge - Interoperability

1. INTRODUCTION

Snohomish County Public Utility District (PUD), a public electric utility, developed and constructed a grid-connected microgrid (MG) at its operations center in Arlington, WA. The Arlington Microgrid (AMG) serves loads for the local PUD facilities, including the Clean Energy Center (CEC), operations support infrastructure, and the future North County Local Office. The grid edge solutions also function together as a demonstration hybrid microgrid that operates a battery energy storage system (BESS), solar photovoltaics (PV), and electric vehicle charging infrastructure (EVCI) together with back-up generation. Like any microgrid, it includes “electricity distribution systems containing loads and distributed energy resources, (such as distributed generators, storage devices, or controllable loads) that can be operated in a controlled, coordinated way either while connected to the main power network or while islanded” [1]. In addition, the microgrid automation and controls, together with the advanced grid forming (GFM) power conversion system for the BESS supports seamless transitions from operation supporting the wider PUD grid to resilient, reliable operation as an electric island. A key innovation of the project is in its Vehicle Grid Integration (VGI) that enables the microgrid to use the batteries in the electric vehicles connected to the EVCI as a resource that can both import power from and export power and services to the microgrid. Vehicle-to-grid (V2G) capability from the EVs provides unique energy services for PUD including expanded resilience, renewable integration, and flexibility. More information on the AMG can be found in [2]

The AMG was developed with significant investment from the Washington State Clean Energy Fund, which has funded the “development, demonstration and deployment of clean energy technologies” in Washington state since 2013 [3]. The goals of the project are:

- Provide services to the PUD grid, including energy arbitrage and demand reduction,
- Provide resilient and reliable power to critical microgrid loads, including seamless islanding while regulating voltage and frequency, particularly for disaster recovery [4]
- Renewable integration, including solar smoothing during grid connected operation and running the microgrid with 100% renewable power,
- Deploy one of the first V2G installations in the United States,
- Serve as platform for research into microgrids and other grid edge technologies [5],[6]
- Support the energy transition, including helping public utilities use new technology and educating the public on the future of energy.

2. ARLINGTON MICROGRID ARCHITECTURE

The AMG’s major local supply assets include 500 kW_{AC} of solar PV, 1 MW / 1.4 MWh PowerStore BESS, a 350 kW back-up genset, 350 kW load bank, and two bi-directional 6 kW electric vehicle chargers. The e-mesh Control and SCADA manages and coordinates the hybrid operation of the microgrid. These assets are spread across two 480 V feeders, which step up into the major site distribution feeders at 12 kV. There are two redundant 12 kV circuit breakers that serve as the common point of interconnections with the rest of the PUD grid. The microgrid load feeders off the redundant breakers branch into sub-feeders dependent on the criticality of the loads on each feeder, ensuring multiple layers of redundancy for reliability and resiliency. A simplified single-line diagram of the overall MG electrical layout is shown in Figure 1, including indication of the critical loads that are prioritized during resiliency events. Portions of the Clean Energy Center are prioritized on the critical circuit; during an extended grid disturbance some of the circuits will remain energized while others are curtailed to extend resiliency and maximize the operation on solar generation.

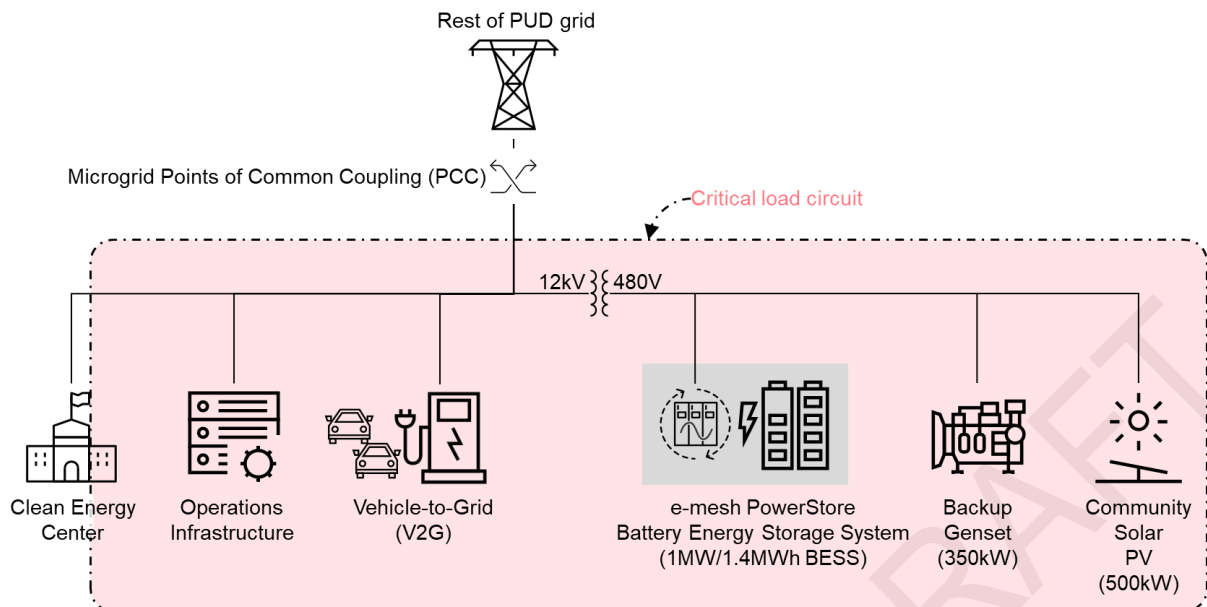


Figure 1 : Simplified single-line diagram of the major microgrid assets and loads

The major assets are shown in Figure 2. The community solar PV array is on the right, with the major microgrid equipment in a vertical line in the middle. From bottom to top, there is a cluster of PV switchgear, transformers, and field control units, then 480V switchgear in the middle, followed by back-up genset and the BESS at the top of the line. The distributed network is entirely underground in duct banks. The Clean Energy Center is shown in the upper left.



Figure 2: Aerial view of the major assets in the Arlington microgrid

3. INCREASING RESILIENCE WITH VEHICLE-TO-GRID (V2G)

The V2G electric vehicle charging interface (EVCI) system features two bi-directional electric vehicle chargers each interface with a light-duty EV. There are two EVs that typically connect to the microgrid, a 2019 Nissan Leaf with 40 kWh battery and a 2020 Nissan Leaf with 62 kWh battery. The batteries in the EVs can be used either to operate the vehicle or,

when connected to the microgrid, discharge to provide energy and energy services to support the microgrid and grid. Figure 3 shows both electric vehicles and the bidirectional chargers that connect them to the PUD MG.



Figure 3 : These light-duty electric vehicles charge and discharge power into the Arlington microgrid and PUD grid

The EVs are standard, commercially available vehicles that have not been modified to perform grid support, and this application is within the EV manufacturer’s specification.

PUD communicates with the Arlington microgrid by a mixture of human operator control and automated control through the local communications network. The automated control communications for V2G are through MQTT, a lightweight messaging protocol common in Internet of Things (IoT) applications.

Figure 4 shows measured results of BESS and EV performance from the Site Acceptance Test, providing a sample of V2G resiliency automation for the AMG while islanded.

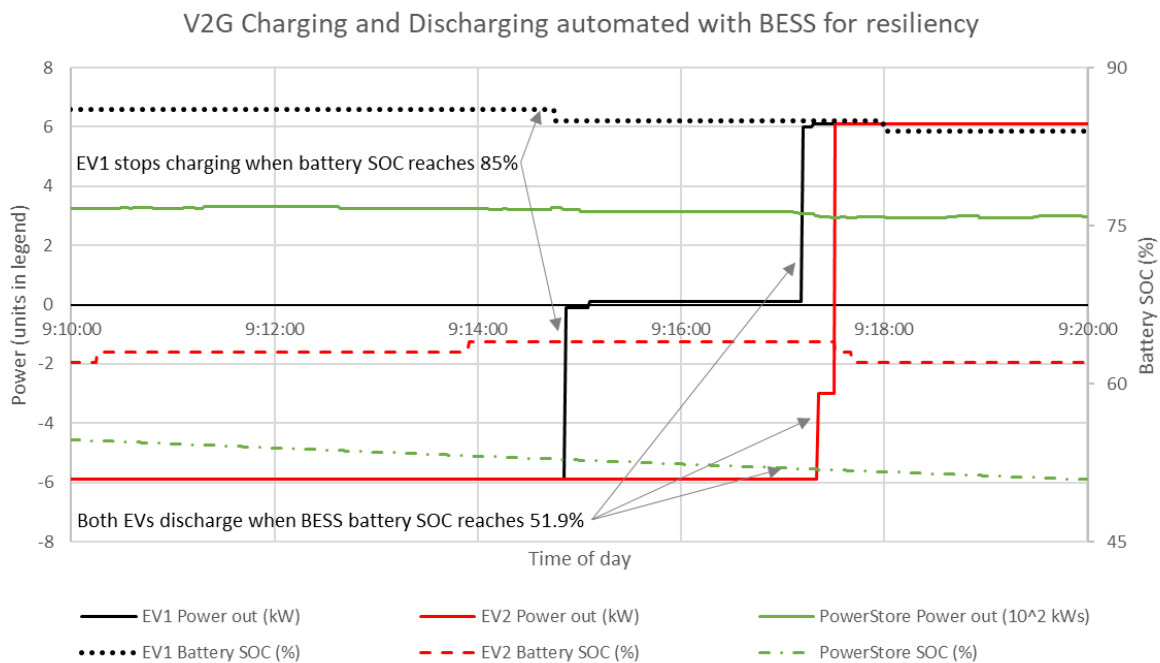


Figure 4 : V2G charging and discharging to support BESS resiliency during Site Acceptance Testing (Jan 19, 2022)

The solid lines are the power discharged and charged from the two V2G EVCI and the BESS, whereas the dashed lines represent the state of charge (SOC) of their respective batteries. For all three assets, a positive value indicates the amount of power discharged from the asset to the microgrid, although the BESS units are displayed in hundreds of kW. The average BESS discharge is 315 kW over the ten-minute plot. EV1 discharges 6 kW until its battery reaches 85% SOC at 9:15am, and then begins to discharge 6 kW when the BESS battery SOC drops to 51.9% just after 9:17am. EV2 does not reach the 85% SOC threshold, so its EVCI only discharges when the BESS SOC reaches the 51.9% threshold.

4. COMMUNICATIONS AND STANDARDS

The communications for the distributed energy resources (DER) in the Arlington microgrid, including the BESS, are all compliant with the Modular Energy System Architecture (MESA) open standard for energy systems. The MESA standard “combines two international standards: IEC 61850 and IEEE 1815 (DNP3) by mapping the IEC 61850-7-420 semantic data model standard for DER to the widely-used IEEE 1815 (DNP3) protocol standard.” [7]. [8] provides more information on MESA. Together, these create an interoperable profile of DER functions, monitored information, and control commands. The BESS and its components, as well as Microgrid Controls, Microgrid SCADA, DERMS, and PUD SCADA are all MESA compliant.

A simplified communications schematic with major protocols is shown in Figure 5.

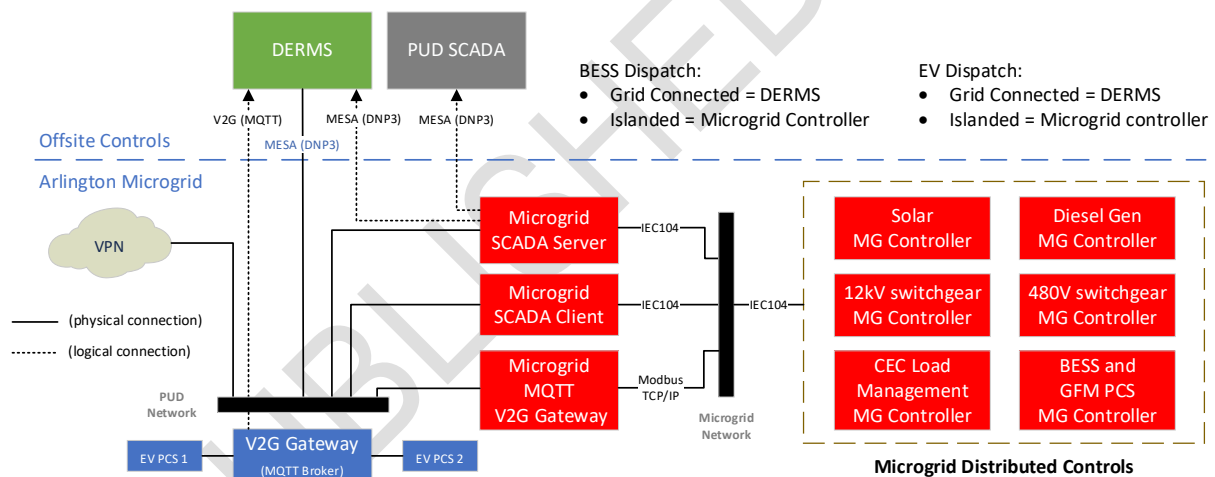


Figure 5 : Simplified communications schematic of protocols in the Arlington Microgrid

The EVCI equipment was specified in 2018 and installed in mid-2020. There was manual V2G in late 2020, and automated V2G functionality was enabled in mid-2021, with final automated V2G capabilities in Jan 2022. The protocol for the V2G communications was selected during the project, using MQTT with custom point list definitions and mapping.

5. SAFETY

A key design criterion during the development of the Arlington microgrid site was maintaining safe operations, with a particular focus placed on the battery system. The methodology for protecting the battery system has evolved over time as standards for battery storage systems, along with recent industry events, continue to present new challenges and opportunities for improvement. The result of this effort is a robust system that has seen input from the owner, the system vendor, the local fire authority, and national research entities.

The final design for the fire suppression system (FSS) comprises a tiered response that elevates the level of intervention based on the current conditions within the container. This response is driven by data collected from a series of different sensors located within the container. These data points are provided to both the local controller as well as an external remote fire panel to allow for immediate automated responses and, if required, a level of human intervention and monitoring. The stages are summarized in Figure 6.

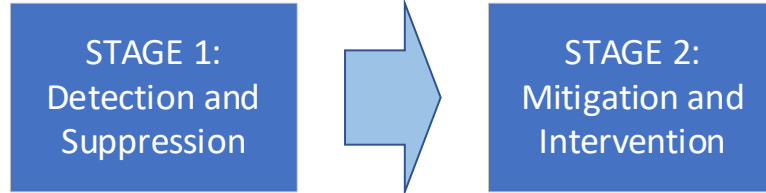


Figure 6 : Stages in the fire safety strategy for the battery energy storage system

STAGE 1: Detection and Suppression

A variety of sensors exist within the container, all of which are constantly monitoring for any deviation from the normal operating and environmental conditions. Examples include:

- Temperature sensors within the battery modules
- Heat and smoke detectors in the container
- Li-Ion Tamer off-gas detection
- VESDA system (very early smoke detection alarm)

Each sensor mentioned above provides its own specific monitoring, and when they detect an issue, they will initiate a different response from the protection system. A Kiddie AEGIS[®] Fire Systems primary control panel integrates some of these sensors and coordinates the response of the NOVEC[®] 1230 dry-agent suppression system. See Table 1.

Table 1 : Fire safety sensors and detection responses

Sensor	Detection Response
Module Temperature	BMS opens contactors for battery racks
Heat and Smoke Detectors	Triggers dry-agent release from fire panel
Li-Ion Tamer	Registers E-Stop to controller, BMS opens contactors for battery racks and immediately activates venting
VESDA System	Triggers alarms and dry-agent release from fire panel

In the event the sensors detect that conditions have changed, the applicable device in the container will initially respond according to the above table. All these elements are intended to function without human interaction and prevent escalation to a more severe event.

STAGE 2: Mitigation and Intervention

Once the system has detected unsafe conditions and responded with the initial suppression action the subsequent response works to reduce the potential for deflagration by mitigating the build-up of any explosive gases within the building. An intake and exhaust system is used to draw air through the container and vent gases outside of the container envelope. This venting is nominally set to operate 10 mins after the NOVEC system has discharged.

Yet another approach to managing conditions in the container and providing for intervention is the newly developed Pacific Northwest National Laboratory’s IntelliVent device [9]. This technology allows an operator to remotely release the container doors in front of the battery racks and force them open. This action allows for both a visual inspection of the battery racks as well as the ability to directly spray water, if required, on any affected areas.

The final remediation for the FSS involves the deluge water system. This is a manually controlled dry pipe connection, which can be opened by the local fire department under specific conditions to flood the container with water. It is assumed that both the injection of

water from the deluge system or direct spray of water through the doors will permanently damage both the batteries and the controllers. For this reason, these manual interventions are considered a last resort in responding to any events.

6. LESSONS LEARNED FOR ENERGY STORAGE, MICROGRIDS, AND V2G

The Arlington Microgrid is an innovative project that provides valuable lessons learned during all stages of the project including planning, design, construction, as well as commissioning. Each of these project stages faced challenges that were successfully addressed to develop an operating microgrid with V2G. The lessons are captured and organized against thematic elements here to guide development of future projects, further research, standards development, replication of the microgrid, as well as future microgrid execution.

6.1 Standards are especially important for Energy Storage, Microgrids, and V2G.

A cross-cutting lesson reinforced throughout the project was the need for standards that support communications and controls between the major assets in the microgrid, including the BESS and V2G. To address these challenges, the MESA standard was specified for the BESS and the associated control and automation systems. However, the V2G system used MQTT communication with custom protocols, which added complexity and necessitated significant interaction and collaboration between the EVCI manufacturer and control system providers. Within the EV space, the increased adoption of standard protocols such as OCPP [10] and IEC 61851 [11] enable easier integration, although both standards have evolved significantly within the past five years and in practice many EVCI vendors do not comply with the latest version. For less common EV uses like V2G this creates challenges, since it may limit the choice of EVCI suppliers and requires careful specification and evaluation. As standards evolve, there is a need for clear understanding of requirements, whether assisting with design and specification development or simplifying connection and operation of assets. Near term solutions for these challenges are to take careful consideration with communication and control standards, as well as working with experienced partners and integrators. Longer term solutions include supporting standards like MESA.

6.2 Battery safety is important and still changing and improving.

Robust fire safety requirements were incorporated early in the design process of the AMG. Even with careful consideration, the safety strategies for the BESS in the AMG have evolved between design and commissioning, and they continue to evolve. The safety issue is complex along several fronts. There are changing codes and standards. For example, in the U.S., both NFPA 855 [12] and IFC [13] have undergone very frequent changes with large adjustments related to secondary battery systems. At the same time the technology is new and Authorities Having Jurisdiction (AHJ) may struggle with regulating them, particularly in the face of changing codes and standards. Proactive engagement with local first responders and code officials can help to address some of these challenges. In addition, there are many new engineered solutions becoming increasingly available to address the safety issues. As with many of the lessons learned, the challenge is reduced by working with an established vendor focused on safety code and standard compliance.

6.3 The value microgrids offer is evolving

The value of microgrids is evolving, both in terms of how the value is quantified, and how it is captured. Microgrids offer a range of values that can be stacked together to justify the investment. Each of the use cases needs to be identified and quantified, ensuring that they provide values that are not mutually exclusive. For example, the BESS in a microgrid can provide both capacity firming and renewable smoothing, but they cannot be done at the same

time. However, renewable smoothing can be compatible with seamless back-up since these do not conflict with each other in operations. The BESS can provide renewable smoothing during normal operation, but when there is a grid outage, when combined with a microgrid, it can quickly provide back-up. These values can be successfully stacked together to justify the value. Quantifying these benefits requires careful consideration [14], [15], particularly as electricity markets and technologies evolve.

6.4 Energy Storage, Microgrids, and V2G technologies require changes to traditional utility approaches.

PUD justified the value of the AMG not just by the resilient infrastructure, but also by factoring the benefits of learning and preparing PUD as an organization for the future. The current structure for many utilities, particularly those with more traditional utility structures, is not well suited for a technology like microgrids. The technology spans several groups at PUD, including the substation group, the system planning and protection group, the generation group, the underground distribution group, information technology and network group, and the facilities group; this mis-alignment between the infrastructure needs and utility structure makes investment a challenge and fragments operation. There was broad support at PUD for this project, but planning, ownership, and day-to-day operations are all a challenge without dedicated resources from a lead group. Some utilities have addressed this with the development of grid modernization groups focused on technologies that face these hurdles. For PUD, this project provided clear benefits for helping the organization to understand the implications of the technology and guide policy in a grounded way.

6.5 Energy Storage, Microgrids, and V2G technologies have specific integration and performance characteristics.

There are several integration and performance lessons learned from the BESS, MGs, and V2G technologies at the AMG. Many of these technologies were new to PUD. With new technologies, robust quality assurance and review of installation is critical to simplify integration. Thorough review of field wiring, reviewing all interconnections, ensuring that all devices have the appropriate firmware, and aligning equipment to all operate on the same version of the standards are all critical to efficient deployment of technologies. Erratic behavior stemming from these issues can create confusion and inhibit integration, particularly with new technologies where installers or owners may have less familiarity. In terms of ensuring stable operation of the grid, the system protection settings needed to be adjusted to match the needs of the site. When properly set, modern BESS with coordinated protections enables the seamless transition from grid connected operation into an electrical island. The process of tuning the parameters and setting protections was finalized in the field. Even with tuning, it is important to remember that microgrid dynamics are different than large grid dynamics. For example, when islanded the MG frequency and voltage will be less stiff, and sudden changes in load can cause perturbations different from when grid connected. In the first version of the V2G site acceptance test plan, the load bank rapidly applied its 350 kW load which caused a frequency excursion that exceeded the protection settings of the V2G converters, and required manually resetting the EVCI to resume automation. This was addressed by adjusting the test plan to apply the load bank in 25% steps every 10 seconds, rather than a step load change. The issue was quickly identified because the project included experienced vendors with extensive microgrid experience.

6.6 Remote management and operation are valuable and viable.

The major assets of the AMG were deployed during 2020 and 2021. This coincided with the global COVID-19 pandemic. Accordingly, the team adapted to expand what could be done remotely. Large portions of the commissioning were done with team members offsite, and there is strong confidence in the technology's ability to be tested and operated off-site. In

addition to supporting social distancing, the expansion of remote access helped to increase efficiency and provided an opportunity to further expand the importance of strong automation and controls. With this, the project was able to reduce team travel and share from a pool of resources from around the globe, not just locally.

7. CONCLUSION

The Arlington Microgrid proves that the bidirectional flow of electricity from EVs can provide services to electrical grids, particularly when managed as part of a grid edge solution like a microgrid. The technologies around EVs are evolving rapidly, including the interface, communications, and interactions with the power grid. Projects like the Arlington Microgrid demonstrate that utilities can actively support standards that make it easier and safer to integrate diverse electrification and renewable technologies. When utilities like PUD develop innovative projects with these technologies, they are creating living laboratories to help build the utility of the future, and ultimately reduce costs while improving services for ratepayers with clean technologies.

BIBLIOGRAPHY

- [1] CIGRÉ, Working Group C6.22 “Microgrids 1 Engineering, Economics, & Experience”, Technical Brochure 635, October 2015, ISBN 978-2-85873-338-5.
- [2] Daniel S. Kirschen and Chanaka Keerthisinghe, “Snohomish Public Utility District Arlington Microgrid,” University of Washington report for the Washington Clean Energy Fund, 2022. Online: <https://labs.ece.uw.edu/real/library.html>
- [3] B. Bonlender, “Clean Energy Fund Program Status per 2EHB1115 (2015), Section 1028(11)”, State of Washington Department of Commerce, April 2017, <http://www.commerce.wa.gov/wp-content/uploads/2017/04/Commerce-Clean-Energy-Fund-2017.pdf>.
- [4] S. Gibson, A. Swaney, “Lessons from the Microgrid”, *T&D World*, Sept. 2019, p. 16-22.
- [5] C. Keerthisinghe, E. Mickelson, D. S. Kirschen, N. Shih and S. Gibson, "Improved PV Forecasts for Capacity Firming," in *IEEE Access*, vol. 8, pp. 152173-152182, 2020. doi: 10.1109/ACCESS.2020.3016956
- [6] C. Keerthisinghe and D. S. Kirschen, "1 Real-Time Digital Simulation of Microgrid Control Strategies," 2020 IEEE Power & Energy Society Innovative Smart Grid Technologies Conference (ISGT), Washington, DC, USA, 2020, pp. 1-5.
- [7] MESA, “MESA-ESS Specification,” Version 1.0, December 2018. Accessed December 2020. <http://mesastandards.org/wp-content/uploads/MESA-ESS-Specification-December-2018-Version-1.pdf>
- [8] MESA, “Open standards for Energy Systems”, Web. Accessed Jan 2022, <http://mesastandards.org/>.
- [9] Pacific Northwest National Laboratory, IntelliVent Technology Overview, Accessed December 2021, <https://www.pnnl.gov/available-technologies/intellivent>.
- [10] Open Charge Alliance, “The Importance of Open Protocols”, Accessed January 2022. <https://www.openchargealliance.org/protocols/>
- [11] IEC, Electric vehicle conductive charging system, Standard 61850, <https://www.iecee.org/>
- [12] NFPA 855, “Standard for the Installation of Stationary Energy Storage Systems”, National Fire Protection Association, 2020.
- [13] International Code Council. “International Building Code”. Falls Church, Va. International Code Council, 2021.
- [14] E. Lightner, J. Leader, S. Berdahl, et al, “Voices of Experience: Microgrids for Resiliency”. United States: N. p., 2021. Web. <https://sepapower.org/resource/voices-of-experience-microgrids-for-resiliency/>
- [15] Hitachi Energy, “Ensuring reliable power for commercial and industrial sites”, Web, 2021, <https://search.abb.com/library/Download.aspx?DocumentID=4CAE000425&LanguageCode=en&Action=Launch>

Appendix E: Real-Time Digital Simulation of Microgrid Control Strategies

Real-Time Digital Simulation of Microgrid Control Strategies

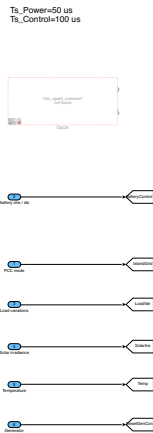
Chanaka Keerthisinghe, *Member, IEEE*, and Daniel S. Kirschen, *Fellow, IEEE*

Department of Electrical and Computer Engineering, University of Washington, Seattle, Washington 98195, USA

Email: chanakak@uw.edu and kirschen@uw.edu

Abstract—This paper describes the real-time digital simulation of a microgrid control strategy prior to actual implementation. The microgrid mode of operation is studied: grid-connected mode with the battery and islanded operation when the battery is discharged.

Index Terms—microgrid, real-time digital simulation, RT², Simulink[®]



REAL-TIME digital simulation and design methodology prior to actual deployment.

This paper describes the real-time digital simulation of a microgrid control strategy prior to actual deployment. The microgrid mode of operation is studied: grid-connected mode with the battery and islanded operation when the battery is discharged. The emergency generator will only be used when the battery is discharged and there is insufficient PV generation. The batteries of the EVs are capable of supporting the microgrid and the electrical grid. The simulation models developed in MathWorks[®] Simulink[®] using the Simscape Power Systems[™] (formerly SimPowerSystems[™]) toolbox are available to the public and could be adapted to model other microgrids [10].

The rest of the paper is structured as follows: Section II presents the Simulink[®] models of the microgrid. Section III describes the setup used for the real-time digital simulation. Section IV presents simulation results for different operating scenarios. Section V draws conclusions and outlines future work.

II. MICROGRID MODEL

Figure 1 shows the connections between the various components of the microgrid. The following subsections describe

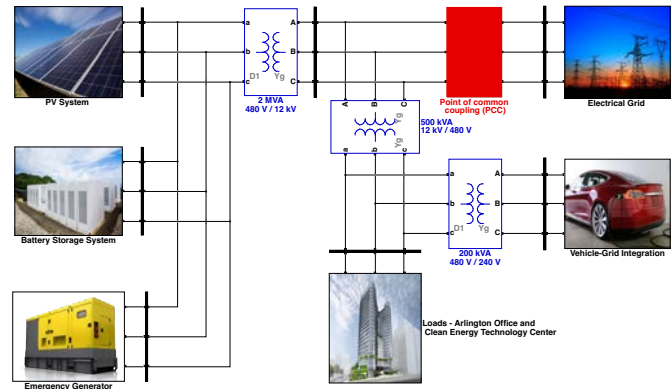


Fig. 1. Components of the Arlington Microgrid.

TABLE I
SPECIFICATIONS OF THE REC TWINPEAK 2S MONO 72 SERIES 375 W PV MODULE

Parameters	Values
Maximum power	375 W
Open circuit voltage (V_{oc})	48 V
Rated Voltage (V_r)	40.1 V
Short circuit current (I_{sc})	9.06 A
Rated current (I_r)	9.86 A
Temperature coefficient of V_{oc}	-0.28 %/C
Temperature coefficient of I_{sc}	0.04 %/C
Number of cells per module	144

in detail how each of these components is modeled.

A. PV System

The PV system consists of the PV array, maximum power point tracker (MPPT) and an inverter. The PV array [11] consists of multiple PV modules connected in series and parallel to achieve the desired voltage and current. Table I provides the specifications of the PV modules. The PV array consists of 1640 modules divided into four sub-arrays, each of which contains 410 modules organized in 41 strings of 10 series-connected modules, and is rated at 615 kWdc.

Fig. 2 shows the current-voltage and power-voltage characteristics of each sub-array for different solar irradiances and temperatures. Each array is equipped with an MPPT to keep the voltage at the the maximum power point (MPP) as the solar irradiance and the temperature of the panel change. This tracking is achieved using a DC-DC converter that implements a *perturb and observe* algorithm. Note that the voltages on the

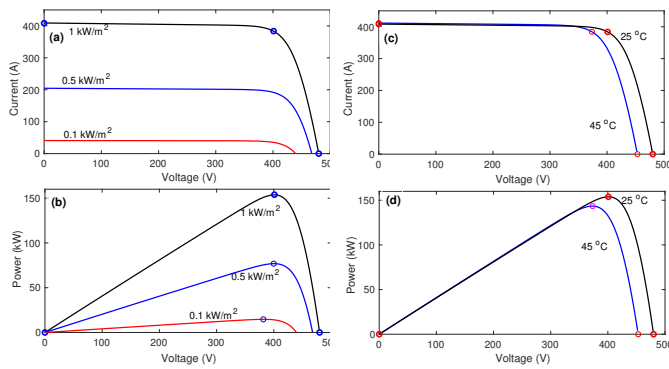


Fig. 3. PV inverter characteristics and temperature dependence for

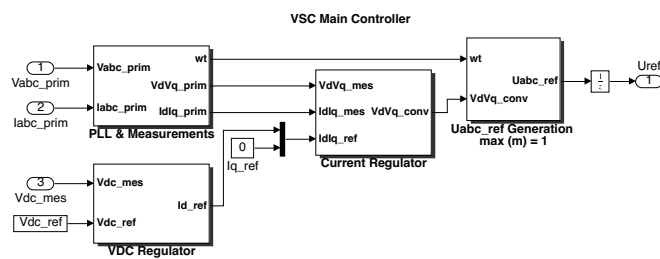


Fig. 3. Control of the PV inverter for grid-following

PV array and the dc link can therefore be option would be to connect the PV array link of the inverter and to incorporate the the controller of this inverter [12].

The PV inverter is a two-level three-br converter (VSC) that operates in grid-fol 3 summarizes the inverter control algorit voltage and current signals for phase-loc measured from the inverter output. The PLL block calculate the angle synchronized (crossing of the fundamental of the ref transform both voltages and currents from reference frames.

When the input power from the solar to variation in irradiance or temperature, t also changes because the power obtained 1 not match the power delivered to the grid. voltage regulator is thus to change the acti current (I_d) of the current regulator so tl from the solar array matches the power d [13].

The current regulator uses the current r (reactive current) to calculate the required for the inverter. The reactive current refe in this model, as the system only supplies grid. More details about this controller can this model, the harmonics produced by the using a single inductor (L). However, of are possible [13].

TABLE II
SPECIFICATIONS OF THE BATTERY

Parameters	Values
Nominal voltage	800 V
Rated capacity	1250 Ah
Fully charged voltage	931.2 V
Maximum capacity	1320 Ah
Capacity @nominal voltage	1250 Ah
Nominal discharge current	1250 A

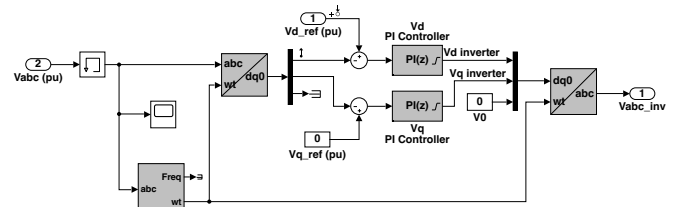


Fig. 4. Battery inverter operation as a voltage regulator during islanded operation.

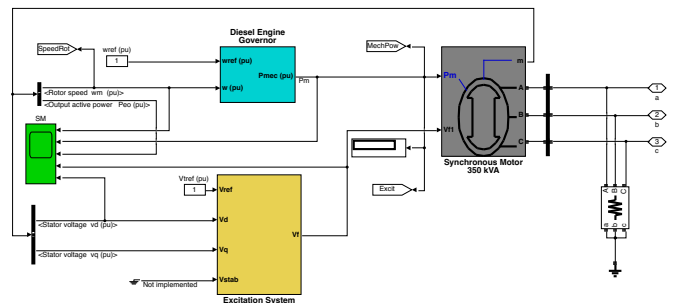


Fig. 5. Emergency generator model including synchronous machine, excitation system and diesel engine governor.

B. Battery Energy Storage

The battery energy storage system consists of a Li-ion battery, a dc-dc converter and an inverter with both grid-forming and grid-following capabilities. Table II provides the specifications for the battery model [15]. A bi-directional DC-DC converter is inserted between the inverter and the battery to control the battery charge and discharge rates in grid-following mode [16]. The battery inverter control for grid-connected mode, which is similar to the PV inverter controller [12]. In islanded mode, this inverter controller operates as a voltage regulator as shown in Fig. 4.

C. Emergency Generator

The emergency diesel generator consists of a synchronous generator, diesel engine governor and an excitation system, as shown in Fig. 5. The model of the synchronous machine takes into account the dynamics of the stator, field, and damper windings and is represented using a sixth-order model [17]. Table III. provides the specifications of this emergency generator.

TABLE III
SPECIFICATIONS OF THE EMERGENCY GENERATOR

Parameters	Values
Power rating	350 kW
Voltage rating	480 V
Frequency	60 Hz
Stator resistance	0.0036 Ω
Inertia coefficient	20
Pole pairs	4

TABLE IV
SPECIFICATIONS OF THE EV BATTERY

Parameters	Values
Nominal voltage	200 V
Rated capacity	500 Ah
Fully charged voltage	232.8 V
Maximum capacity	500 Ah
Capacity @nominal voltage	452.2 Ah
Nominal discharge current	217.4 A
Exponential zone voltage	216.1 V
Exponential zone capacity	24.6 Ah
Internal resistance	0.004

In order to synchronise the emergency generator it's frequency, voltage magnitude and phase angle must be matched with those of the microgrid. The frequency of the emergency generator, f_g is given by:

$$n_s = \frac{120f_g}{P} \quad (1)$$

where n_s is the synchronous speed of the generator in revolutions per minute and P is the number of poles. The desired frequency is obtained by changing the speed reference of the diesel engine governor, such that 1 pu corresponds to $f_g=60$ Hz, $P=4$, $n_s=1800$ rpm [18].

The generator voltage is adjusted by controlling the reference voltage of the excitation system. Note that a reference of 1 V (pu) corresponds to the rated voltage of the generator. The emergency generator is connected to the microgrid when the phase angle difference is close to zero [18].

D. Vehicle-grid integration

The vehicle-grid integration system is modeled using an EV battery and an inverter that controls the charge and discharge rates. The EV battery has the specifications given in Table IV. An average model has been used for the DC-AC inverter, which is based on the work described in [19]–[21].

III. REAL-TIME SIMULATION

Simulating this microgrid at 50 μ s fixed time-steps in Simulink[®] over a long period of time requires an excessive amount of computing time. We also wanted to have the ability to perform hardware-in-the-loop simulations to test some of the components and their controllers. The Simulink[®] model was therefore ported to an OPAL-RT[®] eMEGAsim real-time digital simulator [22]. The simulator hardware consists of an OP5600 chassis equipped with up to 12 parallel 3.3-GHz processor cores, a flexible high-speed front-end processor and a signal conditioning stage. The solver used is called

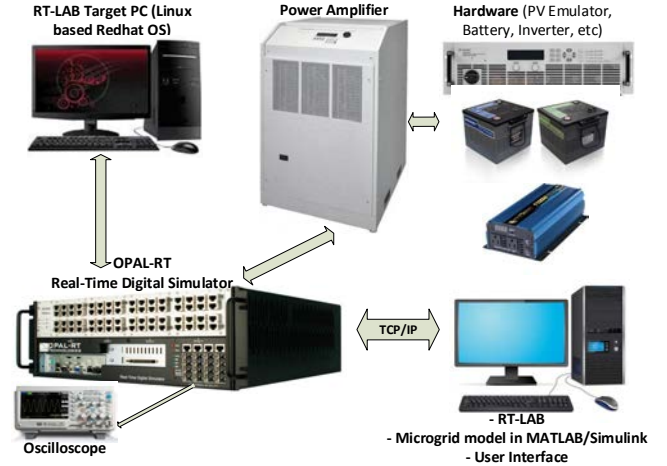


Fig. 6. Setup for power hardware-in-the-loop and software-in-the-loop testing.

ARTEMiS (advanced real-time electromagnetic simulation). Fig. 6 illustrates this real-time digital simulation testbed.

The Simulink[®] model of the microgrid is first to run as an effective platform for developing and testing the real-time microgrid. The Simulink[®] microgrid model has to be separated into different subsystems (master, slave, and console) in order to execute the model on several cores, before being compiled using RT-LAB. Each master and slave subsystem in RT-LAB is assigned to a separate core to perform their parallel processes in a fast and efficient way.

Power system models are typically decoupled at large transmission lines because these lines introduce a delay in signal propagation. Because there are obviously no such lines in a microgrid, we decoupled the system at dc busses. Another option is to use OPAL-RT's ARTEMiS state-space nodal (SSN) solver, which results in the same solution.

IV. SIMULATION RESULTS AND DISCUSSION

This section discusses the simulation of three operating scenarios.

A. Scenario A: Grid-connected operation

The microgrid is operated in grid-connected mode, with the PV system injecting a variable amount of power into the grid as solar irradiance changes. From $t = 1$ second to $t = 60$ seconds, the battery is used for solar smoothing. From $t = 60$ second to $t = 100$ seconds, the battery charges and discharges at a constant rate. From $t = 50$ second to $t = 90$ seconds, the active load varies. The EV is discharged at 50 kW from $t = 0$ second to $t = 40$ seconds and charges from $t = 40$ seconds to $t = 80$ seconds at the same rate. Fig. 7 shows the corresponding simulation results.

The output current of the PV array (b.2) decreases when the solar irradiance (a.1) decreases, however, the voltage (b.1) is maintained around the same value. This is because the voltage corresponding to the MPP does not change significantly with changing solar irradiance as shown in Fig. 2. Note that the voltage and current corresponding to the MPP at 25^oC and 1000 W/m² are 401 V and 383.8 A, respectively. The dc link

voltage of the PV inverter is not affected by the changing solar irradiance, in fact it is regulated at a constant value to supply the required output voltage.

During the first 60 seconds of Scenario A, since the battery is used for solar smoothing, the power output at the point-of-common-coupling (PCC) is regulated at the chosen 600 kW (f.1) regardless of the changing solar irradiance. From 60 to 80 seconds the battery is charged at 500 kW and from 80 to 100 seconds, the battery is discharged at 500 kW. Note that the frequency at the PCC is fixed at 60 Hz because the microgrid is in grid-connected mode. Small spikes in frequency (e.4 and f.4) are due to minor simulation glitches.

B. Scenario B: Battery operating in grid-forming mode

Initially (from $t = 0$ to $t = 10$ seconds), the microgrid is grid-connected and the PV system injects power into the grid assuming a constant irradiance. The battery neither charges nor discharges. When the microgrid is suddenly islanded at $t = 10$ seconds, the battery controller switches to islanded mode to maintain the microgrid's desired voltage and frequency. The load varies between $t = 50$ and $t = 90$ seconds while the EV charges from $t = 0$ to $t = 30$ seconds and discharges from $t = 60$ to $t = 100$ seconds. Fig. 8 shows the results of the simulation for this scenario.

While in grid-connected mode, the voltage at the PCC (f.3) is slightly less than 1 p.u. because the microgrid does not control the voltage at that point. When the microgrid is suddenly islanded at 10 seconds, the voltage regulator in Fig. 4 increases the voltage at the PCC (f.3) to 1 p.u. The active load also slightly increases because the load model is voltage dependent. Since the microgrid is islanded when the power flow at the PCC is not zero, a power spike occurs (d.1, e.1, f.1). The battery then manages to maintain the voltage (d.3, f.3) and the frequency (d.4, f.4) at a constant value even when the load varies (between $t = 50$ and $t = 90$ seconds) and the solar irradiance decreases (between $t = 20$ and $t = 30$ seconds).

C. Scenario C: Emergency generator operation in islanded mode

In this scenario, the microgrid operates in islanded mode and the emergency generator maintains the desired voltage and frequency. The load varies between $t = 50$ and $t = 90$ seconds. The battery charges at 100 kW between $t = 10$ and $t = 100$ seconds. The EV charges at 50 kW between $t = 0$ and $t = 100$ seconds. Fig. 9 shows the simulation results.

The variable load between $t = 50$ and $t = 90$ seconds as well as the decision to charge the battery at $t = 10$ seconds cause frequency oscillations (b.4, d.4, h.4). However, the frequency always stays within ± 5 Hz and extending the simulations over a longer duration shows that these oscillations die out. Their amplitude can be reduced by increasing the inertia of the generator, however this causes these oscillations to last longer. There are voltage and power spikes (Fig. 9 (d.1, d.3, g.1, g.3)) and a sudden drop in load (Fig. 9 (f.3)) when the battery starts charging at 10 seconds.

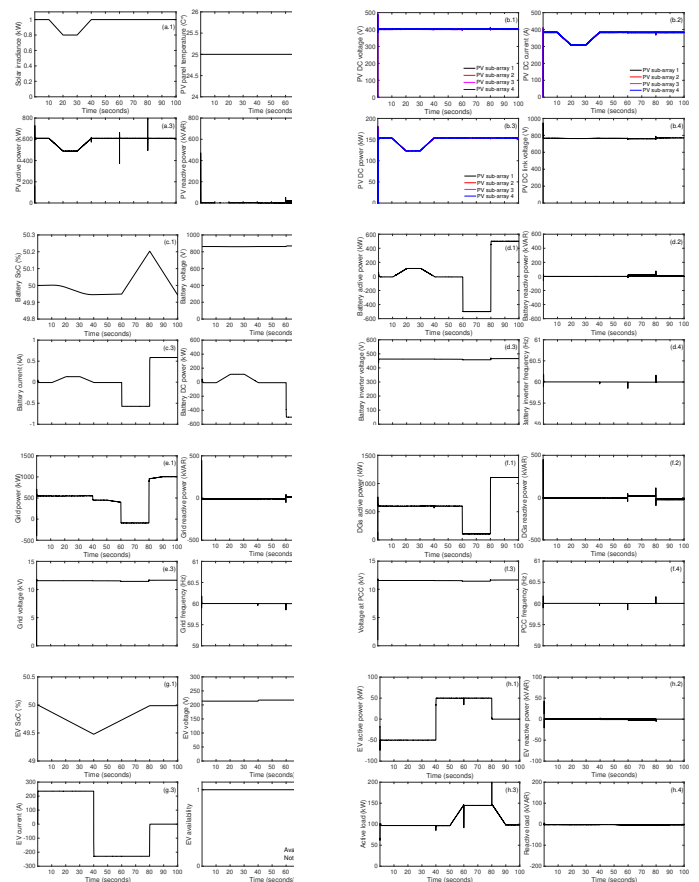


Fig. 7. Simulation results for Scenario A: PV system (a.1-b.4), battery (c.1-d.4), electrical grid (e.1-e.4), PCC (f.1-f.4), EV (g.1-h.2) and load (h.3-h.4).

CONCLUSIONS

This paper presented a real-time digital simulation on an OPAL-RT real-time digital simulator of a microgrid being built in by Snohomish PUD in Arlington, WA. This model supports the study of different operating conditions before the microgrid is deployed in the field at the end of 2021.

Once the microgrid is operational, we will compare our simulation results with the actual measured data.

ACKNOWLEDGMENTS

The authors would like to thank Scott Gibson from Snohomish PUD and Bob Kirchmeier from Washington State Department of Commerce for the guidance and financial support.

REFERENCES

- [1] M. Farzinfar and M. Jazaeri and N. C. Nair and F. Razavi, "Stability evaluation of microgrid using real-time simulation," in *2014 Australasian Universities Power Engineering Conference (AUPEC)*, Sep. 2014, pp. 1–6.
- [2] X. Meng, C. Yang, K. Lin, F. Zhang, J. Wu, and J. Shen, "Research on photovoltaic power system of microgrid based on real-time simulation," in *2017 IEEE Conference on Energy Internet and Energy System Integration (EI2)*, Nov 2017, pp. 1–5.
- [3] L. Ghomri, M. Khiat, and S. A. Khiat, "Modeling and real time simulation of microgrids in Algerian Sahara area," in *2018 IEEE International Energy Conference (ENERGYCON)*, June 2018, pp. 1–5.

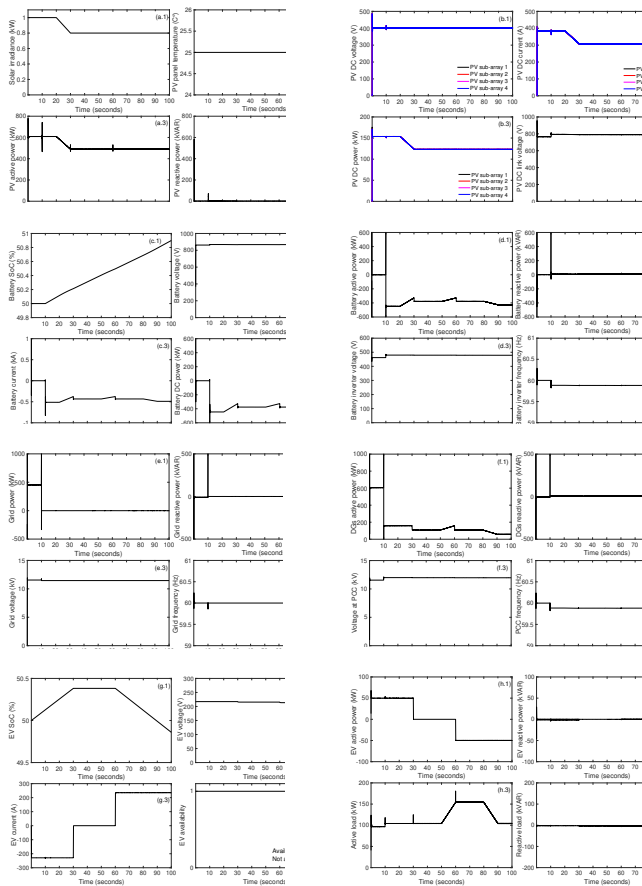


Fig. 8. Simulation results for Scenario B: PV system (a.1-b.4), battery (c.1-c.4), electrical grid (e.1-e.4), PCC (f.1-f.4), EV (g.1-h.2) and load (h.3-h.4)

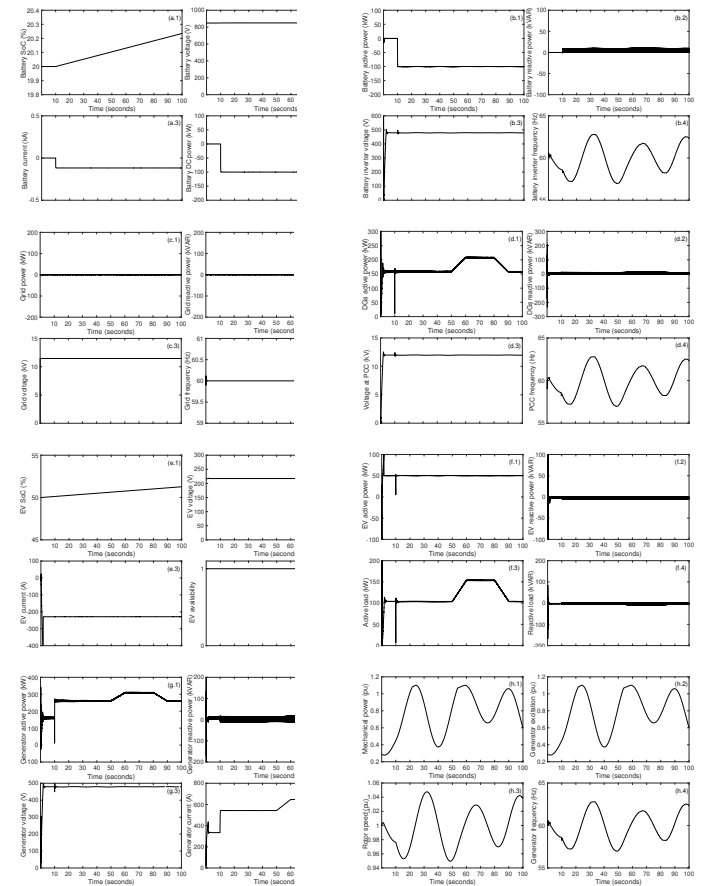


Fig. 9. Simulation results for Scenario C: Battery (a.1-b.4), electrical grid (c.1-c.4), PCC (d.1-d.4), EV (e.1-f.2), load (f.3-f.4) and generator (g.1-h.4).

- [4] I. Leonard, T. Baldwin, and M. Sloderbeck, "Accelerating the custom-driven microgrid through real-time digital simulation," in *2009 IEEE Power Energy Society General Meeting*, July 2009, pp. 1–3.
- [5] O. Nzimako and A. Rajapakse, "Real-time simulation of a microgrid with multiple distributed energy resources," in *2016 International Conference on Cogeneration, Small Power Plants and District Energy (ICUE)*, Sep. 2016, pp. 1–6.
- [6] F. Baccino, A. Brissette, D. Ishchenko, A. Kondabathini, and P. Serra, "Real-time hardware-in-the-loop modeling for microgrid applications," in *2017 6th International Conference on Clean Electrical Power (IC-CEP)*, June 2017, pp. 152–157.
- [7] A. Yamane and S. Abourida, "Real-time simulation of distributed energy systems and microgrids," in *2015 International Conference on Sustainable Mobility Applications, Renewables and Technology (SMART)*, Nov 2015, pp. 1–6.
- [8] M. Chlela, G. Joos, M. Kassouf, and Y. Brissette, "Real-time testing platform for microgrid controllers against false data injection cybersecurity attacks," in *2016 IEEE Power and Energy Society General Meeting (PESGM)*, July 2016, pp. 1–5.
- [9] Snohomish County Public Utility District. Arlington Microgrid Project. [Online]. Available: <https://www.snopud.com/?p=3326>
- [10] C. Keerthisinghe and D. S. Kirschen. (2019) Real-Time Digital Simulation of Microgrid Control Strategies. Renewable Energy Analysis Lab, University of Washington. [Online]. Available: <https://labs.ece.uw.edu/real/RTDSmain.html>
- [11] MathWorks. PV array. [Online]. Available: <https://www.mathworks.com/help/physmod/sps/powersys/ref/pvarray.html>
- [12] —. (250-kw grid-connected PV array). [Online]. Available: <https://www.mathworks.com/help/physmod/sps/examples/250-kw-grid-connected-pv-array.html>
- [13] Mohsin Noman Mustafa, "Design of a grid connected photovoltaic power electronic converter," Master's thesis, Universitet i Tromsø, Jun. 2017.
- [14] P. Giroux, G. Sybillé, C. Osorio, S. Chandrachud. Average

- model of a 100-kw grid-connected PV array. MathWorks. [Online]. Available: <https://www.mathworks.com/help/physmod/sps/examples/average-model-of-a-100-kw-grid-connected-pv-array.html>
- [15] MathWorks. Simulink battery model. [Online]. Available: <https://www.mathworks.com/help/physmod/sps/powersys/ref/battery.html>
- [16] M. Saleh, Y. Esa, Y. Mhandi, W. Brandauer, and A. Mohamed, "Design and implementation of CCNY DC microgrid testbed," in *2016 IEEE Industry Applications Society Annual Meeting*, Oct 2016, pp. 1–7.
- [17] MathWorks. Simplified synchronous machine. [Online]. Available: <https://www.mathworks.com/help/physmod/sps/powersys/ref/simplifiedsynchronousmachine.html>
- [18] G. Sybillé and Tarik Zabaïou. Emergency diesel-generator and asynchronous motor. MathWorks. [Online]. Available: <https://www.mathworks.com/help/physmod/sps/examples/emergency-diesel-generator-and-asynchronous-motor.html>
- [19] IDE4L: ideal grid for all. [Online]. Available: <https://ide4l.eu>
- [20] L. Vanfretti, W. Li, A. Egea-Alvarez, and O. Gomis-Bellmunt, "Generic VSC-based DC grid EMT modeling, simulation, and validation on a scaled hardware platform," in *2015 IEEE Power Energy Society General Meeting*, July 2015, pp. 1–5.
- [21] L. Vanfretti, N. A. Khan, W. Li, M. R. Hasan, and A. Haider, "Generic VSC and low level switching control models for offline simulation of VSC-HVDC systems," in *2014 Electric Power Quality and Supply Reliability Conference (PQ)*, June 2014, pp. 265–272.
- [22] OPAL-RT Technologies. Microgrid. [Online]. Available: <https://www.opal-rt.com/microgrid-overview/>

Appendix F: Capacity Firming Using Deep Learning

Received July 21, 2020, accepted August 7, 2020, date of publication August 17, 2020, date of current version August 28, 2020.

Digital Object Identifier 10.1109/ACCESS.2020.3016956

Improved PV Forecasts for Capacity Firming

CHANAKA KEERTHISINGHE^{1,2}, (Member, IEEE), EVAN MICKELSON¹, DANIEL S. KIRSCHEN¹, (Fellow, IEEE), NATHAN SHIH¹, (Student Member, IEEE), AND SCOTT GIBSON³, (Member, IEEE)

¹Department of Electrical and Computer Engineering, University of Washington, Seattle, WA 98195, USA

²Systems Integration Testbed, Washington Clean Energy Testbeds, Seattle, WA 98105, USA

³Snohomish County Public Utility District, Everett, WA 98201, USA

Corresponding author: Chanaka Keerthisinghe (chanakak@ieee.org)

ABSTRACT Some balancing authorities give owners of medium to large photovoltaic (PV) generation plants a choice between firming the production of their plants using battery energy storage or paying the balancing authority for the cost that these imbalances impose on the system. If the owner of a PV plant decides to do capacity firming, the net production of the PV plant and the battery must match a forecast value. A more accurate forecast of the PV production reduces the energy throughput of the battery and hence its degradation. This article compares capacity firming using persistence forecasts with predictions based on long short-term memory recurrent neural networks (LSTM-RNN), encoder-decoder LSTM-RNN and multi-layer perceptrons. This article also proposes to use the type-of-day, such as sunny, cloudy etc, which can be generated by clustering historical PV generation data according to the total daily PV generation, as a feature of the PV forecasting model. Results based on the Snohomish County Public Utility District's Arlington Microgrid show that the machine learning techniques perform significantly better than the persistence method in forecasting PV generation. In particular, encoder-decoder LSTM-RNN would reduce the yearly battery energy throughput by 29% and the number of battery cycles with a greater than 10% depth-of-discharge (DoD) by 51%. Including the day-type as a feature in PV forecasting reduces the battery energy throughput by 5.3% and the number of cycles with a DoD larger than 10% by 5.9%.

INDEX TERMS Capacity firming, solar smoothing, PV forecasting, encoder-decoder long short-term memory networks, recurrent neural networks, multi-layer perceptrons, battery energy storage, battery degradation, sequence2sequence time-series prediction.

I. INTRODUCTION

Providing the resources needed to balance the increasing amount of naturally variable and uncertain generation from solar and wind can be very costly for the balancing authorities (BA) that are responsible for maintaining the balance between load and generation within their territory. Some have therefore given the owners of these resources a choice between paying a balancing fee and firming up the output of their plants using their own resources.

This work is motivated by the capacity firming requirements of medium to large photovoltaic (PV) generation plants in the balancing area of the Bonneville Power Administration (BPA) and presents results based on the 500 kWac PV system of the Arlington Microgrid owned by Snohomish County Public Utility District (Snohomish PUD) [1].

The associate editor coordinating the review of this manuscript and approving it for publication was Ning Kang¹.

Snohomish PUD can either pay a fee for capacity firming to BPA or compensate deviations between the actual and forecast PV generation using the 1MW/1.385MWh battery energy storage system (BESS) of the microgrid.

Capacity firming is based on a one-hour-ahead target PV generation determined considering the PV forecast, the maximum allowed ramp rate of the PV profile and the battery state-of-charge (SoC) that should be achieved at the next time-step. The BESS is charged when the PV generation is above the target value or discharged when the PV generation is below this value. In most cases the BESS has enough power and energy capacity to achieve this goal. However, the more inaccurate the forecast is, the more the battery has to compensate with deeper cycles. Since deeper cycles cause more battery degradation [2], [3], it may be more economical in the long run to pay the fee for capacity firming to BPA rather than firming the capacity using the battery. Since more accurate forecasts extend the life of the battery,

a careful analysis of the benefits of improved accuracy is thus required.

This article compares state-of-the-art PV forecasting techniques, such as long short-term memory recurrent neural networks (LSTM-RNN), encoder-decoder LSTM-RNN, multi-layer perceptrons (MLP), and the persistence method suggested by BPA. The paper also proposes to use the type-of-day as a feature in the PV forecasting model. The type-of-day is generated by clustering historical PV generation data according to the total daily PV output. The cluster with the highest PV generation is classified as sunny while the cluster with the least PV generation is classified as cloudy. These forecasting methods are compared using not only the root-mean-square error (RMSE), mean-absolute error (MAE) and mean-bias error (MBE), but also the resulting number and depth of the battery cycles.

The remainder of this article is structured as follows: Section II explains capacity firming; Section III reviews the existing PV forecasting techniques and discusses the machine learning based forecasting techniques; Sections IV and V describe the model, while Section VI presents and discusses the simulation results. Section VII concludes the paper.

II. CAPACITY FIRING

This section explains the incentive scheme for capacity firming (Section II-A), formulates this problem mathematically (Section II-B) and describes the PV forecasting technique proposed by BPA (Section II-C).

A. INCENTIVE SCHEME FOR PV CAPACITY FIRING

BPA, the balancing authority for the Snohomish PUD service region has decided to charge \$5400 per year as the cost of capacity firming for the 500 kWac PV system of the Arlington Microgrid. Snohomish PUD could save this cost by ensuring that the actual PV production matches their one-hour-ahead prediction. If Snohomish PUD chooses this option, BPA has proposed to use the persistence approach for PV forecasting described in Section II-C.

B. FORMULATION OF THE CAPACITY FIRING PROBLEM

The one-hour-ahead PV generation can be firmed using a BESS. The battery is charged when the PV generation is above the target value and discharged when the PV generation is below this value. Fig. 1. shows the energy flow diagram for this capacity firming application of the BESS.

The decision to do capacity firming or not depends on a cost/benefit analysis. While Snohomish PUD could avoid paying this fee to BPA if they did capacity firming, the extra battery cycling required would increase battery degradation and carry a long term cost. More accurate PV forecasts would require fewer battery cycles, cause less battery degradation costs and hence improve the cost/benefit ratio from capacity firming.

The capacity firming problem can be formalized as follows:

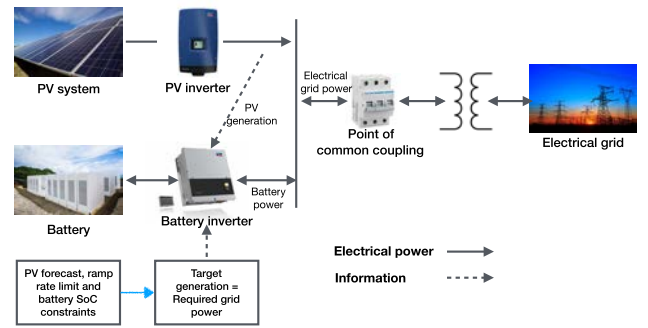


FIGURE 1. Electrical power and information flows in a PV-battery microgrid. The battery power is calculated using (1).

- A sequence of time-steps, $\mathcal{K} = \{1 \dots k \dots K\}$, where K and k represent the total number of time-steps and a particular time-step in a day, respectively. We choose 30 minute intervals because this is the duration that BPA uses to assess capacity firming.
- A set of variables to define the energy flows in the system. The battery charge/discharge rate p_k^b , is the difference between the actual PV generation $p_k^{pv,actual}$ and the target output p_k^t :

$$p_k^b = p_k^t - p_k^{pv,actual} \quad (1)$$

where a positive value for p_k^b means the battery is discharging and a negative value that is charging.

- The target output p_k^t is estimated considering the PV forecast, the maximum allowed ramp rate of the PV profile and the desired battery SoC at the next time step. The target PV generation is calculated as follows:

$$p_k^t = p_k^{pv,forecast} + 2C \left(B_k^{SoC} - B^{SoC,50\%} \right) \quad (2)$$

where B_k^{SoC} is the battery SoC at time-step k in kWh, $B^{SoC,50\%}$ is the battery 50% SoC in kWh and C determines how close to the 50% level the SoC should remain. A higher value of C keeps the SoC closer to 50%. The factor “2” is needed to convert energy into power because we use 30 minute intervals. The BESS system is assumed to have enough power and energy capacities to correct the expected range of deviations in PV generation. Finally, the target PV generation submitted to BPA cannot violate the ramp rate limits:

$$|p_k^t - p_{k-1}^t| < \gamma_r \quad (3)$$

where γ_r is the ramp rate limit.

The battery SoC, $B_k^{SoC} \in [s_k^{SoC,min}, s_k^{SoC,max}]$, evolves according to:

$$B_{k+1}^{SoC} = B_k^{SoC} - 0.5\eta_b p^b \quad (4)$$

where η_b is the battery efficiency.

The number of battery cycles that a lithium-ion battery can undergo before its capacity falls below an acceptable threshold depends on the depth-of-discharge (DoD) of

these cycles. The number of battery cycles and their magnitudes are calculated using the rainflow cycle counting algorithm and these numbers are then used to quantify the battery degradation.

The net present value (NPV) of capacity firming is calculated by subtracting the present value of the battery replacement cost after the lifetime of the project from the present value of all the revenue over the lifetime of the battery. The battery replacement cost is the expected degraded battery capacity over the lifetime multiplied by the battery replacement cost per kWh.

C. PERSISTENCE APPROACH TO FORECASTING

Because of its simplicity, BPA has suggested to Snohomish PUD to use the persistence forecasting technique for one-hour-ahead PV forecasting. For example, under 30/30 persistence forecasting, the net generation for the 2:00 PM to 2:30 PM interval is calculated by taking the average of the generation output from 1:00 PM to 1:30 PM. Similarly, the schedule for the 3:00 PM to 3:30 PM interval is calculated by taking the average of the generation output from 2:00 PM to 2:30 PM.

III. PV FORECASTING USING MACHINE LEARNING

This section first presents a brief review of existing PV forecasting techniques and then the state-of-the-art techniques that have been shown to provide the best PV forecasts.

A. BRIEF REVIEW OF EXISTING SOLUTION TECHNIQUES

A range of techniques have been proposed to optimize capacity firming [4]–[10] but these approaches did not include state-of-the-art machine learning techniques discussed in this article.

The underlying PV forecasting problem is a sequence-to-sequence (seq2seq) time series prediction because the PV generation has to be predicted two time-steps ahead. PV forecasting can be categorized into physical models and data-driven models. Physical models use numerical weather prediction, which shows good performance for forecast horizons from several hours up to six days [11], [12]. Data-driven models can be further divided into statistical and machine learning models. Statistical models include auto-regressive integrated moving average, auto-regressive moving average, coupled auto-regressive and dynamic system, Lasso, and Markov models. Machine learning models include support vector machine, feed-forward neural networks, and RNN such as LSTM networks [13]–[28]. These approaches can be further subdivided according to the type of input features that are used to train the model. A forecasting model that uses only a target time-series as an input feature (solar irradiance in this case) is referred to as a nonlinear auto-regressive (NAR) model. On the other hand, if a model uses additional exogenous inputs, such as temperature and humidity, it is referred to as a nonlinear auto-regressive with exogenous inputs (NARX) model. According to [13], [18], a vector

output LSTM-RNN performs the best at forecasting day-ahead PV generation.

Section III-B describes feedforward neural networks, also known as multi-layer perceptrons, while Section III-C is devoted to LSTM-RNN and encoder-decoder LSTM-RNN. The encoder-decoder LSTM-RNN was first proposed and applied to speech recognition problems [29], [30] in order to effectively solve seq2seq time-series problems with multiple outputs. Our encoder-decoder LSTM-RNN implementation is based on [18].

B. MULTI-LAYER PERCEPTRONS

In general, MLPs are feedforward neural networks with multiple layers of perceptrons. A perceptron is a single neuron model that has weighted input signals and produces an output signal using an activation function.

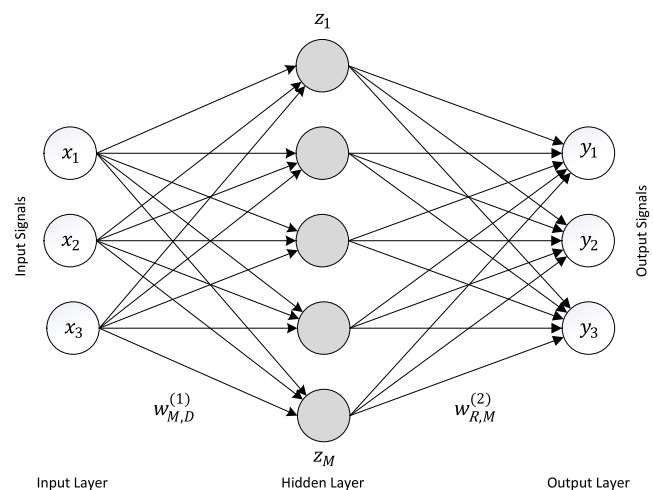


FIGURE 2. Feed-forward neural network. The circles represent the nodes of the input, hidden, and output layers. The arrows show the direction of forward propagation.

An MLP consists of at least three layers: an input layer, one or more hidden layers and an output layer, as depicted in Fig. 2. The input, hidden and output nodes are defined as $\mathbf{x} = [x_1 \dots x_d \dots x_D]$, $\mathbf{z} = [z_1 \dots z_m \dots z_M]$ and $\mathbf{y} = [y_1 \dots y_r \dots y_R]$, respectively. Here the total number of input, hidden and output nodes are D , M and R , while d , m and r denote a particular node. The output value for y_r is calculated using:

$$y_r(\mathbf{x}, \mathbf{w}) = \sigma \left(\sum_{m=1}^M w_{rm}^{(2)} \mathcal{H} \left(\sum_{d=1}^D w_{md}^{(1)} x_d + b_m^{(1)} \right) + b_r^{(2)} \right), \quad (5)$$

where σ and \mathcal{H} are the activation functions for output and hidden layers, respectively. The biases $b_m^{(1)}$ and $b_r^{(2)}$ are for the hidden node m and the output node r , respectively. The weight matrices of hidden-input and output-hidden are $w_{md}^{(1)}$ and $w_{rm}^{(2)}$, respectively.

MLPs utilize a supervised learning technique called back propagation for training and the training data needs to be arranged in a 2-dimensional (2D) matrix of samples

and features. Therefore, the only way to use MLPs for time-series prediction is to use the time sequence data as a feature (more details in Section IV). The other option is to use a RNN, which is explained in the next section.

C. LONG SHORT-TERM MEMORY RECURRENT NEURAL NETWORKS

LSTM networks are a special type of RNN that are capable of learning long-term dependencies. Fig. 3 illustrates the RNN and Fig. 4 the LSTM cells [13].

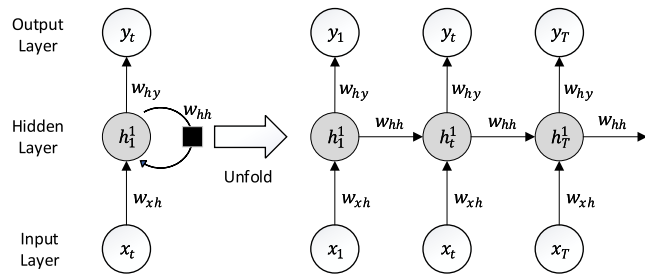


FIGURE 3. Recurrent neural network. The circles represent the input, hidden and output layers and the weights are above the lines. The arrows show the direction of forward propagation.

A RNN has a feedback connection where the output depends on the current input to the network, and the previous inputs, outputs, and/or hidden states of the network, as depicted in Fig. 3. Given an input sequence $\mathbf{x} = (x^1 \dots x^t \dots x^T)$, RNNs compute the hidden vector $\mathbf{h} = (h^1 \dots h^t \dots h^T)$, and output vector sequence $\mathbf{y} = (y^1 \dots y^t \dots y^T)$ by iterating (6) and implementing the calculation shown in (7).

$$h_t = \mathcal{H}(W_{xh} \cdot x_t + W_{hh} \cdot h_{t-1} + b_h), \tag{6}$$

$$y_t = W_{hy} \cdot h_t + b_y, \tag{7}$$

where \mathcal{H} is the activation function of the hidden layer. W_{xh} , W_{hh} and W_{hy} are the weight matrices of the input-hidden, hidden-hidden, and hidden-output connections, respectively. The hidden and output bias vectors are b_h and b_y .

The error gradients of RNNs that are trained using back-propagation through time can accumulate during an update and result in very large gradients. These gradients result in large updates to the network weights, and in turn, an unstable network. At an extreme, the weights can become so large as to overflow and result in non-computable values. LSTM networks have been developed to overcome the exploding back-propagated gradients of RNNs by providing explicit memory to the network. LSTM units are building units for layers of RNNs. A typical LSTM unit consists of an input gate, forget gate, output gate, and a cell unit.

The operations of the LSTM unit can be described as follows. The most important component is the cell state c_t , which serves as a memory and remembers values over an arbitrary time interval. The input gate i_t , forget gate f_t , and output gate o_t control the flow of information into and out of the cell and has the same size as the hidden vector \mathbf{h} .

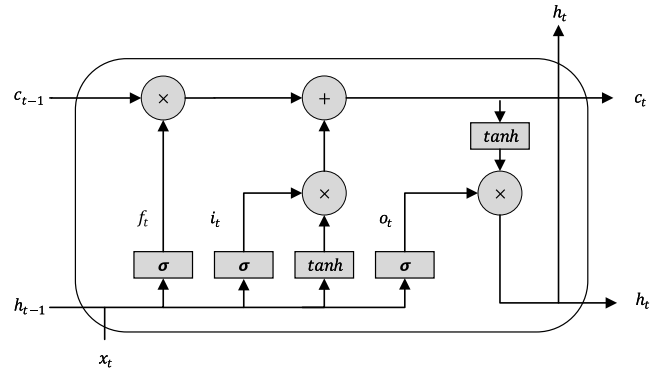


FIGURE 4. Long short-term memory cell.

The forget gate f_t outputs a 0 or 1 for each number in cell state to decide what information we want to put out from the previous cell state c_{t-1} , according to:

$$f_t = \sigma(W_f \cdot x_t + W_f \cdot h_{t-1} + b_f), \tag{8}$$

where σ is the sigmoid activation function. W_f and b_f are the weight matrix and bias of the forget gate, respectively.

Similarly, the input gate output i_t decides the new input information that should accumulate in the memory cell:

$$i_t = \sigma(W_i \cdot x_t + W_i \cdot h_{t-1} + b_i), \tag{9}$$

where W_i and b_i are the weight matrix and bias of the input gate, respectively.

The LSTM cell state is then updated as follows, but with conditional self-loop weights W_c and b_c :

$$c_t = f_t \cdot c_{t-1} + i_t \cdot \tanh(W_c \cdot x_t + W_c \cdot h_{t-1} + b_c). \tag{10}$$

The output hidden state h_t of the LSTM cell depends on the cell state c_t and the output gate o_t :

$$h_t = o_t \cdot \tanh(c_t). \tag{11}$$

The output gate o_t is calculated using:

$$o_t = \sigma(W_o \cdot x_t + W_o \cdot h_t + b_o), \tag{12}$$

where W_o and b_o are the weight matrix and bias of the output gate. Note that the hidden state h_t can be shut off via the output gate o_t , which uses a sigmoid activation function.

Encoder-decoder LSTM-RNN further improve the solution quality. This architecture, as depicted in Fig. 5, involves two models: one for reading the input sequence and encoding it into a fixed-length vector, and a second for decoding the fixed-length vector and outputting the predicted sequence. Next section models the PV forecasting problem.

IV. PV FORECASTING

PV forecasting using machine learning involves three steps: (1) Preparing the dataset, (2) Training, and (3) Predicting. Steps one and two are done day-ahead while step three is done in real-time.

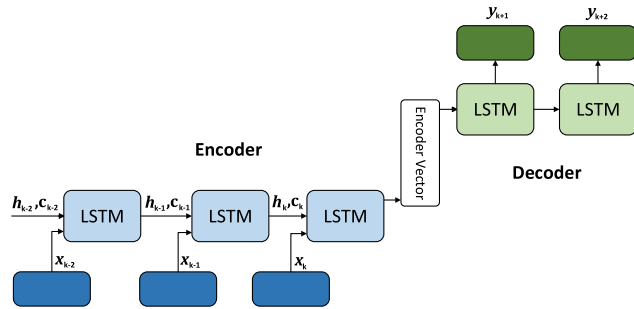


FIGURE 5. Encoder-decoder architecture.

A. DATA PREPARATION

We used two datasets for the analysis: Dataset A has the actual PV generation from the Arlington Microgrid from June 5, 2019 to June 4, 2020 and Dataset B has the PV generation data generated using the empirical formulas from [31] at the approximate location of the Arlington Microgrid (latitude 48.17 and longitude -122.14) and based on National Renewable Energy Laboratories (NREL) historical solar insolation and meteorological data over 6 years (2013 to 2018).

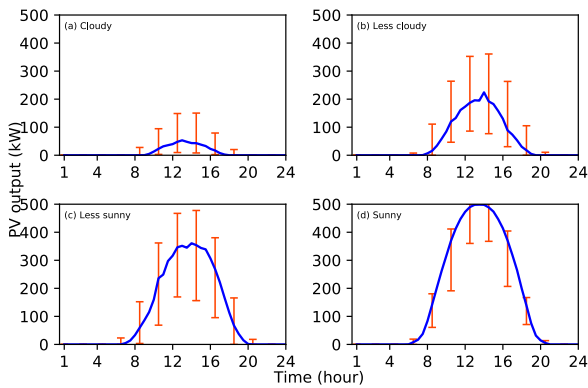


FIGURE 6. Median PV profiles for the four day-types in a year. The upper and lower limits of the error bars show the 95th and 5th quartiles.

Historical data are separated into training and testing sets and arranged in a 3D matrix (samples, time sequence, features) for RNNs and 2D matrix (samples, features) for MLPs. We use PV output, temperature, time-of-the day, season and day-type as features. Days are classified into sunny, less sunny, less cloudy and cloudy day-types by clustering historical PV generation data according to the total daily PV output using a k-means algorithm. Fig. 6 shows the median PV profiles for the four day-types over a year. When predicting, the day-type is estimated on the day ahead using a weather forecasts or a day-ahead PV-forecast. Preliminary simulations showed that the optimum length of the input time-sequence is 47 time-steps (i.e. one day). Outputs are the PV generation for the next two time-steps.

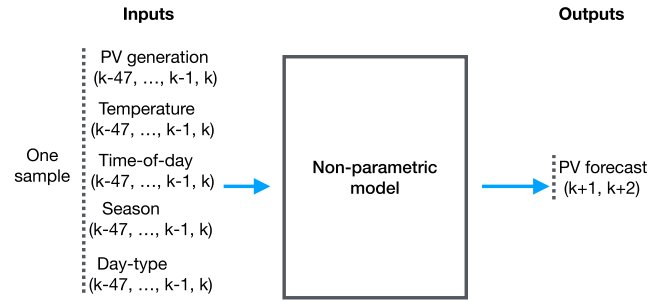


FIGURE 7. Inputs and outputs of the LSTM model.

TABLE 1. Simulation parameters of the two datasets.

	Snohomish PUD (~1 year)	NREL (>6 years)
Features	PV generation (clustered into four day-types)	PV generation Temperature Time-of-day Season Day-type
Training	~ 2 months for each cluster	5 years
Testing (days)	28 days for each cluster	365 (1 year)
Length of time sequence	One day	One day
LSTM units	25-100	25-100
Epochs	20	20-25
Batch size	1 to 16	1 to 16
Activation	Rectified Linear	Rectified Linear
Optimizer	adam	adam

B. TRAINING

Training the non-parametric model maps inputs and outputs as shown in Fig. 7. The parameters of the LSTM-RNN are given in Table 1.

Since Dataset A covers only a year, we cluster the PV generation data into four day-types according to the total daily PV generation using a k-means algorithm. The aim here is to identify the performance of the machine learning techniques on different types of days. Each of these clusters is trained separately and, because of the limited sample size, only the PV generation was used as a feature (i.e. we implemented a NAR model). On the other hand with the NREL dataset (Dataset B) we were able to use all the features mentioned in Fig. 7 (i.e. we implemented a NARX model). Therefore, we used the Dataset B for the economic analysis.

C. TESTING

The testing dataset was used to make real-time predictions for the next two time-steps, i.e. one hour-ahead forecasts. For Dataset A, 28 days in each cluster are used for testing and the remainder is used for training, as shown in Table 1. On the other hand, the NREL dataset used one year for testing and five years for training.

The machine learning models were trained and tested using Keras, which is a high-level neural networks application programming interface, written in Python, on a computer with a 2.8 GHz Intel Core i7 processor and a 16 GB 2133 MHz LPDDR3 memory card.

V. BATTERY MODELING

Operation of the 1 MW/1.385 MWh Lithium-ion battery of the Arlington Microgrid is limited to the 10% to 90 % SoC range. Fig. 8 shows the expected degradation of this battery over ten years assuming one energy throughput cycle per day, i.e. if there are multiple cycles, the total discharge equals 800 kWh. The average charge and discharge rate is assumed to be 1 C. Note that after ten years, this BESS is expected to have 1 MWh of capacity after degradation.

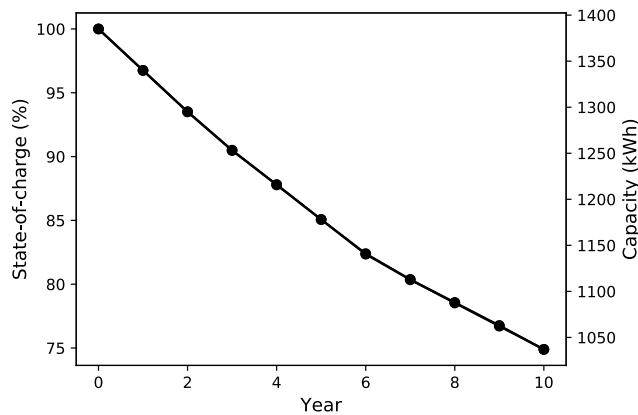


FIGURE 8. Estimated battery life of the Arlington Microgrid’s BESS over ten years assuming one energy throughput cycle per day.

In order to compare the battery degradation from the four PV forecasting methods, we generated battery SoC profiles for given actual and forecast PV generation using (1)-(3). The battery charging, battery discharging and inverter efficiencies are assumed to be 98%, 92% and 92%, respectively. The value of *C* is set to 1.2. Based on these SoC profiles, we use the rainflow algorithm to calculate the battery cycles and their magnitudes.

VI. SIMULATION RESULTS AND DISCUSSION

Figures 9, 10, and 11 show the PV generation forecasts and the battery SoC for typical cloudy, less sunny and sunny days, respectively. Tables 2 (Dataset B) and 3 (Dataset A) compare the RMSE, MAE, MBE and the resulting battery cycles of the LSTM-RNN, encoder-decoder LSTM-RNN, MLPs and the 30/30 persistence forecasting techniques. In all cases, machine learning forecasts are significantly better than the 30/30 persistence forecasts. The RMSE and MAE over a year from the encoder-decoder is 35.7% and 42.6% better than the persistence method (Table 2). The accuracy of the PV forecast varies with the type of day and machine learning technique, as shown in Table 3. For example, LSTM-RNN produced the best PV forecasts on sunny and less sunny days

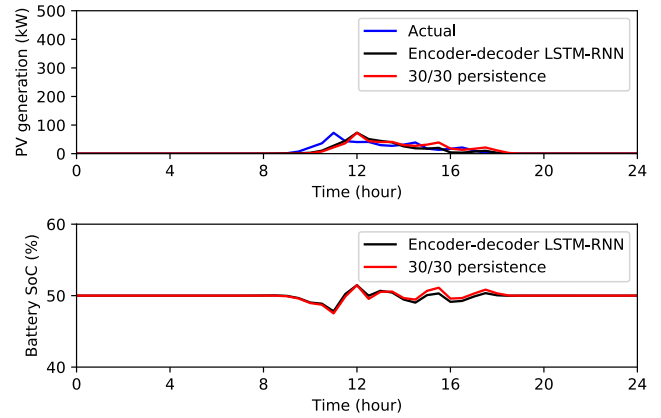


FIGURE 9. PV generation and battery SoC on a cloudy day using encoder-decoder LSTM-RNN and persistence method.

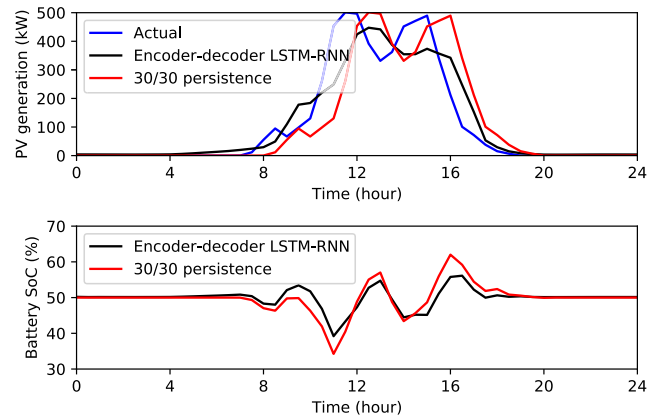


FIGURE 10. PV generation and battery SoC on a less sunny day using encoder-decoder LSTM-RNN and persistence method.

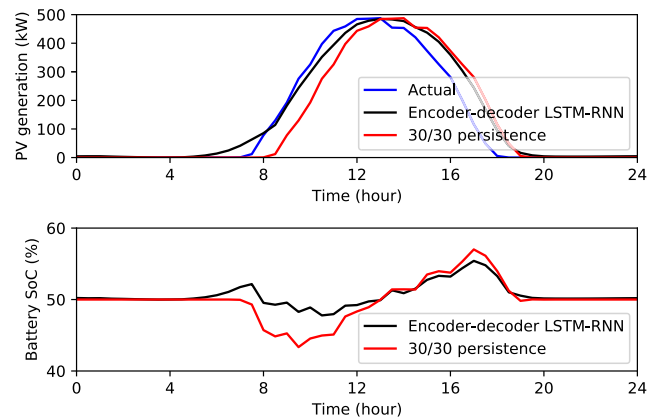


FIGURE 11. PV generation and battery SoC on a sunny day using encoder-decoder LSTM-RNN and persistence method.

while encoder-decoder LSTM-RNN performed the best on less cloudy days.

The number of yearly energy throughput cycles can be reduced by 29.1% (66 cycles per year) using the encoder-decoder LSTM-RNN forecasts. Battery cycles involving more than a 10% Depth of Discharge (DoD) can be reduced

TABLE 2. Simulation results based on NREL data over a year using five years training data. The improvements from the persistence method are given as percentages in parenthesis. The “e”, “b” and “h” in the training time column are the epochs, batch size and number of hidden units, respectively. A positive value for MBE indicates an under-prediction while a negative value indicates an over-prediction.

	RMSE (kW)	MAE (kW)	MBE (kW)	Battery cycles (energy throughput)	Battery cycles above 10% DoD	Training time (minutes)
30/30 Persistence	51.12	27.86	0	227	286	-
LSTM-RNN (no day-types)	35.88 (29.8%)	14.41 (48.3%)	0.55	180 (20.7%)	175 (38.8%)	14.7 e=20 b=32 h=100
LSTM-RNN (with day-types)	32.73 (36%)	13.64 (51.0%)	1.24	168 (26%)	153 (46.5%)	14.2 e=20 b=32 h=100
MLP (no day-types)	35.95 (29.7%)	18.18 (34.8%)	-2.1	177 (22%)	163 (43%)	1.3 e=20 b=16 h=200
MLP (with day-types)	34.53 (32.5%)	17.85 (35.9%)	1.9	163 (28.2%)	142 (50.4%)	1.4 e=20 b=16 h=200
Encoder-decoder LSTM-RNN (no day-types)	35.59 (30.4%)	15.79 (43.3%)	1.8	173 (23.8%)	157 (45.1%)	21.7 e=20 b=16 h=50, 25
Encoder-decoder LSTM-RNN (with day-types)	32.87 (35.7%)	15.98 (42.6%)	-1.85	161 (29.1%)	140 (51%)	21.4 e=20 b=16 h=50, 25

by 51%. Such deep cycles have a disproportionate effect on lithium-ion battery degradation. Unfortunately, due to the limited amount of data available about battery degradation, it has not been possible to quantify this effect more accurately. The benefit of using machine learning based forecasts is much higher during sunny days because incorrect forecasts result in higher battery energy throughput, as shown in Fig. 11.

The PV forecast from any of the machine learning techniques are significantly improved by using the type-of-day as a feature, as shown in Table 2. The battery energy throughput, the number of cycles above 10% DoD and the RMSE are improved by 5.3%, 5.9%, and 5.3%, respectively, by using day-type as feature in the encoder-decoder LSTM-RNN. Similar improvements are seen with the MLPs and LSTM-RNN.

In general, over-forecasting and under-forecasting have different effects on the battery usage because the PV output can be curtailed instead of charging the battery to meet the target generation. However, since the PV array of the Arlington Microgrid is part of a community solar project where each panel is owned by a different individual, the PV array is expected to always operate at maximum power (i.e. PV curtailment is not allowed). Given this, the only effect over-forecasting and under-forecasting have in our capacity firming problem is because of the different battery charging and discharging efficiencies. For the sake of completion, we compare the MBE (mean-bias-error) of the PV forecasts

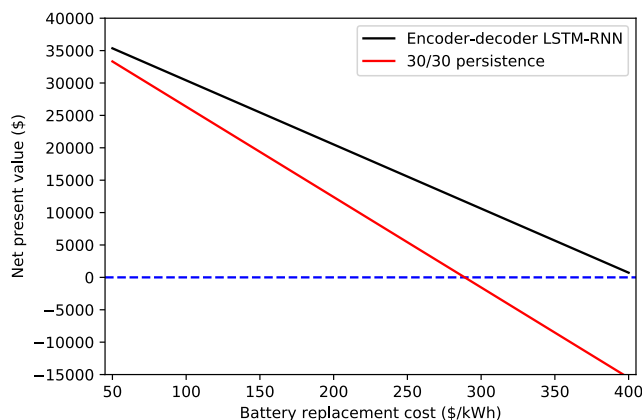


FIGURE 12. Net present value of capacity firming using encoder-decoder LSTM-RNN and 30/30 persistence after 10 years vs. battery replacement cost in 10 years. The revenue is fixed at \$5400 per year, the discount rate is assumed to be 5% and the battery degradation per cycle is based on Fig. 8.

in Tables 2 and 3. The small values for MBE in Table 2 means that our yearly forecasts consist of equal amounts of over-forecasts and under-forecasts. According to Table 3, all the machine learning techniques over-forecasts on sunny and less sunny days. This could be because our Dataset A is limited in size.

Tables 2 and 3 show that the time required for training MLPs is significantly smaller than for LSTM-RNN and encoder-decoder LSTM-RNN. However, the testing time is

TABLE 3. Simulation results from actual PV generation data of the Arlington Microgrid that are clustered into four day-types. The improvements from the persistence method are given as percentages in parenthesis. A positive value for MBE indicates an under-prediction while a negative value indicates a over-prediction.

	RMSE (kW)	MAE (kW)	MBE (kW)	Battery cycles (energy throughput)	Battery cycles (above 10% DoD)	Training time (seconds)
Sunny						
30/30 Persistence	68	41.75	0	14.8	30.5	-
LSTM-RNN	32.48 (52.2%)	16.79 (59.8%)	-10.46	9.3 (37.2%)	6 (80.3%)	31
MLP	33.28 (51.1%)	21.86 (47.6%)	-7.72	12.75 (13.9%)	6 (80.3%)	5.7
Encoder-decoder LSTM-RNN	35 (48.6%)	21.8 (47.8%)	-7.42	9.8 (33.8%)	6 (80.3%)	32.1
Less sunny						
30/30 Persistence	70.45	40.76	0	27.9	40.5	-
LSTM-RNN	52.08 (26.1%)	27.57 (32.4%)	-6.86	22.3 (20.1%)	26 (35.8%)	59
MLP	54.18 (23.1%)	31.43 (22.9%)	-11.87	24.4 (12.5%)	21 (48.1%)	7.2
Encoder-decoder LSTM-RNN	52.2 (25.9%)	31.02 (23.9%)	-12.49	22 (21.1%)	24.5 (39.5%)	55.3
Less cloudy						
30/30 Persistence	63.85	32.99	0	28.3	37.5	-
LSTM-RNN	52.62 (17.6%)	25.95 (21.3%)	4.50	21.7 (23.3%)	25.5 (32%)	43.5
MLP	50.56 (20.8%)	26.85 (18.6%)	-1.35	23.8 (15.9%)	26.5 (29.3%)	6.5
Encoder-decoder LSTM-RNN	49.78 (22%)	24.99 (24.3%)	2.31	21.7 (23.3%)	30 (20%)	42.7
Cloudy						
30/30 Persistence	24.67	10.4	0	8.8	6.5	-
LSTM-RNN	20.93 (15.2%)	8.4 (19.2%)	4.82	7.2 (18%)	3 (53.9%)	71.8
MLP	20.18 (18.2%)	9.24 (11.2%)	2.69	7.8 (11.4%)	2 (69.2%)	7.8
Encoder-decoder LSTM-RNN	21.91 (11.2%)	8.76 (15.8%)	-2.70	7.24 (17.7%)	3 (53.9%)	68.4

similar for all three techniques. Given that the offline training is done on a fast computer, the training time should not be considered when deciding the best PV forecasting method.

Fig. 12 compares how using the best machine learning forecast and persistence forecast affects the NPV (net present value) of capacity firming. Since it is difficult to know what the battery replacement cost will be in ten years, these values have been calculated for a range of replacement costs. This figure shows that encoder-decoder LSTM-RNN based PV forecasting makes capacity firming more profitable than persistence forecasting. If the battery replacement cost is high, capacity firming is not profitable if persistence forecasting is used. In these NPV calculations, the revenue from capacity firming is assumed to be \$5400 per year (i.e. the amount that Snohomish PUD would not have to pay to BPA), the interest rate is assumed to be 5%, the battery degradation is assumed to be 0.00687945% per cycle based on Fig 8, and the yearly battery cycles are from Table 2.

Our analysis shows that it is beneficial to do capacity firming if the PV forecasts are based on a state-of-the-art machine learning technique and the capacity firming is

already implemented in the BESS or the cost of implementing capacity firming in the BESS is low.

VII. CONCLUSION

This article compared capacity firming using photovoltaic (PV) forecasts based on long short-term memory recurrent neural networks (LSTM-RNN), encoder-decoder LSTM-RNN, multi-layer perceptrons and the 30/30 persistence approaches. The results showed that the encoder-decoder LSTM-RNN performs significantly better than the persistence method in forecasting PV generation and therefore significantly reduces the battery degradation cost of capacity firming.

REFERENCES

- [1] *Snohomish County Public Utility District*. Accessed: May 1, 2020. [Online]. Available: <https://www.snopud.com/?p=3326>
- [2] B. Xu, A. Oudalov, A. Ulbig, G. Andersson, and D. Kirschen, "Modeling of lithium-ion battery degradation for cell life assessment," in *Proc. IEEE Power Energy Soc. Gen. Meeting*, Jul. 2017. p. 1.
- [3] B. Xu, J. Zhao, T. Zheng, E. Litvinov, and D. Kirschen, "Factoring the cycle aging cost of batteries participating in electricity markets," in *Proc. IEEE Power Energy Soc. Gen. Meeting (PESGM)*, Aug. 2018. p. 1.

- [4] A. Marinopoulos and P. Bakas, "Evaluation of a very large scale PV power system with energy storage for capacity firming," in *Proc. IEEE Eindhoven PowerTech*, Jun. 2015, pp. 1–6.
- [5] A. K. Bhattacharjee, I. Batarseh, H. Hu, and N. Kutkut, "An efficient ramp rate and state of charge control for PV-battery system capacity firming," in *Proc. IEEE Energy Convers. Congr. Expo. (ECCE)*, Oct. 2017, pp. 2323–2329.
- [6] J. Cardo-Miota, H. Beltran, P. Ayuso, J. Segarra-Tamarit, and E. Perez, "Optimized battery sizing for merchant solar PV capacity firming in different electricity markets," in *Proc. IECON - 45th Annu. Conf. IEEE Ind. Electron. Soc.*, Oct. 2019, pp. 2446–2451.
- [7] S. A. Abdelrazek and S. Kamalasadán, "Integrated PV capacity firming and energy time shift battery energy storage management using energy-oriented optimization," *IEEE Trans. Ind. Appl.*, vol. 52, no. 3, pp. 2607–2617, May 2016.
- [8] S. Abdelrazek and S. Kamalasadán, "A weather-based optimal storage management algorithm for PV capacity firming," *IEEE Trans. Ind. Appl.*, vol. 52, no. 6, pp. 5175–5184, Nov. 2016.
- [9] S. A. Abdelrazek and S. Kamalasadán, "An optimal storage management algorithm for PV capacity firming based on weather patterns," in *Proc. IEEE Ind. Appl. Soc. Annu. Meeting*, Oct. 2015, pp. 1–8.
- [10] S. Abdelrazek and S. Kamalasadán, "Integrated control of battery energy storage management system considering PV capacity firming and energy time shift applications," in *Proc. IEEE Ind. Appl. Soc. Annu. Meeting*, Oct. 2014, pp. 1–7.
- [11] J. Mathe, N. Miolane, N. Sebastien, and J. Lequeux, "PVNet: A LRCN architecture for spatio-temporal photovoltaic PowerForecasting from numerical weather prediction," 2019, *arXiv:1902.01453*. [Online]. Available: <http://arxiv.org/abs/1902.01453>
- [12] N. Holland, X. Pang, W. Herzberg, S. Karalus, J. Bor, and E. Lorenz, "Solar and PV forecasting for large PV power plants using numerical weather models, satellite data and ground measurements," in *Proc. IEEE 46th Photovoltaic Specialists Conf. (PVSC)*, Jun. 2019, pp. 1609–1614.
- [13] M. Husein and I.-Y. Chung, "Day-Ahead Solar Irradiance Forecasting for Microgrids Using a Long Short-Term Memory Recurrent Neural Network: A Deep Learning Approach," *Energies*, vol. 12, no. 10, pp. 1–21, May 2019. [Online]. Available: <https://ideas.repec.org/a/gam/jeners/v12y2019i10p1856-d231480.html>
- [14] Li, Wang, Zhang, Xin, and Liu, "Recurrent neural networks based photovoltaic power forecasting approach," *Energies*, vol. 12, no. 13, p. 2538, Jul. 2019. [Online]. Available: <https://www.mdpi.com/1996-1073/12/13/2538>
- [15] D. Lee and K. Kim, "Recurrent neural network-based hourly prediction of photovoltaic power output using meteorological information," *Energies*, vol. 12, no. 2, p. 215, Jan. 2019. [Online]. Available: <https://www.mdpi.com/1996-1073/12/2/215>
- [16] L. Cho, C.-Y. Hsu, C.-W. Li, W.-C. Chen, H.-R. Wang, and C.-P. Lin, "Study of features and number of time steps to improve hourly solar power forecasting via LSTM," in *Proc. IEEE 8th Global Conf. Consum. Electron. (GCCE)*, Oct. 2019, pp. 303–304.
- [17] Y. Yu, J. Cao, and J. Zhu, "An LSTM short-term solar irradiance forecasting under complicated weather conditions," *IEEE Access*, vol. 7, pp. 145651–145666, 2019.
- [18] J. Brownlee. (2019). *How to Develop Multi-Step LSTM Time Series Forecasting Models for Power Usage*. [Online]. Available: <https://machinelearningmastery.com/how-to-develop-lstm-models-for-multi-step-time-series-forecasting-of-household-power-consumption/>
- [19] J. Antonanzas, N. Osorio, R. Escobar, R. Urraca, F. J. Martinez-de-Pison, and F. Antonanzas-Torres, "Review of photovoltaic power forecasting," *Sol. Energy*, vol. 136, pp. 78–111, Oct. 2016. [Online]. Available: <http://www.sciencedirect.com/science/article/pii/S0038092X1630250X>
- [20] S. Theocharides, R. Alonso-Suarez, G. Giacosa, G. Makrides, M. Theristis, and G. E. Georghiou, "Intra-hour forecasting for a 50 MW photovoltaic system in uruguay: Baseline approach," in *Proc. IEEE 46th Photovoltaic Specialists Conf. (PVSC)*, Jun. 2019, pp. 1632–1636.
- [21] Y. Tao and Y. Chen, "Distributed PV power forecasting using genetic algorithm based neural network approach," in *Proc. Int. Conf. Adv. Mech. Syst.*, Aug. 2014, pp. 557–560.
- [22] M. Alrashidi, M. Alrashidi, M. Pipattanasomporn, and S. Rahman, "Short-term PV output forecasts with support vector regression optimized by cuckoo search and differential evolution algorithms," in *Proc. IEEE Int. Smart Cities Conf.*, Sep. 2018, pp. 1–8.
- [23] G. Mosaico and M. Saviozzi, "A hybrid methodology for the day-ahead PV forecasting exploiting a clear sky model or artificial neural networks," in *Proc. 18th Int. Conf. Smart Technol.*, Jul. 2019, pp. 1–6.
- [24] S. Leva, M. Mussetta, A. Nespoli, and E. Ogliari, "PV power forecasting improvement by means of a selective ensemble approach," in *Proc. IEEE Milan PowerTech*, Jun. 2019, pp. 1–5.
- [25] F. Wang, Z. Xuan, Z. Zhen, K. Li, T. Wang, and M. Shi, "A day-ahead PV power forecasting method based on LSTM-RNN model and time correlation modification under partial daily pattern prediction framework," *Energy Convers. Manage.*, vol. 212, May 2020, Art. no. 112766. [Online]. Available: <http://www.sciencedirect.com/science/article/pii/S0196890420303046>
- [26] Y. Jung, J. Jung, B. Kim, and S. Han, "Long short-term memory recurrent neural network for modeling temporal patterns in long-term power forecasting for solar PV facilities: Case study of South Korea," *J. Cleaner Prod.*, vol. 250, Mar. 2020, Art. no. 119476. [Online]. Available: <http://www.sciencedirect.com/science/article/pii/S095965261934346X>
- [27] M. P. Almeida, M. Muñoz, I. de la Parra, and O. Perpiñán, "Comparative study of PV power forecast using parametric and nonparametric PV models," *Sol. Energy*, vol. 155, pp. 854–866, Oct. 2017. [Online]. Available: <http://www.sciencedirect.com/science/article/pii/S0038092X17306175>
- [28] M. Q. Raza, M. Nadarajah, and C. Ekanayake, "On recent advances in PV output power forecast," *Sol. Energy*, vol. 136, pp. 125–144, Oct. 2016. [Online]. Available: <http://www.sciencedirect.com/science/article/pii/S0038092X16302547>
- [29] K. Cho, B. van Merriënboer, C. Gulcehre, D. Bahdanau, F. Bougares, H. Schwenk, and Y. Bengio, "Learning phrase representations using RNN encoder-decoder for statistical machine translation," 2014, *arXiv:1406.1078*. [Online]. Available: <http://arxiv.org/abs/1406.1078>
- [30] I. Sutskever, O. Vinyals, and Q. V. Le, "Sequence to sequence learning with neural networks," in *Proc. 27th Int. Conf. Neural Inf. Process. Syst.*, Cambridge, MA, USA, 2014, p. 3104–3112.
- [31] M. G. Masters, *Renewable Efficient Electric Power System*. Hoboken, NJ, USA: Wiley, 2004.

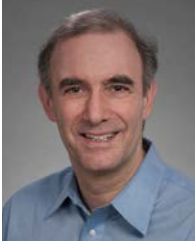


CHANAKA KEERTHISINGHE (Member, IEEE) was born in Sri Lanka. He received the B.E. (Hons.) and M.E. degrees in electrical and electronic engineering from The University of Auckland, Auckland, New Zealand, in 2011 and 2014, respectively, and the Ph.D. degree in electrical engineering from The University of Sydney, Sydney, NSW, Australia, in 2017.

He is currently the Lead Electrical Engineer with the Systems Integration Testbed, Washington Clean Energy Testbeds, and a Postdoctoral Researcher with the Department of Electrical and Computer Engineering, University of Washington, Seattle, WA, USA. He has work experience at Mitsubishi Electric Research Laboratories, Cambridge, MA, USA. He holds a U.S. patent and publications in microgrids, energy management in smart homes, wireless power transfer, disaster response, electricity markets, stochastic optimization, and machine learning.



EVAN MICKELSON is currently pursuing the bachelor's degree in electrical engineering with a focus on sustainable power systems with the University of Washington. His mission is to facilitate the integration of clean energy into the grid.



DANIEL S. KIRSCHEN (Fellow, IEEE) received the Ph.D. degree from the University of Wisconsin–Madison and the Electromechanical Engineering degree from the Free University of Brussels, Belgium. He is currently the Donald W. and Ruth Mary Close Professor of electrical engineering with the University of Washington. His research interests include the integration of renewable energy sources in the grid, power system economics, and power system resilience. Prior to joining the University of Washington, he taught for 16 years at The University of Manchester, U.K. Before becoming an Academic, he worked at Control Data Corporation and Siemens on the development of application software for utility control centers. He is the author of two books.



NATHAN SHIH (Student Member, IEEE) is currently pursuing the bachelor's degree in electrical and computer engineering with the University of Washington. He was an Undergraduate Researcher with the University of Washington's Renewable Energy Analysis Laboratory and has previously interned at the National Renewable Energy Laboratory and the NASA Ames Research Center. His research interests include renewable energy, energy poverty, and sustainability.



SCOTT GIBSON (Member, IEEE) received the B.S.E.E. degree from the University of Wyoming, in 1987. He is currently a Principal Engineer with Snohomish County PUD. After graduation, he worked at Boeing and then with a consulting company designing building electrical systems. In 2000, he joined PUD, where he is working on new electrical generation projects. He worked on the development of a tidal generation project and helped to design and constructs two run-of-the-river hydroelectric projects. He is the Project Manager of the PUD's latest energy storage project Arlington Microgrid.

...